Aerodynamic performance of a small-scale ducted rotor in hover

An experimental study on the effect of the tip gap

Reinier Goudswaard

Aerodynamic performance of a small-scale ducted rotor in hover

An experimental study on the effect of the tip gap

by

Reinier Goudswaard

to obtain the degree of Master of Science
at the Delft University of Technology,
to be defended publicly on Tuesday December 13, 2021 at 13:00 PM.

Student number:	4375793	
Project duration:	November 2, 2020 – December 3, 2021	
Thesis committee:	Dr.ir. W.J. Baars	TU Delft, supervisor
	Dr. D. Ragni	TU Delft, chairman
	Prof.Dr.ir. L.M.M. Veldhuis	TU Delft, examiner

An electronic version of this thesis is available at `http://repository.tudelft.nl/`.

TU Delft

Preface

Most graduates can attest that a master thesis is a real ordeal. The year-long process can be difficult at times, because the contestant is challenged to outline by him- or her-self what work needs to be done, and more importantly: *Why?*

This becomes challenging even more so, when a pandemic comes around that shuts down the university for over a year. Never have I seen the four walls of my room more. I think it is needless to devote more words to that situation, as I'm quite sure that everyone has experienced the effects of a lockdown to some extent.

However challenging, last year has also been an incredibly edifying and educational experience. I know that it is not very original to thank my supervisors in this paragraph, but....yes I truly want to thank my supervisors. Woutijn and Dani, you have shown a very sincere interest in my thesis as well as me personally. I was always welcome to ask questions, which were even answered at unorthodox times. Your advises really have supported me through the moments where I was stuck. Moreover, at times it even was fun! (Who would have thought)

I could use the remaining space on this page to describe in more detail the technical challenges I encountered and overcame. But I think if the interest is there, it's better to just read this thesis. Instead, here is a poem by Marilyn Shepperson:

Swirling widdershins, round and around
To enter it, is to leave the sane world behind
It drags me down to unexplored depths
I step in, only when I dare
Sometimes, if I am lucky, it's quite safe and benign
But more often than not, it contains
The stuff of dreams and nightmares,
What is this vortex, that's so fascinating
Why it's only my mind.

Reinier Goudswaard
Delft, November 2021

Abstract

The growing demand for efficient propulsion systems that operate primarily in hover, has led the ducted rotor configuration to emerge as an increasingly popular design solution. One of the major design parameters for the ducted-rotor assembly is the radial distance between the blade tip and the circumferential wall of the duct, referred to as the tip gap. How a variation in the tip gap affects the performance of the ducted-rotor assembly is addressed in this current research work.

The aerodynamic characteristics and performance of the ducted-rotor assembly are experimentally investigated for a parametric variation of the tip gap. The aerodynamic performance of both the rotor and the duct are characterized through force measurements with load cells. These types of measurements reveal that, for typical operating conditions, the duct generates more than half of the total thrust of the assembly. The thrust performance of the duct was also characterized with a detailed mapping of the static pressure distribution over the duct inner-wall, confirming that the thrust-generating mechanism of the duct is a direct consequence of the relatively low pressure over the inlet area of the duct. Even though the diffuser of the duct generates a small amount of pressure drag, its presence is critical for the below-the-rotor pressure recovery and for establishing a high axial throughflow. From detailed flow measurements using the particle image velocimetry method it was furthermore found that the performance deterioration—with an increase of the tip gap—is associated with a contraction of the rotor slipstream in the duct-diffuser, since the less rapid breakdown of the tip vortices reduce the axial momentum near the diffuser wall. A set of preliminary acoustic experiments were also conducted and show that the noise radiated by the system is also strongly dependent on the size of the tip gap.

Contents

List of Figures

List of Tables

List of Symbols and Abbreviations

Abbreviations

2D	2-Dimensional
BEM	Blade Element Momentum
BPF	Blade Pass Frequency
CAD	Computer Aided Design
CFD	Computational Fluid Dynamics
FOR	Frame Of Reference
FOV	Field Of View
MAV	Micro Air Vehicle
Min.	Minutes
PIV	Particle Image Velocimetry
RPM	Revolutions Per Minute
Sec.	Seconds
UAM	Urban Air Mobility
VTOL	Vertical Take-Off and Landing

Symbols

α	Blade angle of attack [deg]
β	Blade twist angle [deg]
δ^*_{tip}	Tip gap ratio [%]
δ_{tip}	Tip gap [m]
Ω	Angular velocity [RPM]
ω_z	Vorticity in Z-direction (out of X-Y plane) [1/s]
ϕ	Blade Inflow angle [deg]
ψ	Microphone position angle relative to rotor [deg]
ρ	Air Density [kg/m^3]
σ_d	Duct diffuser ratio [-]
θ	Rotor position phase [deg]
θ_d	Duct diffuser angle [deg]
C_d	Drag force coefficient [-]
C_l	Lift force coefficient [-]
C_P	Power coefficient [-]
C_T	Total thrust coefficient [-]
$C_{p,stat}$	Static pressure coefficient [-]
$C_{T,r}$	Rotor thrust coefficient [-]
D_d	Duct throat diameter [m]
D_r	Rotor diameter [m]
f	Frequency [Hz]
f_b	Blade pass frequency [Hz]
F_d	Drag force [N]
F_l	Lift force [N]
F_{tot}	Total force acting on rotor [N]
FM	Total figure of Merit [-]
FM_r	Rotor figure of Merit [-]
$G_{pp}(f)$	Autospectrum of the sound pressure time series $p(t)$
L	Length coordinate of the duct profile [m]
L_d	Diffuser length [m]
$OASPL$	Overall sound presure level [dB]
$p(t)$	Sound pressure time series [Pa]
P	Mechanical power [W]
p_{atm}	Atmospheric pressure [Pa]
p_{ref}	Standard reference sound pressure [Pa]
p_{rms}	Root mean square of the sound pressure time series $p(t)$ [Pa]
p_{stat}	Static pressure [Pa]
Q	Torque [Nm]
R_r	Rotor radius [m]
r_{lip}	Duct inlet lip radius [m]
Re_c	Reynolds number (chord based) [-]
SPL	Sound presure level [dB/Hz]
t	Time [s]

T_d	Duct thrust [N]
T_r	Rotor thrust [N]
T_{tot}	Total thrust (combined rotor and duct thrust) [N]
v_{tip}	Rotor blade tip speed [m/s]
V_{tot}	Total flow velocity [m/s]
V_x	Velocity in X-direction [m/s]
V_y	Velocity in Y-direction [m/s]
V_z	Velocity in Z-direction [m/s]
W	Total velocity component [m/s] (blade section FOR)
W_a	Axial velocity component [m/s] (blade section FOR)
W_t	Tangential velocity component [m/s] (blade section FOR)
X	X-dimension of Cartesian coordinate system [m]
Y	Y-dimension of Cartesian coordinate system [m]
Z	Z-dimension of Cartesian coordinate system [m]
A	Rotor disc area [m2]
c	Blade chord length [m]

1 Introduction

1.1. Background

In the past decade, the multi-rotor configuration has become an increasingly popular design solution for rotary wing aircraft. The emerging market of Urban Air Mobility (UAM) as well as the rapidly evolving Micro Air Vehicle (MAV) drone market, are the driving stimulus behind this development. In 2018, the Vertical Flight Society reported the existence of more than 100 fully electric UAM concepts for human transport [33] that are under development. And, when it comes to MAV's, a complete industry branch has already been established that produces drones for many applications in today's society: e.g., aerial photography, geographical mapping, cropfield monitoring, emergency shipment deliveries.

For these new types of aerial vehicles, the multi-rotor concept is often chosen because of its VTOL (Vertical Take-Off and Landing) capabilities and manoeuvrability in confined areas. Furthermore, practical considerations such as accessibility, ease of use and low cost of small motors are often named as advantages of this concept. On the other hand, a major challenge arise when increasing the number of (smaller-scale) rotors, because they result in a lower overall efficiency; this then reduces the flight time. A multitude of smaller-scale rotors are aerodynamically less efficient because of the following reasons:

1. Multi-rotor aircraft generally result in a design with a smaller total area of all rotors combined compared to single rotor aircraft (e.g. a helicopter). According to the ideal actuator disc theory [26], this results in a higher required power to produce a certain amount of thrust.

2. Even when the combined area of all rotors on a multi-rotor aircraft equals the area of a single rotor aircraft, small rotors still have the disadvantage of operating at a lower Reynolds number [10].

In attempts to counteract the decreased overall efficiency of relatively small-scale multi rotors, the ducted rotor configuration was introduced. When an axisymmetric duct is placed around a rotor – and optimized for the given rotor-duct assembly – the aerodynamic performance can be improved. This means that for a given rotor-disc area, a ducted rotor needs less power to generate a certain amount of thrust, compared to a rotor in open air [23] [26]. As for any addition of major structural component on aerospace vehicles, there are several practical challenges when including ducts. One major challenge is the weight of the duct; if the duct weighs too much this can cancel out all the gains associated with the higher aerodynamic efficiency. For this reason, ducted rotors are often not used in the design of traditional rotor craft. However, for propulsion systems of smaller diameter, these practical issues turn out to be resolvable. The scaling laws of weight ($\propto$ size^3) and power required for a certain amount of thrust ($\propto$ size^{-1}) are for example in favor for ducted rotors of smaller scale [16]. Therefore, with the growing markets for multi-rotor aircraft, there also is an increasing interest in the research and development of the ducted rotor configuration.

1.2. Problem analysis

With a ducted rotor configuration, the rotor is not the only device that generates thrust. The duct itself also produces a significant amount of thrust, due to the pressure distribution over the inner wall-profile of the duct [23] [26]. The total performance of the system is subject to the aerodynamic interaction between the rotor and duct: In hover flight, the thrust-performance of the duct is fully dependent on the flow induced by the rotor. Conversely, the rotor performance is also affected by the presence of the duct; the velocity distribution at the rotor plane changes, and towards the tip of the blade the rotor vortex dynamics are affected by the close proximity of the duct wall [32].

The degree of interaction between rotor and duct strongly depends on the tip gap δ_{tip}, which is defined as the radial distance between the blade tip and circumferential wall of the duct. The tip gap is therefore a major parameter in the design of a ducted rotor system. Several studies have (partially) investigated how the tip gap affects the aerodynamics of a ducted rotor: The experimental work of Pereira [26] and Martin and Tung [23] showed that a smaller tip gap δ_{tip} significantly improves the overall performance of a ducted rotor. Pereira observed that this performance increase is mostly related to an increase of suction at the duct inlet lip, which causes the duct to generate more thrust. There is however no study that explains in detail what mechanism causes this increase of suction. Some papers highlight an isolated flow effect that is related to a smaller tip gap, such as the faster breakdown of the rotor tip vortices [32] [5] or the reduction of blockage due to tip leakage [4], but this does not present a complete explanation. Moreover, it is hard to compare the separate results of these studies, because different designs, scales and operating conditions were investigated.

Getting an understanding in of how the flow inside the duct changes for different tip gaps, and how this affects the performance of the ducted rotor system, would be a valuable extension to the existing scientific literature of ducted rotor systems. Gaining insight in the complex interaction between rotor and duct can ultimately contribute to improving the designs of ducted rotors.

1.3. Objective and research questions

The aim of the current study is to investigate in detail how the tip gap affects the aerodynamic performance of a small-scale ducted rotor in hover. In order to achieve this, three types of experiments are performed on a ducted rotor system that is well representative for MAV's in hover: The performance of the ducted rotor system is characterized through force measurements with load-cells, the pressure distribution over the duct profile is measured with static-pressure tabs in the duct inner-wall, and the flow field inside the duct is retrieved and analyzed using PIV- (particle image velocimetry) measurements.

The main research questions is defined as follows:
How does a tip gap affect the aerodynamic performance of a small-scale ducted rotor in hover?

Three sub-questions are defined in support of the main question:

- How is the tip gap related to the aerodynamic efficiency of the ducted rotor system, and the portion of thrust that is generated by the duct?
- How are the initial strength, trajectory and ageing of the rotor tip vortices affected by the tip gap?
- How does the tip gap affect the velocity distribution inside the duct and the pressure distribution over the duct profile?

Even though the main focus of the study is to investigate how the tip gap affects the aerodynamic performance of a ducted rotor system, a preliminary investigation into the aeroacoustic noise is also included. A fourth type of experiments in an anechoic chamber is performed to measure the far field noise for different tip gaps. The corresponding fourth sub-question is defined as follows:

- How is the aeroacoustic noise of the ducted rotor system affected by the tip gap?

1.4. Thesis report outline

This thesis report is composed of the following chapters:
In chapter 2, the relevant background theory of ducted rotors in hover is described. Chapter 3 contains a literature review of the state of the art on how the tip gap affects the aerodynamics of a ducted rotor system. Chapter 4 provides an overview of the methods that are used to obtain the results of this study. The experimental set-ups, working principles and goals of the four types of experiments are described (performance experiments, static-pressure experiments, PIV experiments and acoustic experiments). Also the design is described of the ducted rotor system that is used for all experiments. In chapter 5 the results of all the experiments are analysed and discussed. Finally in chapter 6, the most important findings are summarized in the conclusions. Furthermore, some recommendations are given for future studies.

2

Background theory: ducted rotors in hover

This chapter covers the relevant background of ducted rotor aerodynamics. In section 2.1, the basic theory of open rotor aerodynamics is introduced. In section 2.2, a description is given of the duct shape and its placement around the rotor. Section 2.3 describes how the rotor is affected by the presence of a duct, and section 2.4 explains how the duct itself can generate thrust, and thus favorably contribute to the performance.

2.1. Open rotor aerodynamics: basic theory

One of the most commonly used models to assess the aerodynamic performance of rotors is the so-called Blade Element Momentum (BEM) theory. This BEM model results from a combination of the blade element theory and the momentum theory [17]. It is not only a very effective method to calculate the performance of a rotor, but has proven to be a useful framework for discussing aerodynamic phenomena of rotors.
With the blade element theory, the blade of a rotor is divided in small 'elements' [17] [12]. Each element can be seen as a 2D airfoil profile, as shown in figure 2.1. For each element the resulting aerodynamic force can be calculated with the help of a velocity diagram (see figure 2.2). The total air velocity relative to the blade section can be obtained by summing the axial and tangential velocity vectors. The tangential velocity results from the rotational speed of the blade, and the axial velocity component is caused by the fact that the rotor accelerates air in axial direction (which is called the induced axial velocity) [12]. If the total relative velocity W is known, the resulting lift coefficient C_l and drag coefficient C_d can be derived from the polar diagrams of the airfoil that corresponds to the blade section [17]. The airfoil polars can be obtained from windtunnel data or models such as Xfoil [11].

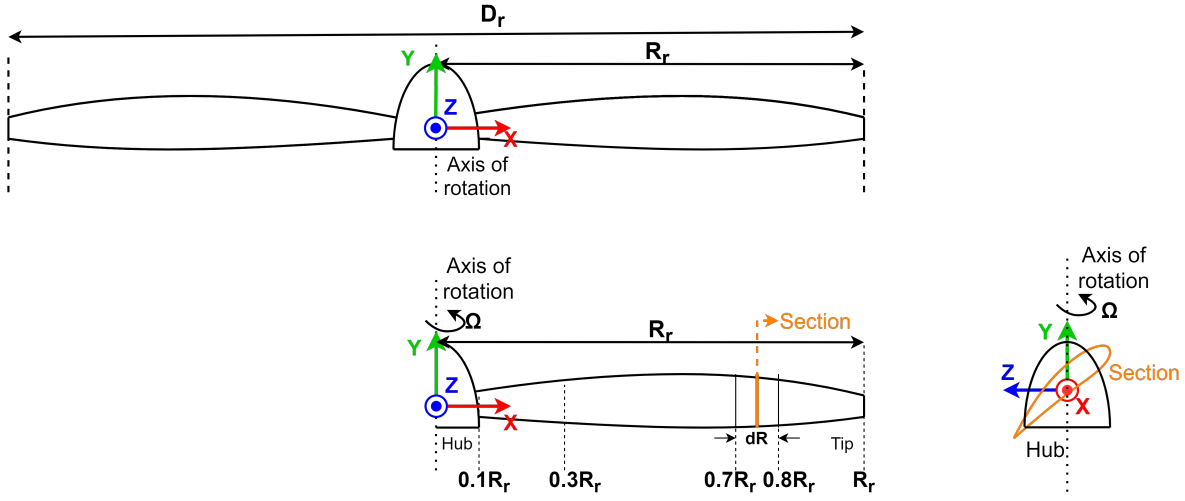

Figure 2.1: Blade element theory: discretizing the rotor blade into small 2D elements (pictures: [14])

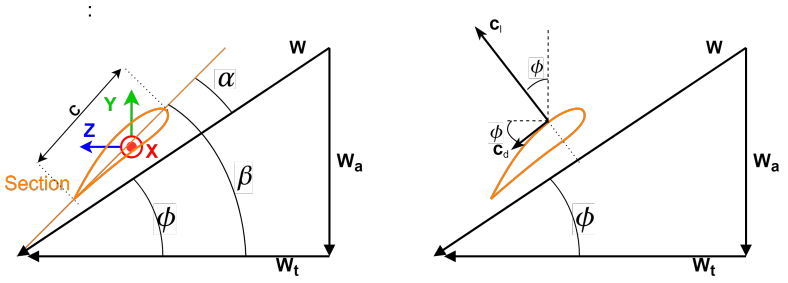

Figure 2.2: Blade crosssection velocity diagrams: W_a=axial vel., W_t=tangential vel., W=total vel., ϕ=inflow angle, β=blade twist angle, α=angle of attack, C_l=lift force coef., C_d=drag coef.

If the lift and drag forces of all blade elements are integrated over the span of the blade, and multiplied by the number of blades, the total force acting on the rotor can be calculated. Generally, this total force is projected in thrust ($+Y$) direction and torque ($+Z$) direction [12]. This is illustrated in figure 2.3.

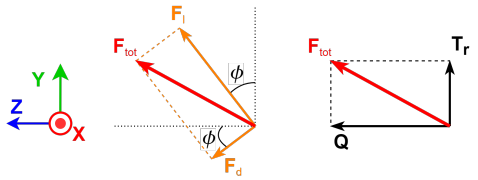

Figure 2.3: Projection of the total force F_{tot} in the rotor thrust T_r and torque Q direction

If the thrust and torque of the rotor are known, the rotor performance coefficients can be derived. These are the power coefficient C_P, rotor thrust coefficient $C_{T,r}$, and rotor figure of merit FM_r. In equation set 2.1 it is defined how these coefficients are calculated [26] [23] [30]. It can be seen that C_P and $C_{T,r}$ depend on the rotational speed Ω, rotor thrust T_r and rotor torque Q. With the power and thrust coefficients, the figure of merit FM_r is calculated. The figure of merit is equal to the mechanical power of an ideal actuator disc (without losses), divided by the actual mechanical power of a rotor at a certain level of thrust [26]. Therefore it expresses the aerodynamic efficiency of a rotor.

$$v_{tip} = \Omega \cdot \frac{2\pi}{60} \cdot R_r \tag{2.1a}$$

$$P = \Omega \cdot \frac{2\pi}{60} \cdot Q \tag{2.1b}$$

$$C_P = \frac{P}{\rho A v_{tip}^3} \tag{2.1c}$$

$$C_{T,r} = \frac{T_r}{\rho A v_{tip}^2} \tag{2.1d}$$

$$FM_r = \frac{\text{ideal power}}{\text{actual power}} = \frac{C_{T,r}^{1.5}}{\sqrt{2} C_P} \tag{2.1e}$$

In a BEM calculation, a few iterations are performed of the calculations that are described above. Initially, the induced axial velocity W_a is set to an arbitrary value because it is not known yet [25]. From the resulting load distribution on the blade, a new axial induced velocity component can be calculated with the help of the momentum theory [17] (which is based on the conservation laws of fluid mechanics [9]). After updating this velocity component, the load distribution can be recalculated, and this iterative process is repeated until convergence is reached [25].
It should be noted that the blade element method does not describe the complete aerodynamics of a rotor, because it involves simplifications. All the blade elements are independent of each other[17], which means that no radial (spanwise) flow is taken into account. This assumption is needed because for each element the lift and drag polar of a 2D-airfoil is evaluated. Also, a laminar steady flow is assumed, and losses associated

with the finite length of the blade are not included (tip vortex losses). For the latter it is however possible to apply some corrections that can account for this [29].
Besides its utility to calculate the aerodynamic forces on a rotor, the blade element method also allows for a relatively straightforward assessment of the influence of design parameters on the rotor performance. For example, in section 2.3, the velocity diagram is directly used to explain how the duct affects the thrust and torque performance of a rotor.

2.2. Duct shape parametrization

Ducts exist in a lot of different shapes and forms, but they all have in common that it is some axisymmetric airfoil-like shape around a rotor. The part above (upstream of) the rotor is referred to as the 'inlet lip', and the part below (downstream of) the rotor is called the 'diffuser'. The 'throat' is located between the inlet lip and diffuser (at the rotor plane), which is were the cross-section of the duct is the smallest.
A clear method to parameterize the shape of a duct is the one as proposed by Pereira [26]. In his study he experimentally investigated the effect of 5 different shape parameters, on the performance of MAV ducted rotors. In table 2.1 and figure 2.4 these shape parameters are summarized.

Table 2.1: Shape parameters to describe the shape of a duct, in the study of Pereira [26]

Description	Symbol	Unit
Duct diameter	D_d	[m]
Inlet lip radius	r_{lip}	[m]
Tip gap ratio	δ_{tip}	[-]
Diffuser length	L_d	[m]
Diffuser angle	θ_d	[deg]

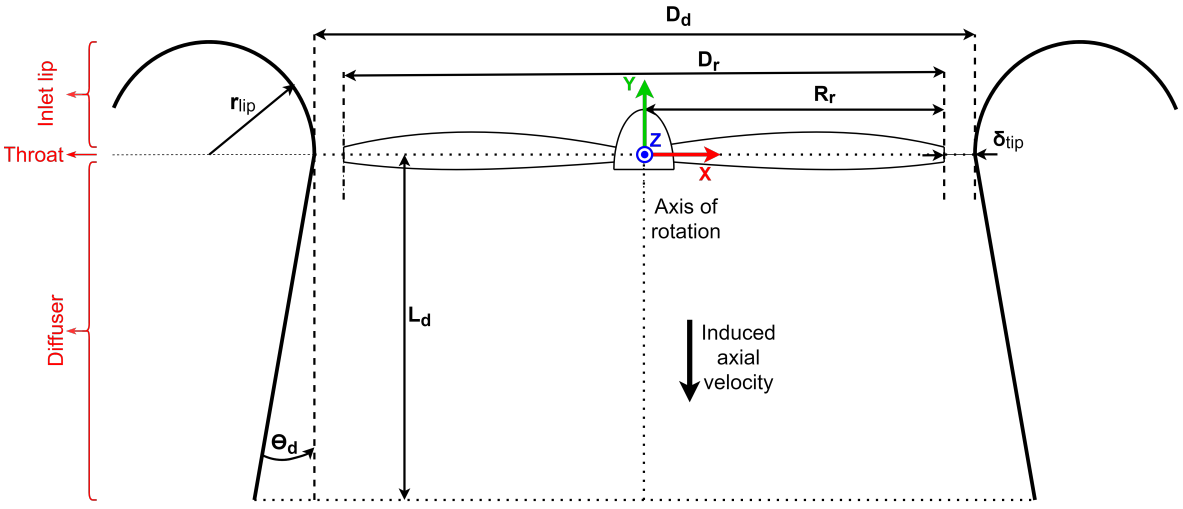

Figure 2.4: Parametrization of a duct shape. The shape is uniquely defined by the duct diameter D_d, inlet lip radius r_{lip}, tip gap ratio δ_{tip}, diffuser length L_d and diffuser angle θ_d.
The rotor diameter D_r and rotor radius R_r over-define the shape, and are stated for terminology purposes.

As can be seen in figure 2.4, the cross-section of a duct that is defined by the shape parameters of Pereira [26], basically consists of a separate semi-circle for the inlet lip, and a straight angled line for the diffuser. This design choice allowed Pereira to easily produce and combine different duct parts, to investigate his extensive test-matrix.
However, most ducts that appear in literature and on existing rotorcraft, instead consist of single spline which

is an airfoil profile (see figure 2.5). Even though Pereira's parameters cannot completely describe these advanced profiles, they are still very relevant to characterize these shapes, similarly to for example the chord, camber and thickness of general airfoils. These definitions will be useful later when discussing the aerodynamic performance of ducts.

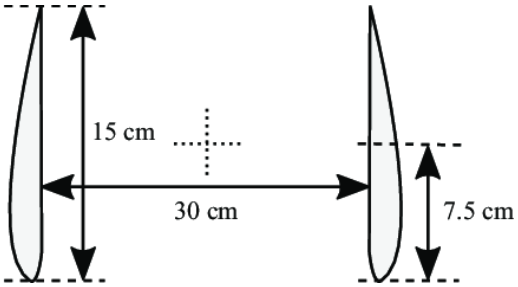

(a)

(b)

Figure 2.5: Examples of an airfoil shaped duct in the study of Malgoezar [21]

2.3. Effect of the duct on the rotor

If a duct is placed around a rotor, the aerodynamic performance of the rotor itself is affected. Two main effects are highlighted that describe the most distinct changes:

Effect 1: increased axial velocity

The presence of a duct changes the inflow profile (velocity distribution at the rotor plane), which subsequently affects the complete load distribution of the rotor. The exact changes in the inflow depend on the shape and placement of the duct, but the most emphatic effect is that the converging inlet of the duct accelerates the flow [35], effectively increasing the axial velocity at the rotor plane compared to open air [37].

The velocity diagram of figure 2.2 can be used to describe how an increased axial velocity affects the performance of a rotor blade. In the figure below (figure 2.6), this is clearly illustrated by comparing the case with lower and higher axial velocity W_a. It can be seen that an increase of the axial velocity W_a increases the inflow angle ϕ and also increases the magnitude of the total velocity vector W. The effective angle of attack α is therefore reduced, as the blade pitch angle β remains the same. The increased inflow angle ϕ also causes the vector corresponding to the lift coefficient C_l to point more towards the torque direction and less towards the thrust direction. In practice, placing a duct around a rotor therefore generally reduces the thrust-to-torque ratio compared to its performance in open air (if the blade geometry and pitch is the same for the open air and ducted case). Effectively this means that more power is required to generate a certain amount of rotor thrust, indicating that the rotor itself operates at a lower figure of merit FM_r (lower efficiency) due to the presence of a duct. The effect that the performance of a rotor decreases in a duct due to the increased axial velocity, is also observed and explained in the experimental study of Pereira (p. 154 of [26]).

It should be noted that all statements above regarding the performance decrease of rotors in a duct only refer to the performance of the rotor itself. Together with the thrust that is generated by the duct, a ducted rotor assembly can be more efficient than an open rotor after all [26], [23]. This is explained in more detail in section 2.4.

Clearly, because a different air inflow profile causes the inflow angle ϕ to change for each blade element, the pitch distribution of the rotor blade needs to be changed accordingly to ensure that each blade element operates at the right angle of attack α that is optimum for performance. Therefore, a rotor that is optimized to be in a duct will have a much more aggressive blade pitch than a rotor that is optimized for open air.

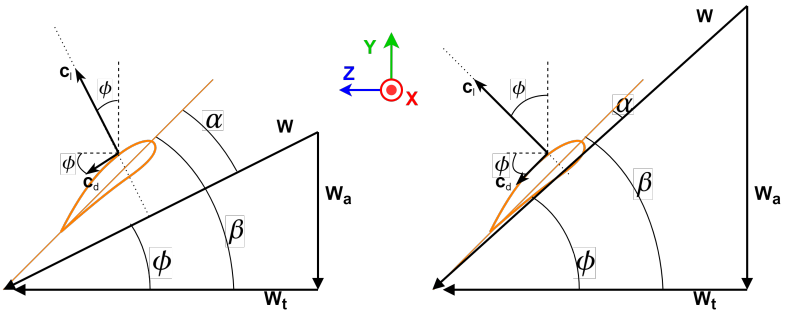

Figure 2.6: Velocity diagram: comparison of a case with lower axial velocity W_a (left), and higher axial velocity W_a (right)

Effect 2: reduced tip losses

The presence of a duct also affects the formation of vortices at the rotor blade tips [7], [26], [32]. The easiest way to explain this is that the duct acts as a physical boundary that prevents the air rolling up from the high pressure to low pressure at the blade tip. This has a beneficial effect on the performance of the rotor, because the tip vortices are a cause of significant efficiency losses for rotors in open air.

The extent to which the duct wall can prevent the formation of tip vortices largely depends on the distance between the blade tip and the duct wall, thus the tip gap δ_{tip}.

2.4. The duct as thrust device

For ducted rotors, the rotor is not the only device that generates thrust. In the studies of Pereira [26] and Martin [23], around 40% of the total amount of thrust is generated by the duct. Clearly, the portion of thrust that is generated by the duct and rotor depends on the shape and size of the duct.
The thrust generating mechanism of a duct is similar to the way an airfoil generates lift. If there is a velocity distribution over the duct, there is a pressure distribution as well. A properly designed duct has a shape such that this pressure distribution causes a net force in the thrust direction. All the thrust of the duct is generated by the inlet lip. Namely, this is the only place where the vectors normal to the duct wall point upwards. A low pressure zone is present here because the air is accelerated around the inlet lip into the rotor. The low pressure causes the duct to be 'sucked' upwards, effectively contributing to the total thrust.
The inlet lip of a duct is in literature often referred to as the duct leading edge, because it has the same function and characteristics as a standard airfoil leading edge; the stagnation point of the incoming flow is located somewhere on this leading edge. Here, the velocity is near zero as all dynamic pressure is converted in static pressure. After the stagnation point, the air accelerates over the thickest part of the airfoil (or over the inlet lip in case of a duct), which is accompanied with a very low pressure zone.

Figure 2.7 shows an example of a pressure distribution over the wall of the duct. The distribution shown here was measured experimentally by Pereira [26]. The low pressure at the inlet lip can clearly be observed here. According to Pereira, the inner half of the inlet lip is responsible of roughly 80 % of the thrust, and the outer half of the inlet lip for 20 % of the thrust.

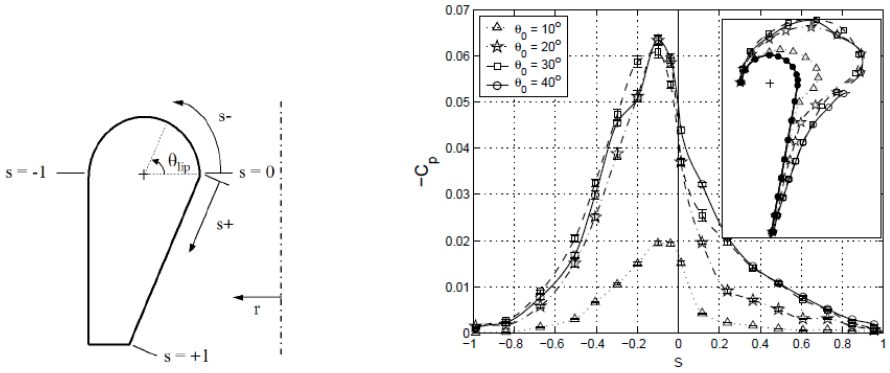

Figure 2.7: Pressure distribution over the wall of a duct, measured experimentally (source: [26])

Even though the low pressure at the inlet lip of the duct physically accounts for all the thrust generated by the duct, the diffuser is also of great importance:
For any conventional open rotor, the air is accelerated upon passing the rotor plane. According to the ideal actuator disc - momentum theory , the velocity of the far wake is twice the induced velocity at the rotor plane [20]. This velocity increase of the far wake causes a contraction of the wake, because of the conservation of mass (see figure 2.8 (a)); If the velocity of the far wake is doubled, this means that the cross-section area of the far wake is halved. With this velocity increase, the far wake contains more kinetic energy, which also means that this effect is accompanied with a power loss.
For ducted rotors on the contrary, the cross-section area of the wake is dictated by the shape of the diffuser (if the flow stays attached to the diffuser walls). In this case, the wake after the rotor plane does not contract but expand (see figure 2.8 (b)). This means that the velocity increase of the far wake is reduced, which also reduces the corresponding power loss (p.16 of [26]).
The flow expansion inside the diffuser is accompanied with a pressure increase from the rotor plane to the duct exit plane. In the ideal case, the duct exit pressure is exactly the same as the ambient pressure. Along the entire wall of the diffuser, an adverse pressure gradient is present (as shown in figure 5.8). This is because starting from the low pressure peak at the inlet lip, the pressure has to increase towards the ambient pressure of the exit plane. Due to this adverse pressure gradient, there is a risk of separation along the duct wall. This has to be taken into account when deciding upon the diffuser angle of the duct (see figure 2.4); a too high diffuser angle may cause the flow to separate, which means that the diffuser cannot effectively expand the

flow anymore.
Whereas the duct inlet lip is analagous to the leading edge of an airfoil, the duct diffuser represents the rear end of an airfoil (from the point of maximum thickness to the trailing edge). The low pressure peaks at the thickest point of the airfoil (for a duct this is the throat), after which it goes back to the ambient pressure in some way. This is called the pressure recovery, and takes place over the trailing edge of the airfoil (or inside a diffuser in case of a duct). A significant difference between the pressure recovery of a standard airfoil trailing edge and a duct diffuser, is that for a duct the air passes through a rotor plane, after which the pressure already significantly increases.

To ensure that the expansion inside the diffuser is just right, the diffuser ratio σ_d is critical. As defined in equation 2.2, this is the ratio between the duct exit area and the duct throat area. Looking at figure 2.4 and table 2.1, it can be seen that the duct length and diffuser angle are the design parameters that determine the diffuser ratio.

$$\sigma_d = \frac{\text{Duct exit area}[m^2]}{\text{Duct throat area}[m^2]} \tag{2.2}$$

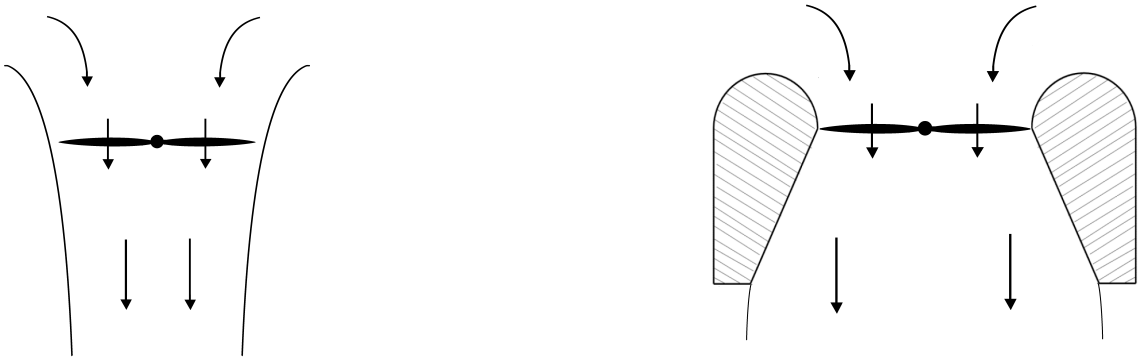

(a) Open rotor flow-field

(b) Shrouded rotor flow-field

Figure 2.8: Schematic representation of flow-fields of open and shrouded rotors. (Source: [26])

Designing an optimal duct quickly becomes a multi-parameter optimization study. That is, aside from the favorable thrust effect, a duct also adds weight and friction drag, particularly when the duct exhibits an excessively long diffuser section. The current research effort is not focused on the optimization of a duct design, but rather on how the aerodynamic performance of an existing duct design is linked to the tip gap.

3

State of the art: effect of the tip gap

As motivated in section 1.2, the current study focuses on the effect of the tip gap on the aerodynamic performance of ducted rotors. In this chapter, a literature review is presented of the studies that (partially) investigated this topic. In section 3.1, it is highlighted what the relation is between the tip gap and the aerodynamic efficiency of a ducted rotor system. Finally, in section 3.2 it is summarized what knowledge is available about the physical flow mechanisms that are associated to the tip gap and the interaction between the rotor and the duct wall.

3.1. Effect of the tip gap on aerodynamic efficiency

The tip gap δ_{tip} is defined as the size of the gap between the tip of the rotor blade and the wall of the duct (see figure 2.4). In literature [26] it is mostly defined in non-dimensional form by dividing by the duct throat diameter D_d. This gives the tip gap ratio δ^*_{tip} (see equation 3.1).

$$\delta^*_{\text{tip}} = \frac{\delta_{tip}}{D_d} \cdot 100 \tag{3.1}$$

A straight forward question is how much the tip gap ratio affects the aerodynamic efficiency of a ducted rotor in hover. This question by itself is relatively easy to investigate, because it can be measured directly and does not require any explanations that go into the underlying cause.
The most common way to express the 'aerodynamic efficiency' of rotors, is the figure of merit FM [23] [26]. This is a non-dimensional number, that is a function of the power coefficient C_P and the thrust coefficient C_T. Earlier in section 2.1, these performance coefficients were defined for rotors in open air (see equation set 2.1 on page 6). For ducted rotors the definitions of these coefficients are slightly different, because now the duct thrust is included in the equations (see equation set 3.2 below).

$$v_{tip} = \Omega \cdot \frac{2\pi}{60} \cdot R_r \tag{3.2a}$$

$$T_{tot} = T_r + T_d \tag{3.2b}$$

$$P = \Omega \cdot \frac{2\pi}{60} \cdot Q \tag{3.2c}$$

$$C_P = \frac{P}{\rho A v_{tip}^3} \tag{3.2d}$$

$$C_T = \frac{T_{tot}}{\rho A v_{tip}^2} \tag{3.2e}$$

$$FM = \frac{\text{ideal power}}{\text{actual power}} = \frac{C_T^{1.5}}{\sqrt{2}C_P} \tag{3.2f}$$

Equation set 3.2 shows that if the rotor torque Q, the rotational speed Ω and the total thrust of the ducted rotor T_{tot} (including duct thrust) can be measured, the figure of merit FM can be calculated.

In several published papers, the effect of the tip gap ratio on the figure of merit is experimentally measured.

In 2004, Martin and Tung [23] experimentally investigated the effect of the tip on the aerodynamic performance of a 10 inch ducted rotor in hover. The thrust coefficient, power coefficient (and with that the figure of merit) were measured for a range of rotational speeds with different tip gap ratio's and various duct shapes. They found that the tip gap ratio has a very significant effect on the the hover efficiency of the ducted rotor. As can be seen in figure 3.1, the FM drastically decreases with an increasing tip gap ratio. Interestingly, the curve is steepest when the tip gap ratio approaches zero.
Besides, they also found that the higher the rotational speed and the smaller the tip gap ratio, the higher the proportion of the total thrust that is generated by the duct (and not the rotor). At the smallest tip gap ratio, the duct generated 38% of the total thrust.
A small remark on the work Martin et al [23], is that their statements about the proportion of thrust generated by the duct are not completely correct. Namely they compare the total thrust of a ducted rotor, to the thrust of the rotor in open air. This means that they assume that at a certain rotaional speed, the rotor itself produces the same amount of thrust whether the duct is placed around it or not. However, as explained in section 2.3, the performance of the rotor its self is also affected by the presence of the duct.

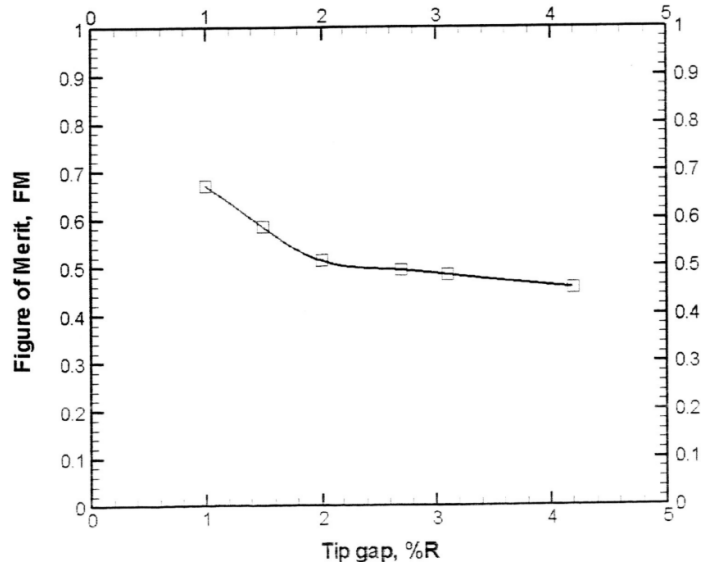

(a)

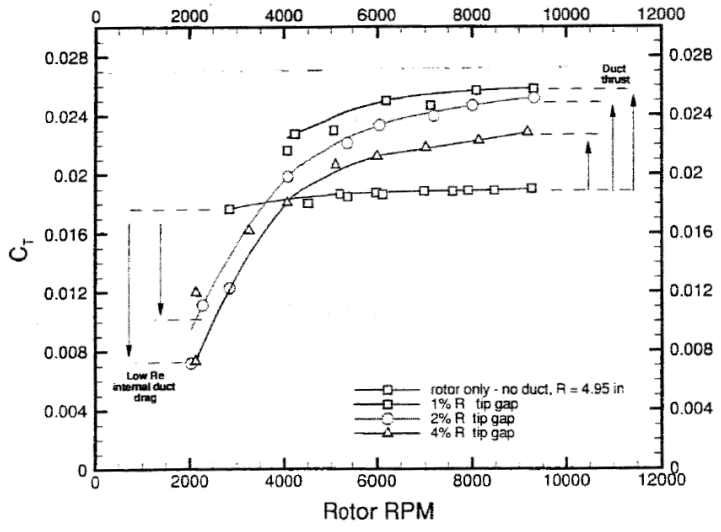

(b)

Figure 3.1: Effect of tip gap ratio on the figure of merit FM (a) and the thrust coefficient C_T (b). (Source: [23])

In 2008, Pereira did an extensive research into the affect of several ducted rotor shape parameters (see table 2.1 of section 2.4) on the aerodynamic performance. One of these parameters was the tip gap ratio, and its effect on the figure of merit. Because Pereira investigated not only one ducted rotor, but different combinations of duct and rotor geometries, his conclusions give a better insight on the effect in general.
In figure 3.2, his results of the effect of the tip gap ratio on the figure of merit are summarized. The four graphs in this figure represent four different duct geometries, and on the x-axis the tip gap ratio is varied. For each duct geometry and tip gap ratio, the experiment is repeated four times with a complete sweep of the rotational speed Ω for four different rotors. Each time, the rotor and Ω combination that results in the maximum FM is selected. That means that each data point in figure 3.2, represents the highest figure of merit that could be found for a specific rotor-duct configuration. The term on the y-axis expresses the maximum FM that could be found for the ducted rotor, normalized (divided) by the highest FM that was found for all open rotor experiments.
It can be seen that for all duct geometries, a higher FM could be found for a smaller tip gap ratio. The top graph is an exception, but Pereira [26] explains in his paper that this deviating graph is caused by an incomplete set of experiments, and therefore should be considered an outlier. Overall, the results of Pereira clearly show that a smaller tip gap ratio always leads to a more efficient ducted rotor. Similarly to the results of Martin [23] in figure 3.1, the curve becomes steeper if the tip gap ratio approaches to zero. This highlights the importance (from an efficiency point of view) to minimize the tip gap ratio as much as possible for ducted rotors in hover.

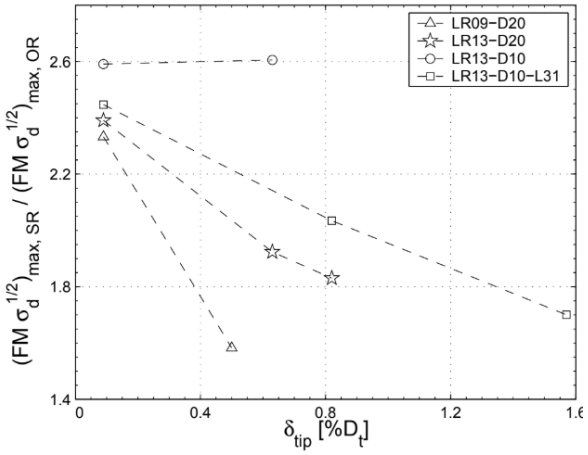

Figure 3.2: Effect of the tip gap ratio on the figure of merit (source: [26])

3.2. Rotor-duct aerodynamic interactions

In subsection 3.2.1 to 3.2.4, four aerodynamic effects are highlighted that are related to the tip gap and the interaction between the rotor and the duct wall.

3.2.1. Increased suction at the duct inlet lip

In section 2.4, it was explained that the duct itself can generate significant amounts of thrust. Figure 2.7 of Pereira [26] showed that the suction (low pressure) at the duct inlet lip is the cause of this thrust component. In the same study, Pereira also experimentally investigated how this suction on the duct inlet lip is affected by the tip gap ratio. In figure 3.3, the pressure distribution over the duct wall is shown for three different tip gap ratios and four different rotors (with varying blade pitch θ_0). Also the thrust coefficient is plotted for the complete duct and separately for the inlet lip and diffuser part of the duct.

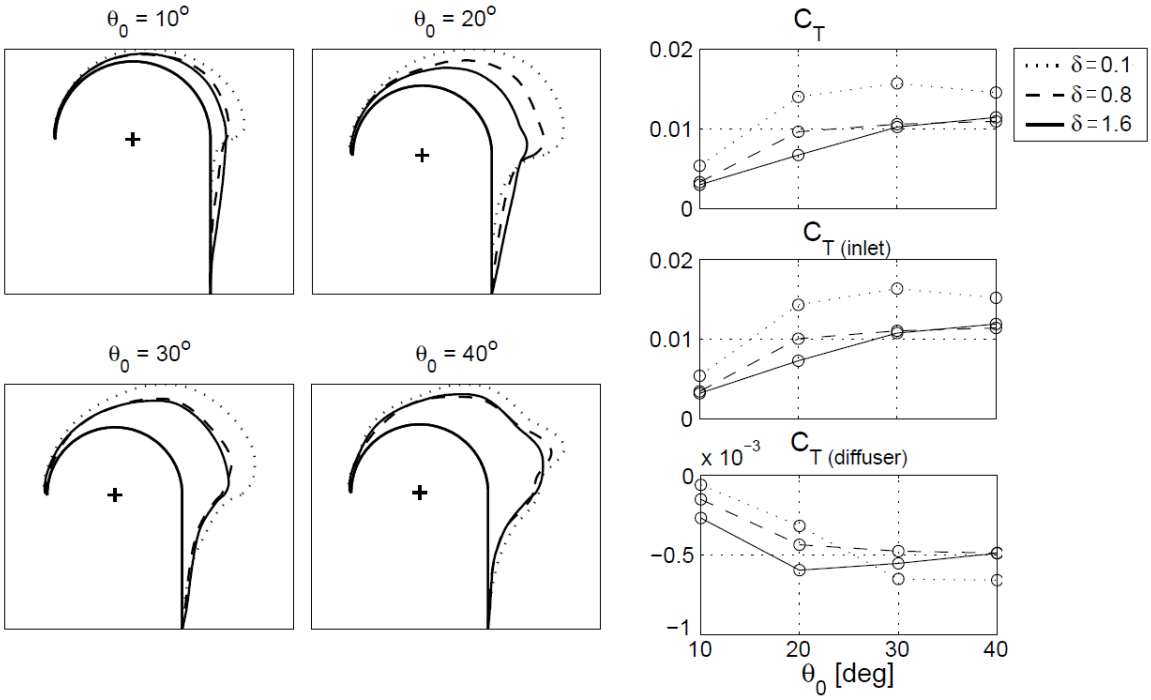

Figure 3.3: Effect of the tip gap ratio on the suction (low pressure) at the duct inlet lip, for rotors with a different collective blade pitch θ_0 (source: [26])

From figure 3.3 it becomes evident that a smaller tip gap causes the suction at the duct inlet lip to increase. This is in line with the findings of section 3.1, where it was said that a smaller tip gap ratio increases the proportion of the total thrust that it is generated by the duct. This means that a higher degree of rotor-duct interaction has a positive effect on the performance of the duct.
Furthermore, Pereira also notices that for some configurations, two distinct suction peaks can be observed on the duct inlet lip, especially for rotor with high blade pitch (θ_0=40%): one somewhere on the middle of the inlet lip, and one very close to the rotor. For rotors with a low pitch, and also for configurations with a high tip gap ratio, these two suction peaks merge into one large suction zone.
Pereira mentions that with his results, the presence of this secondary pressure peak is demonstrated experimentally. In an earlier CFD study of Keys [18], the secondary pressure peak was already predicted (see figure 3.4). Both Pereira and Keys attribute this localized low pressure zone the formation of a blade tip vortex. Pereira hypothesizes that for rotors with higher blade pitch the tip vortex is stronger, which causes the secondary suction peak to be more visible in the static pressure measurements on the wall of the duct.

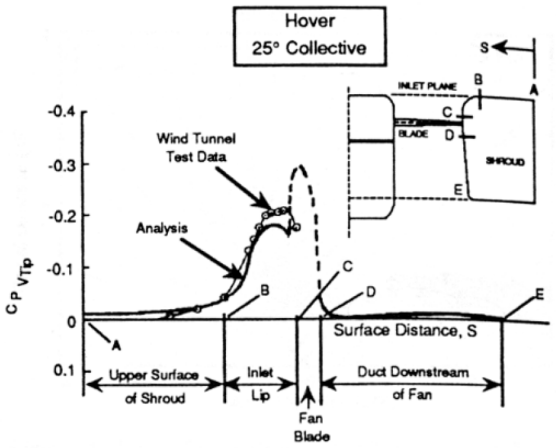

Figure 3.4: CFD prediction of secondary suction peak on the inlet lip of a cuted rotor (source: [18])

3.2.2. Reversed flow below the rotor plane

A second aerodynamic effect that is directly related to the interaction between the rotor tip vortex and duct boundary layer, is the presence of a separation zone at the duct inlet lip just downstream of the rotor plane. This phenomenon is described in two different papers:

In the paper of Martin and Tung [23], it is mentioned that the flow along the wall of the duct immediately separates upon passing the plane of the rotor. As shown in figure 3.5, a zone of zero skin friction is observed at the rotor plane during an oil visualization test. It is argued that this separation occurs due to the 'complex interaction between rotor, tip vortex and duct boundary layer' [23].

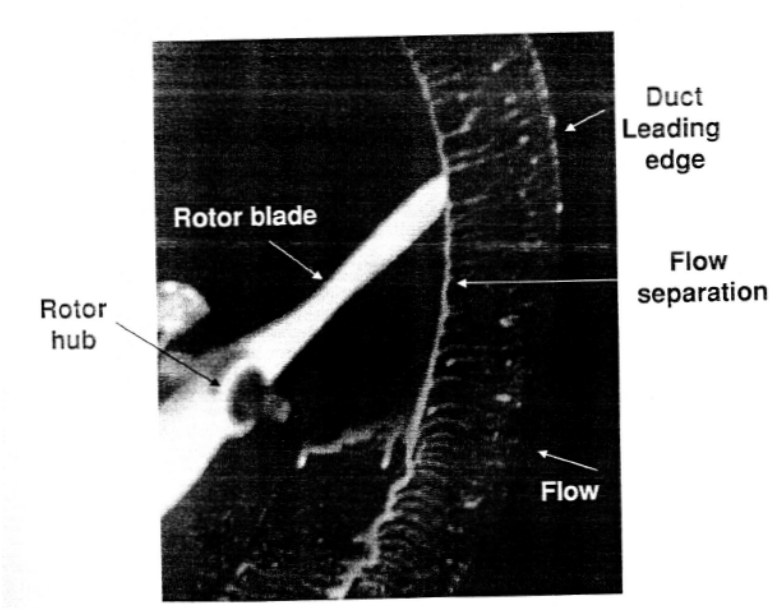

Figure 3.5: Oil visualization on the inlet lip of a ducted rotor (source: [23])

In 2020, Bento et al. [7] published a paper which possibly explains the observed flow separation on the duct wall at the rotor plane by Martin and Tung[23]. In this paper, rans CFD simulations were used to investigate the tip losses for square and circular ducts. Clearly for now, only the circular ducts are of interest.
In figure 3.6, the CFD results of Bento et al. are shown. The plots show the distribution of the pressure coefficient, friction coefficient and vorticity coefficient on the wall of the duct, zoomed in at the location where the rotor-duct interaction takes place. The upper pictures show the uninstalled case (without rotor), and the lower pictures show the installed case (with rotor). The C_p distribution clearly shows that for the installed case, there is a much lower pressure at the inlet lip of the duct. Close to the rotor tip, a strong adverse pressure gradient from low to high pressure can be seen. Also, a strip of low pressure is trailing from the blade tip. The friction coefficient shows that at this strip, a negative skin friction is present in axial direction, indicating flow reversal. The vorticity coefficient plot (f) shows the presence of a tip vortex along the same strip, indicating that the flow reversal takes place due to the interaction of the tip vortex and the duct boundary layer.

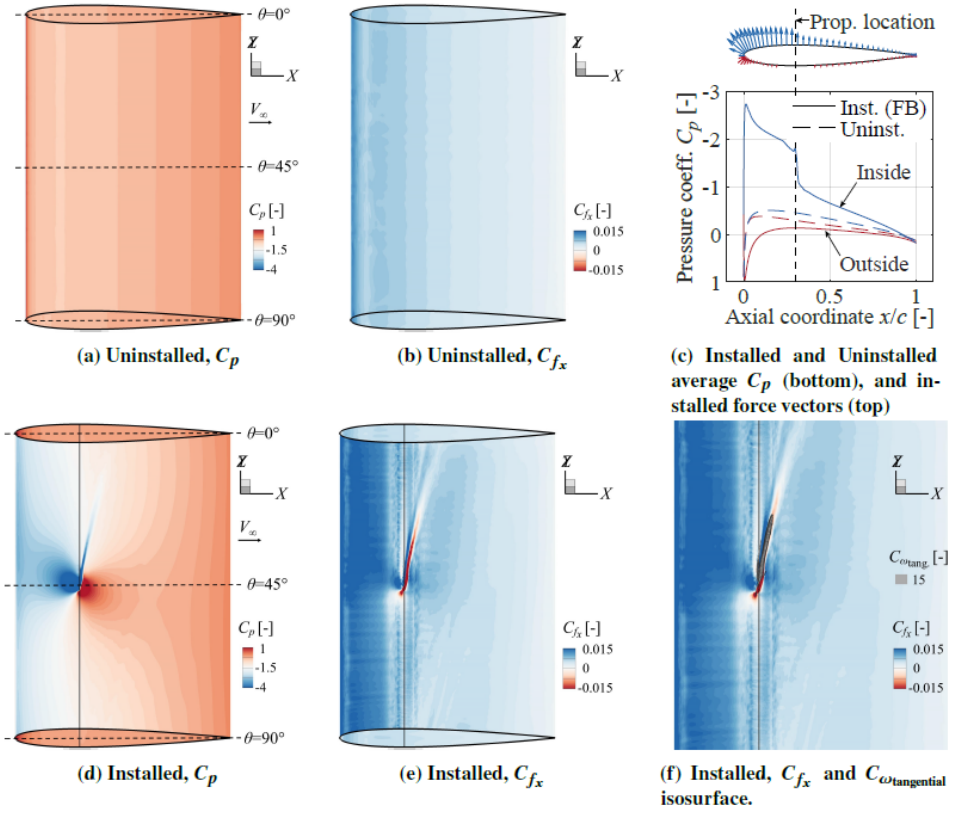

(a) Uninstalled, C_p (b) Uninstalled, C_{f_x} (c) Installed and Uninstalled average C_p (bottom), and installed force vectors (top)

(d) Installed, C_p (e) Installed, C_{f_x} (f) Installed, C_{f_x} and $C_{\omega_{\text{tangential}}}$ isosurface.

Figure 3.6: CFD simulation: comparison of the pressure coefficient C_p and friction coefficient C_{fx} distribution on the duct wall with (installed) and without rotor (installed vs uninstalled). (source: [7])

The separation zone indicated by Bento et al. is probably the same effect that was observed by Martin and Tung with the oil visualization test. The plots of Bento et al. however also show that this separation zone is very small; the strip of negative skin friction is very thin, and only trails up to roughly 45° away from the rotor tip. So whereas the paper of Martin and Tung [23] suggests that a detrimental separation of the flow along the duct wall may occur at the rotor plane, the paper of Bento et al. [7] suggests that the separation zone is very small and should not have a significant effect on the performance. Clearly the results of these papers cannot be compared one to one, because they investigate a different ducted rotor at different operating conditions. What they however agree on, is the presence of a reversed flow zone, which is caused by the interaction between the tip vortex and the duct boundary layer. In figure 3.7 this interaction effect is illustrated in more detail.

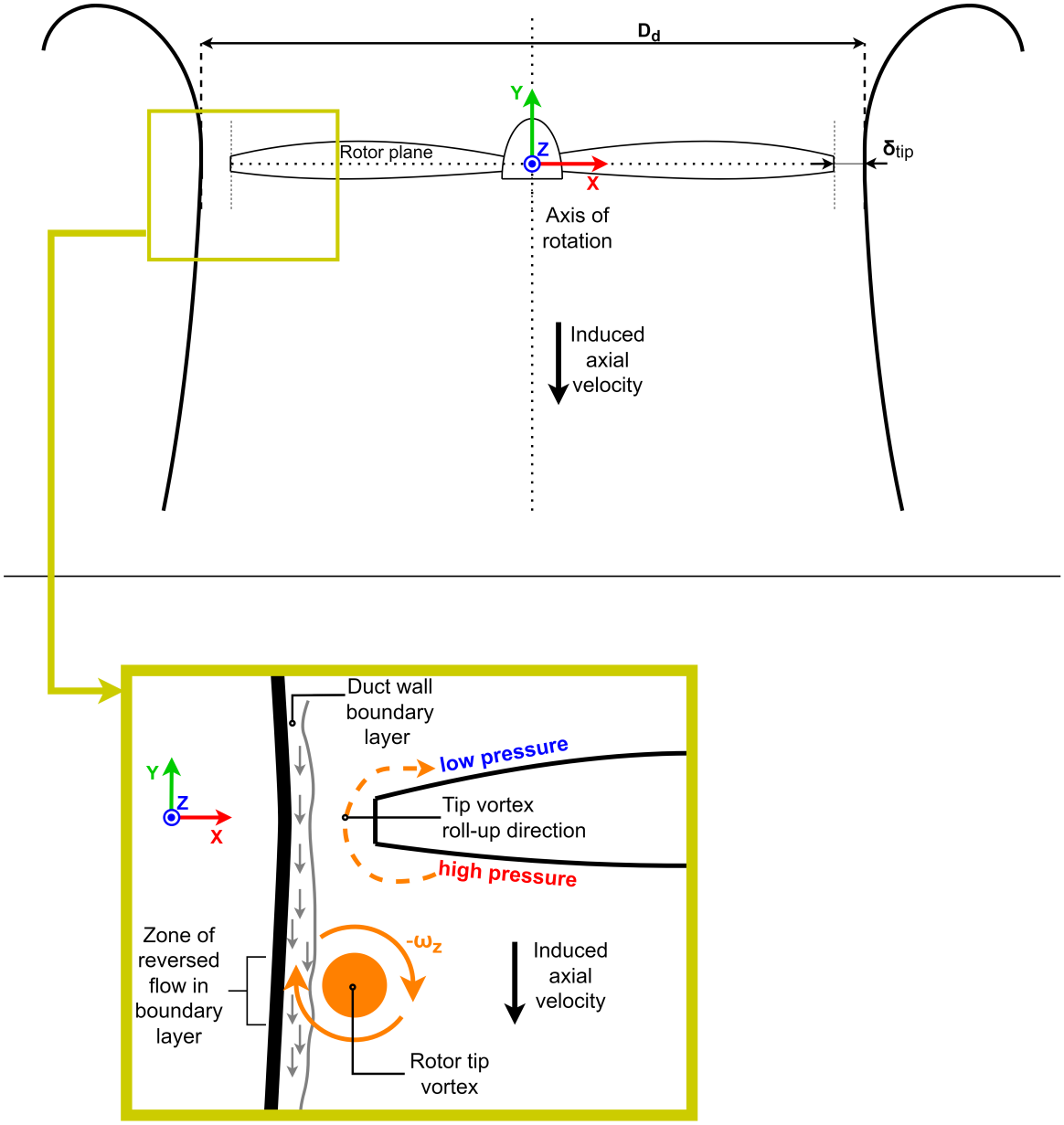

Figure 3.7: Illustration of the interaction between the rotor tip vortex and duct boundary layer for a ducted rotor configuration

3.2.3. Breakdown of the rotor tip vortices

An often mentioned favourable effect of the duct on the rotor, is the reduction of losses associated to the rotor tip vortices. The initial strength and breakdown age of the rotor tip vortices are affected by the close proximity of the duct wall to the blade tip. This is highlighted in the following two papers:

In 2019, Shukla and Komerath [32] investigated the effect of the rotor-duct interaction on the strength and trajectory of the rotor tip vortex, with PIV (particle image velocimetry) experiments. As shown in figure 3.8, an annular ring was placed around a rotor instead of a complete duct. This simplification allowed for an ease in optical access to the area downstream of the rotor.

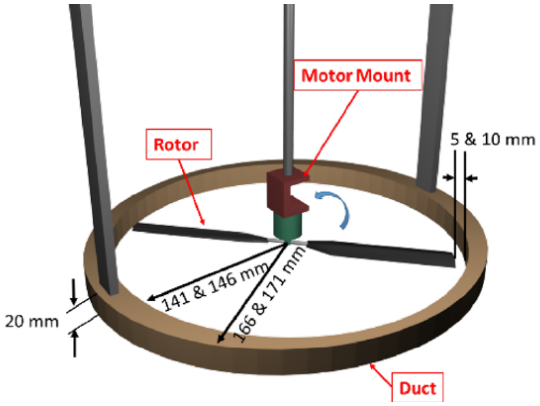

Figure 3.8: Experimental setup of a rotor with an annular ring, to study the rotor duct interaction [32]

In figure 3.9, the PIV results of the experiments are shown. The plots show the instantaneous vorticity contours, for the case with and without duct. When comparing these two cases, a clear difference in the shape and integrity of the vortices can be seen when assessing the strength of out of plane vorticity ω_z. For the case with duct, the vortices start breaking down into a chaotic wake within 180° of the wake age. For the case without duct, all tip vortices remain intact for at least 540°. Shukla and Komerath note that the closer the annular ring is placed to the rotor tip, the more the vortex core interacts with this wall, which causes the tip vortices to lose their coherent structure. Interestingly, the duct also reduces the wake contraction, even though the duct is just an annular ring and has no diffuser. Furthermore, they also measured an improvement of the figure of merit that correlates to the extent of vortex core - duct interaction.
Clearly, the conclusions of Shukla and Komerath are not fully representative for the dynamics of a vortex inside a duct that has a diffuser, like most ducted rotors do. Whereas in the setup of Shukla and Komerath the vortex - duct interaction just takes place at the blade tip, for 'complete' ducts this interaction will occur along the entire length of the duct diffuser wall (and its boundary layer). Nonetheless the results of Shukla and Komerath are interesting, because they indicate that when the tip gap is decreased, it is more likely that the vortices inside the duct will break down sooner into a chaotic structure.

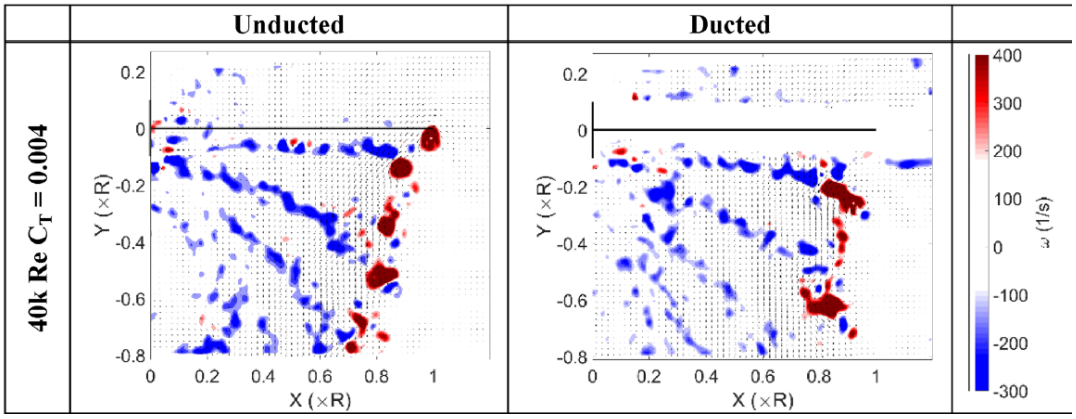

Figure 3.9: PIV experiments: instantaneous vorticity contour plots for the case with and without annular ring, at a Reynolds number of 40k. (source: [32])

The effect of the rotor-duct interaction on the breakdown age of the tip vortex is also highlighted in the study of Avallone et al. [5]. In this study, Lattice-Boltzmann LES simulations were performed for a ducted wind turbine with two different tip gaps. Even though the wind turbine case is exactly the opposite of the rotor case – in the sense that the axial momentum is now *extracted* from the mean flow – there still can be similarities between the two cases. For example how the tip vortex interacts with the boundary layer of the diffuser. It is however important to be aware of the major differences between a wind turbine and rotor propulsion case, such as the rotation direction of the rotor tip vortices (opposite ω_z).

Similarly to the experimental results of Shukla and Komerath, the results of Avallone et al. show that decreasing the tip gap causes a faster breakdown of the rotor tip vortex. As shown in figure 3.10 for the large tip gap (left) the vortices trailing from the blade tips are convected along the diffuser wall, and start breaking down at the very end of the duct. The smaller tip gap case (right) shows a completely different vortex dynamics, where the breakdown starts right behind the rotor plane. This can also be seen in figure 3.11, where for the larger tip gap the vortex cores can be seen until the end of the duct diffuser, and for the smaller tip gap only one vortex core right after the rotor can be seen.

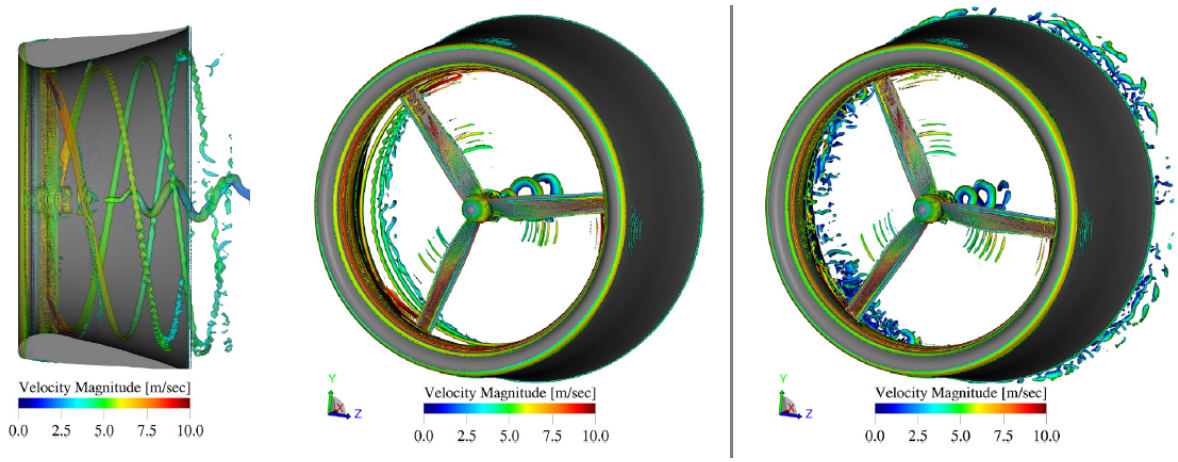

Figure 3.10: LBM-LES simulation: Instantaneous flow field of a ducted wind turbine with a 0.025 tip gap ratio (left) and 0.007 tip gap ratio (right). The vortices (λ_2 iso-surfaces) are plotted and color contoured with the velocity magnitude. (source: [5])

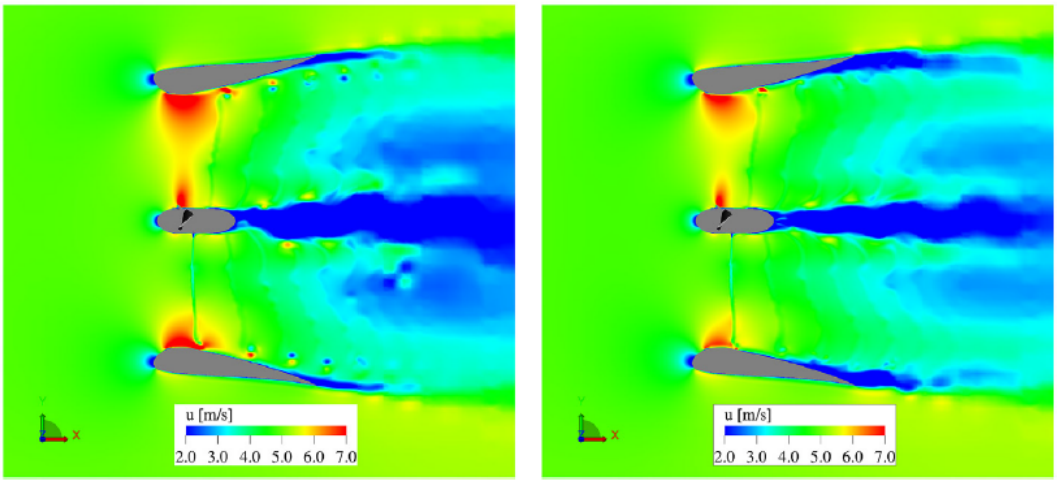

Figure 3.11: LBM-LES simulation: Instantaneous streamwise velocity in the center plane of a ducted wind turbine with a 0.025 tip gap ratio (left) and 0.007 tip gap ratio (right). (source: [5])

3.2.4. Blockage effect due to tip leakage

The interaction between the rotor tip vortex and duct wall is related to a local blockage effect. The size of the tip gap determines to what extend this effect is present.

Akturk and Camci [4] investigated the effect of the tip gap on a 559mm diameter ducted rotor. In their study they highlight the effect of the tip leakage flow on the performance of the system. The tip leakage flow refers to the mass flow rate of the air passing through the gap between the rotor tip and duct wall [4], and is a topic that has been investigated often for the application of axial flow fans and compressors [24] [34] [19]. The tip leakage increases with a larger tip gap, which goes accompanied by a stronger rotor tip vortex. The vortex rolls up from the pressure side to the suction side of the blade, in opposite direction of the axial flow inside the duct. This then induces a blockage effect.

In the CFD results of Akturk and Camci [4], the leakage flow is indicated by a zone of low total pressure close to the duct wall. As shown in figure 3.12, this leakage zone becomes more pronounce with a larger tip gap. Figure 3.13 shows how the velocity distribution downstream of the rotor is affected: near the duct wall the velocity the velocity is significantly lower for the case with larger tip gap. The rotor hub region is not affected.

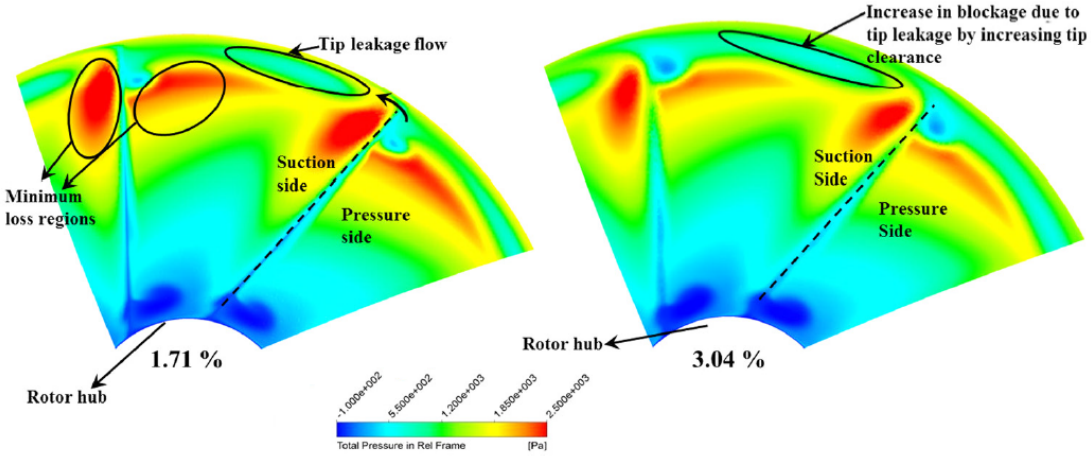

Figure 3.12: Results CFD simulations: Comparison of the relative total pressure at the rotor exit plane (source: [4])

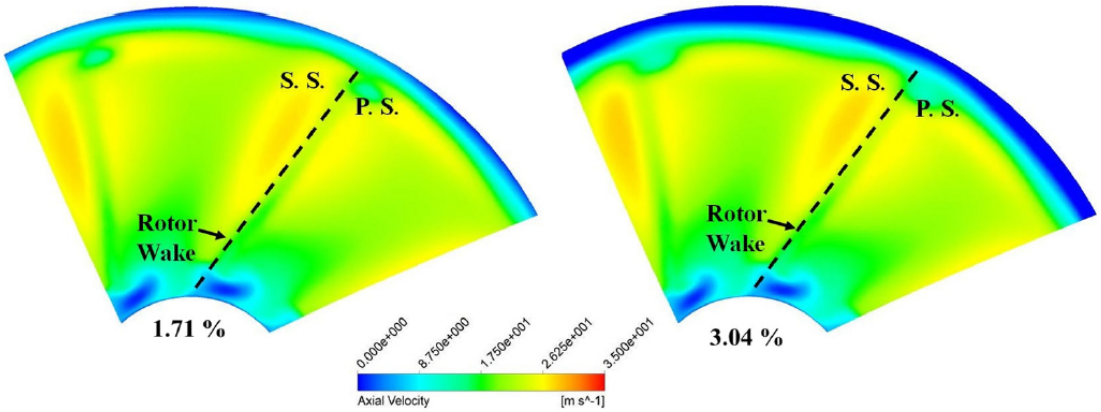

Figure 3.13: Results CFD simulations: Comparison of the axial velocity at the rotor exit plane (source: [4])

The blockage effect due to tip leakage is very closely related to the reversed flow zone that was highlighted earlier in section 3.2.2. Both effects are based on the fact that the rotor tip vortex rolls up in opposite direction of axial velocity inside the duct (illustrated in figure 3.7). The injection of momentum opposite to the boundary layer velocity causes the zone of reversed flow that was observed in the studies of Martin and Tung [23] and Bento [7]. The blockage effect highlighted in the study of Akturk and Camci [4] seems to be a wider interpretation of the same physical effect.

Interestingly, exactly the opposite happens in the study of Avallone et al. [5] on ducted windturbines (see section 3.2.3). This is because for windturbines the pressure and suction sides of the blade are swapped compared to rotors, meaning that the roll-up of the tip vortices is now aligned with the free stream velocity. Therefore, Avallone et al. observed an injection of momentum into the boundary layer, which becomes stronger for a larger tip gap [5]. This improved the performance of the larger tip gap case, because it helps to delay the flow separation in the diffuser from 70% to 90% (as can be seen figure 3.11).

4

Methodology

In the current research, three types of experiments are performed to investigate the aerodynamic performance of the ducted rotor: The performance of the ducted rotor system is characterized through force measurements with load-cells, the pressure distribution over the duct profile is measured with static-pressure tabs in the duct inner-wall, and the flow field inside the duct is retrieved and analyzed using PIV- (particle image velocimetry) measurements. Additionaly, a fourth experiment is performed where the far field noise radiated by the ducted rotor is measured in an anechoic chamber, for a preliminary investigation into the aeroacoustic performance of the system. Section 4.1 describes the design of the ducted rotor assembly that is used for all the experiments. In subsections 4.2-4.5, the purpose and method of each experiment is explained in more detail. Finally, in section 4.6 an oversight is given of the operating conditions at which the experiments are performed.

4.1. Ducted rotor system

The ducted rotor system is provided by Flyability [13], a company that develops MAV drones for indoor inspection. In the pursuit of more efficient propulsion devices, they developed a 5-inch ducted rotor for a quad-copter in hover flight. Both the duct and rotor geometry were optimized to minimize the mechanical power for a certain amount of thrust. For the current study it is a great opportunity to investigate the system provided, as no ducted rotors for hover flight of this scale are commercially available.

In figure 4.1 the design of the duct is shown. Looking at the duct crosssection, the duct consists of four sections: The outer part of the inlet lip (section A) is a quarter circle, and the inner part of the inlet lip (section B) is a quarter ellipse. A straight line (section C) is present at the height of the rotor, such that the tip gap is constant along the complete chord of the rotor tip. The diffuser (section D) consists of a spline tangent to the line above, with an average diffuser angle of 8°. The duct is 3d-printed with a SLS printer (0.1mm precision), and sanded/waxed to smoothen the inner surface.

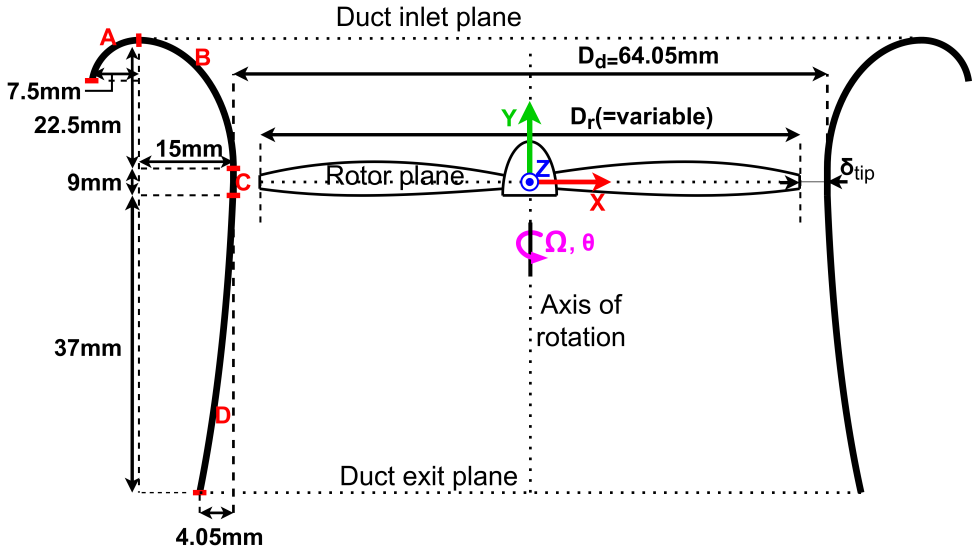

Figure 4.1: Schematic image of the duct design, and the reference system. Rotor phase θ is at 0° in the displayed position (in the X-Y plane)

The geometry of the 2-bladed rotor is optimized to be in a duct. Compared to commercially available standard rotors for open air, it has a much more aggressive blade pitch. The adapted pitch distribution ensures that the blade operates at roughly the right angle of attack along its complete span. This is crucial for current study, because the vortex dynamics of the rotor can only be properly investigated if the rotor blade sections operate at the right angle. Furthermore, the chord of the blade (20mm) remains constant towards the tip, contrary to rotors that are optimized for open air (for rotors in open air the blade chord generally washes out towards the tip to reduce the losses related to the tip vortices). The material of the rotor is injection molded plastic.

4.2. Performance characterization

The objective of the performance characterization is to measure the forces on the duct and rotor, and determine the coefficients that characterize the performance of the ducted rotor system. The parameters that are used for this characterization are the thrust coefficient C_T, power coefficient C_P and figure of merit FM. These performance coefficients were defined earlier in section 3.1 (see equation set 3.2 on page 13). The figure of merit is equal to the mechanical power of an ideal actuator disc (without losses), divided by the actual mechanical power of the rotor at a certain level of thrust [26]. Therefore it can be used to express the aerodynamic efficiency of the rotor.

In the equations of the performance coefficients (equation set 3.2 on page 13), the rotor disc area A appears in the denominator of the thrust coefficient C_T and power coefficient C_P. For all the calculations in this study the duct throat area ($\frac{D_d^2}{4\pi}$) is used for A, instead of accounting for slightly different rotor areas for different tip gaps. This method allows for an easier comparison of the performance for different configurations, and is consistent with the methodology of other studies [23] [26].

The performance coefficients (C_T, C_P and FM) depend on three variables: The rotor tip speed v_{tip}, the mechanical power on the rotor P, and the total thrust of the ducted rotor system T_{tot}. In order to derive these variables, the rotational speed of the rotor Ω, the torque of the rotor Q, the thrust of the rotor T_r and the thrust of the duct T_d need to be measured (see equations 3.2a-3.2c on page 13). In figure 4.2 it is illustrated what setup is used to measure these parameters. By measuring the thrust of the rotor and duct separately (instead of only measuring the total combined thrust T_{tot}), their contribution to the total performance can be distinguished.

As shown in figure 4.2, the ducted rotor system is mounted upside down, such that the thrust is generated downwards and the air is accelerated upwards. The motor is mounted on a stacked Futek LSB200 cell and RTS-25 cell, to respectively measure the thrust T_r and torque Q on the rotor. Two ME KD45 load cells are used to measure the thrust on the duct T_d. The rotational speed Ω is measured with an optical encoder. For each measurement, the signals of the load cells and optical encoder are acquired with a frequency of 25.6 kHz for 10 seconds at constant Ω, after which the time-averaged values are determined.

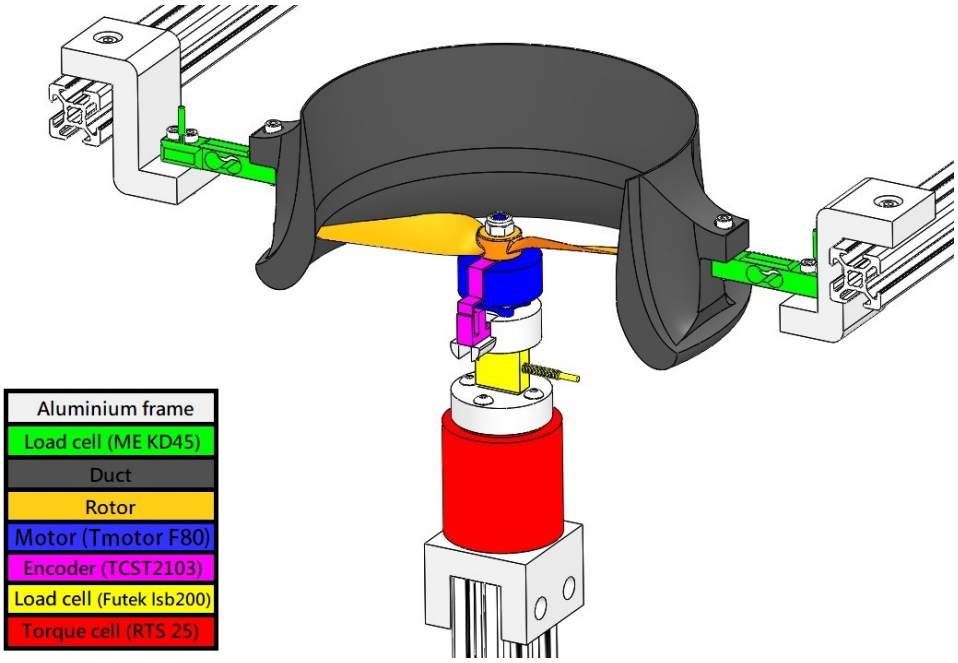

Figure 4.2: Experimental setup for the performance experiments

All the components of the experimental setup are mounted in a aluminium frame box (see figure 4.3). This frame is used for all experiments (performance, static-pressure, PIV and acoustic), and allows to easily move the complete setup to different test locations.

(a) (b)

Figure 4.3: Photos of the experimental setup for the performance experiments

4.3. Static-pressure measurements

The objective of the static-pressure measurements is to obtain the pressure distribution over the duct inner-surface. The results are used to determine which areas of the duct effectively contribute to the generated thrust, and how this changes for different tip gaps. The integrated pressure over the duct should be consistent with the duct thrust as measured in during the load-cell experiments. Furthermore, it is possible to derive certain characteristics of the duct diffuser boundary layer from these pressure profiles.

The static pressure is measured at 24 different axial locations in the duct. At each location, a 3d-printed insert is placed which has a 0.2mm thru hole. The inner surface of the duct is sanded smooth with these inserts. As shown in figure 4.4, the holes are positioned on two diagonal lines. The diagonal spacing allows a finer spacing in the y-direction. The inserts are connected with 1.5mm tubing to a pressure transducer box (2000 Pa range) that measures the pressure of each hole relative to the atmospheric pressure . Each measurement is performed for 30 seconds at constant Ω, after which the average pressure is determined for each channel. The results are presented as the static pressure coefficient, as defined in equation 4.1.

$$C_{p,stat} = \frac{p_{stat} - p_{atm}}{\frac{1}{2}\rho v_{tip}^2} \tag{4.1}$$

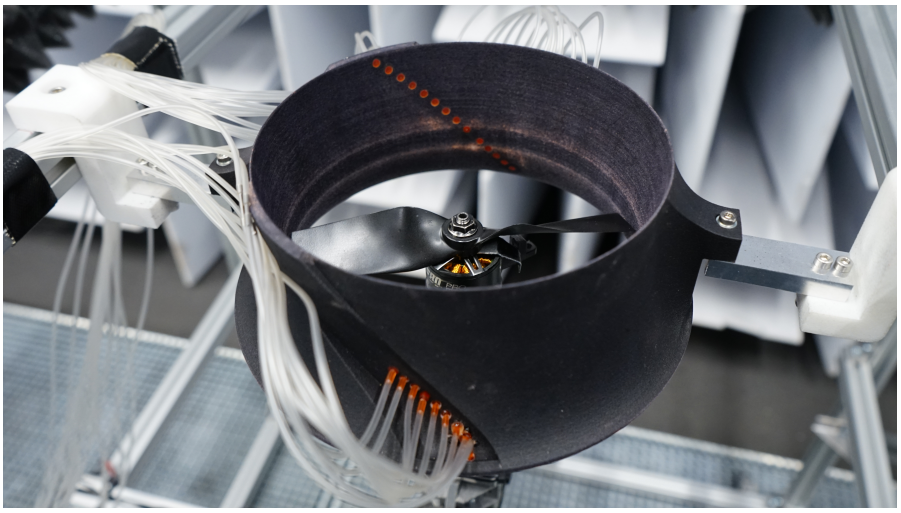

(a)

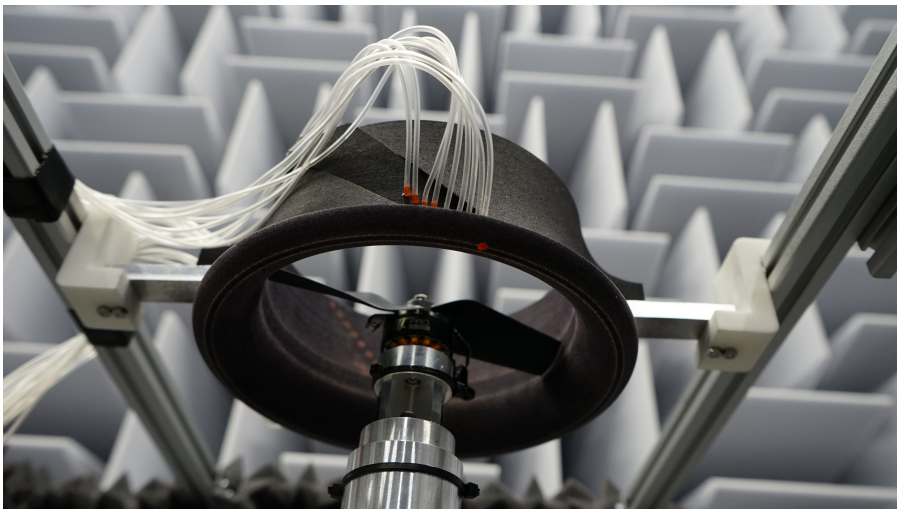

(b)

Figure 4.4: Photos of the experimental setup for the static pressure measurements in the wall of the duct

4.4. Flow measurements using particle image velocimetry

PIV (Particle Image Velocimetry) is an experimental method that allows to measure the velocity in an aerodynamic flow field. The method is based on illuminating tracer particles in the flow with a laser [28] [15]. The particles are illuminated twice in a short time-interval, and a camera captures these two frames. In the post-processing step, the images captured by the camera are divided in interrogation windows [28]. A complex algorithm can determine the displacement of the particles in each interrogation window. This displacement divided by the time-interval between the two frames, then gives the velocity [15]. A setup with a single camera provides two velocity-components in the plane that is illuminated by the laser sheet (2C-PIV). With a stereo setup of two cameras, it is possible to extract the third velocity component as well (3C-PIV) [28].

For the current study, the particle image velocimetry method is deployed to obtain the velocity field in the mid-plane of the duct (X-$Y\,plane$) for different tip gaps. This data gives insight into the aerodynamic flow inside the duct, which is needed to investigate the physical mechanisms that underlie the performance changes for different tip gaps. Specifically of interest is the trajectory of the tip vortex, the vortex strength in terms of its vorticity ω_z, the breakdown of the vortex when it interacts with the duct wall and how this relates to the boundary layer characteristics along the duct's inner wall, from the inlet lip up to the diffuser trailing edge.

As shown in figures 4.5 and 4.3, a stereo-PIV setup is used to acquire the 3 velocity components in an FOV (field of view) at the midplane of the duct. Two SCMOS cameras are used with a 105mm lense. As the cameras are positioned at an angle relative to the mid-plane of the duct, a scheimpflug is used to align the focal plane with the intended FOV in the duct. An Evergreen laser is used in combination with a set of lenses to create a laser sheet. The particles are distributed with a conventional smoke generator with Safex Long Lasting Fluid for PIV.

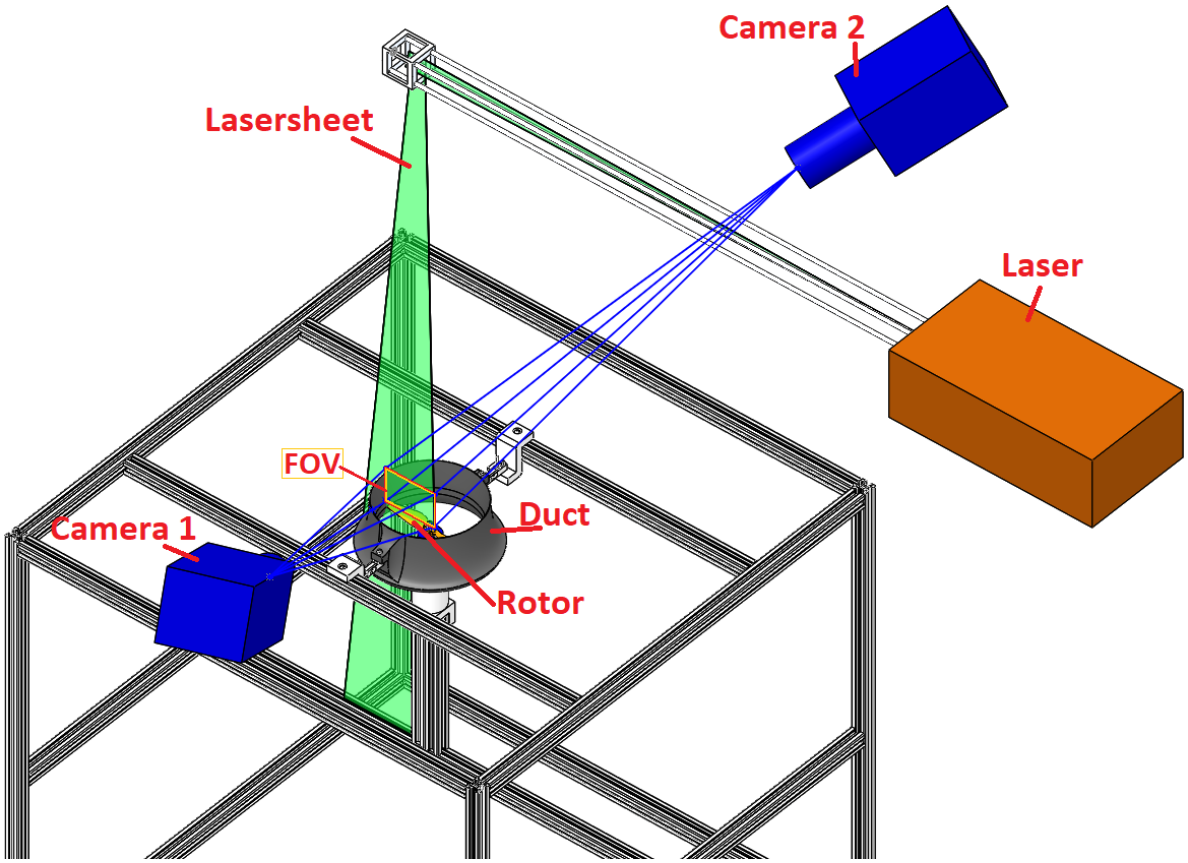

Figure 4.5: Experimental setup for the stereo-PIV experiments

Two different set-ups are used for the PIV experiments: one to measure the velocity in the duct diffuser (downstream of the rotor), and one to measure the velocity in the duct inlet (upstream of the rotor). For the latter, both the duct and rotor are flipped upside down. As shown in figure 4.6, this means that for these measurements in the duct inlet, the air is accelerated in opposite direction compared to all other experiments. The main difference is that the structure which holds the motor, is positioned downstream instead of upstream of the rotor. This should be taken it account when analyzing the results of these two different setups.

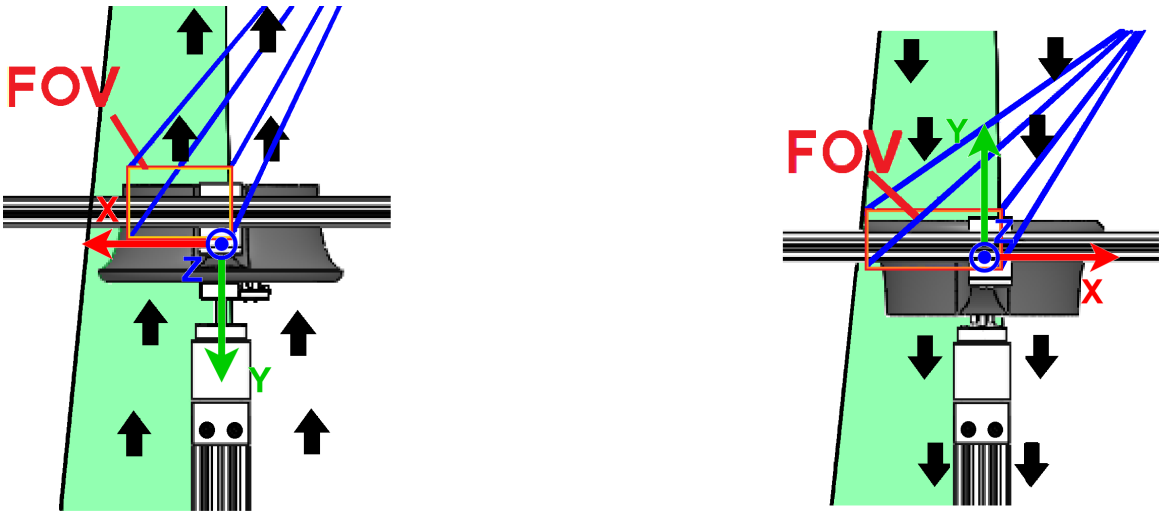

(a) (b)

Figure 4.6: Experimental setup for PIV measurements in the duct diffuser (a) and the duct inlet (b)

The PIV experiments are performed at a single rotational speed (Ω=11000 RPM) and for two different tip gaps. For each tip gap case, 500 random image pairs are acquired to obtain the mean velocity field inside the duct. Furthermore, 500 phase-locked image pairs are acquired at rotor positions θ=45°, θ=90°, and θ=135°. The phase-locked measurements are used to identify the strength and trajectory of the rotor-tip vortices.

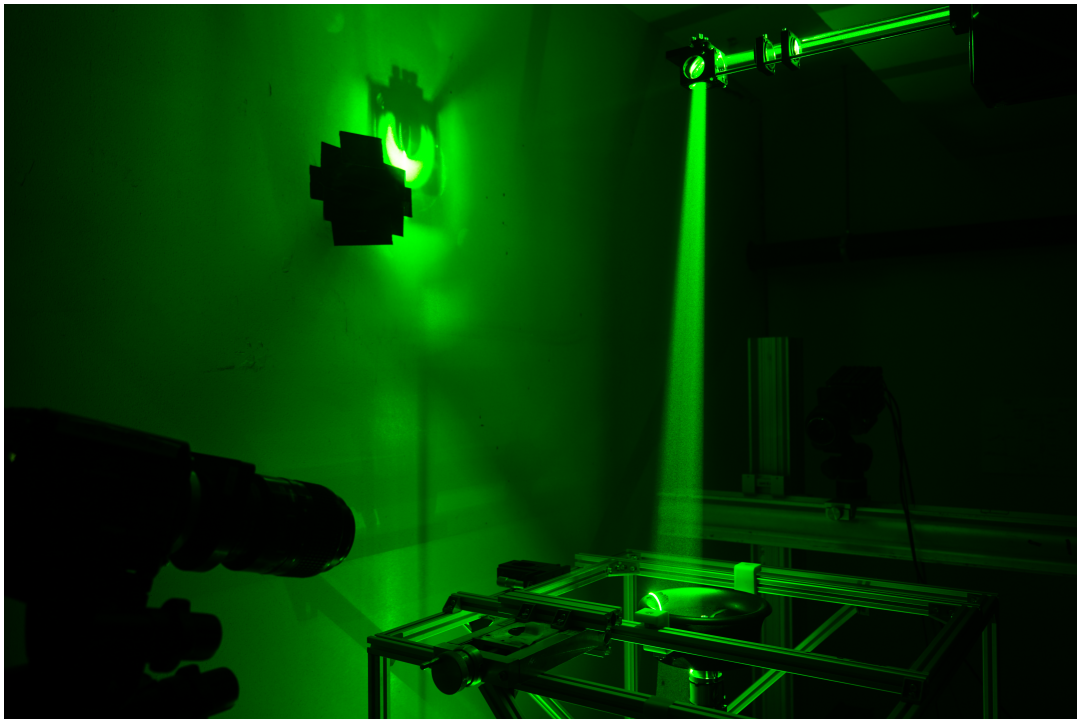

Figure 4.7: Photo of the experimental setup for the stereo-PIV measurements

In figure 4.8 a schematic oversight is shown of the post-processing steps of the PIV measurements. It can be seen that the Lavison Davis software is used to derive the vector fields from the captured images, and Matlab is used for plotting and visualizing the results. The 'substract minimum time filter' proved to be a very effective step to deal with reflections on the duct wall and rotor blade. In the 'stereo-PIV' step, it can be seen that the smallest interrogation window size is 24x24 pixels. This corresponds to a spatial resolution of 0.77mm.

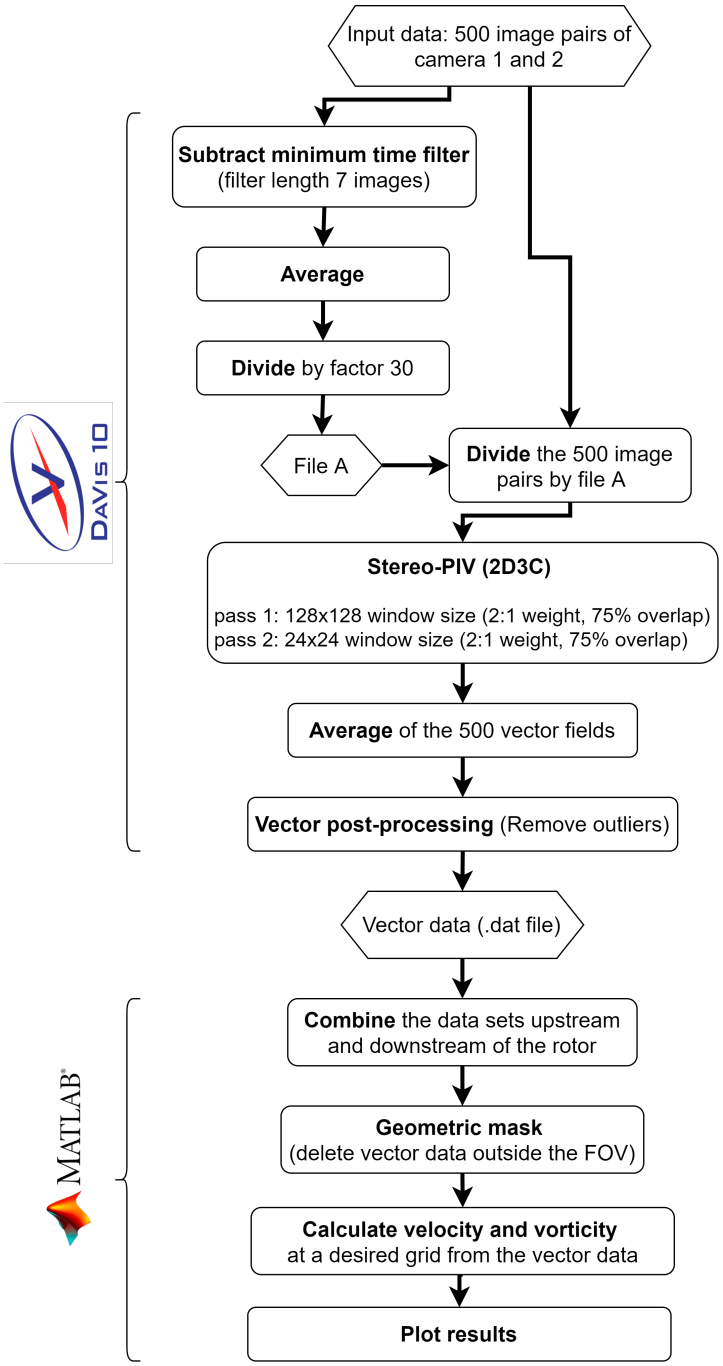

Figure 4.8: Oversight of the post-processing steps of the PIV measurements in Davis and Matlab

4.5. Noise measurements

The objective of the noise measurements is to measure aeroacoustic noise in the farfield of the ducted rotor system. In order to measure only the noise source directly (and not the noise reflected on the walls), the experiments are performed in the Vertical Low Turbulence Wind Tunnel of the TU Delft, which has anechoic properties above 100Hz (see figure 4.9).

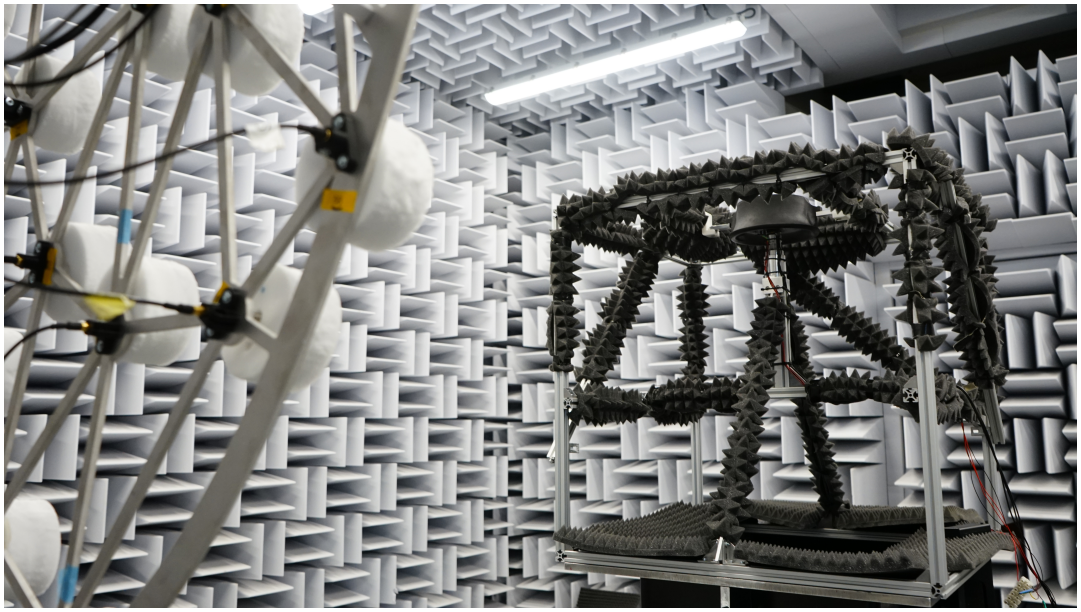

Figure 4.9: Photo of the experimental setup for the acoustic experiments, in the anechoic Vertical Low Turbulence Wind Tunnel at the TU Delft

As shown in figure 4.10, a vertical array of 11 microphones is placed at a distance of 1m of the ducted rotor system, which is equal to ~7.8 times the rotor diameter D_r. The microphones (G.R.A.S. 40PH) have a frequency range of 10Hz to 20kHz. The microphone array is shifted in vertical direction (position 1 to position 2, see figure 4.10) to obtain a greater range of the microphone angles ψ. For each operating condition, the measurement is repeated at the two different positions, and the data is combined later.

For the acoustic experiments, 2 different tip gaps of the ducted rotor are investigated at an Ω=11000 RPM and Ω=12000 RPM (see table 4.1 of section 4.6). For each operating condition, the acoustic pressure is measured for 30 seconds at 51200Hz by the 11 microphones. In a post-processing script, some filters are applied to account for the fact that the facility is not anechoic for frequencies below 100Hz. For each microphone, the overall sound pressure level $OASPL$ is calculated by taking the root mean square of the measured sound pressure p_{rms}, and divide this scalar by the standard reference sound pressure (p_{ref}=20 μPa [8]). To obtain the $OASPL$ in dB, a logarithmic function is applied (see equation 4.2).

$$OASPL = 20 \cdot \log_{10}\left(\frac{p_{rms}}{p_{ref}}\right) \tag{4.2}$$

Besides calculating the overall sound pressure level, a noise spectrum is also developed for each microphone. This allows for a deeper investigation into the acoustic properties of the ducted rotor system. For each microphone, the autospectrum $G_{pp}(f)$ is calculated by applying a fast Fourier transform to the sound pressure time series $p(t)$. This spectrum is divided by the squared reference pressure p_{ref}, and a logarithmic function is applied to obtain the sound pressure level SPL in dB/Hz (see equation 4.3).

$$SPL = 20 \cdot \log_{10}\left(\frac{G_{pp}(f)}{p_{ref}^2}\right) \tag{4.3}$$

As the microphones are positioned in a vertical line and not in a arc, the distance between the ducted rotor and each microphone varies. This affects the results because the acoustic pressure in the farfield is inversely proportional to the distance between the observer and the noise source. This is accounted for by dividing the measured sound pressure of each microphone by its distance to the ducted rotor, and multiplying with a factor $10D_d$ (which is 1.28m). This represents the sound pressure levels at a virtual arc around the ducted rotor at a constant radius of $10D_d$.

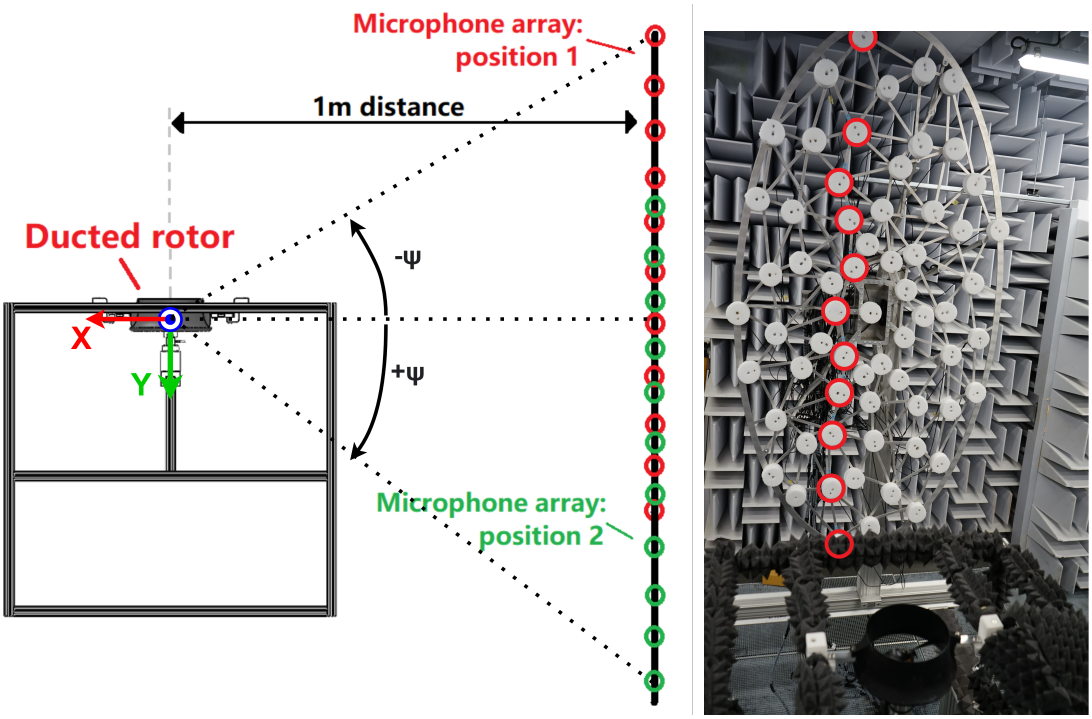

(a) (b)

Figure 4.10: Setup of the microphone array for the acoustic experiments. The red circles in the photo (b) mark the microphones used in position 1

4.6. Operating conditions

All experiments are performed in static hover conditions. In table 4.1 an oversight of the operating conditions for all the experiments can be seen.

The rotational speed is varied between Ω=2000 RPM and Ω=14000 RPM with increments of 1000 RPM for the performance characterization tests. These are the minimum and maximum rotational speeds that the experimental setup can handle without having excessive vibrations. For the smallest tip gap, the rotational speeds of Ω=11000 RPM and Ω=12000 RPM correspond to a total thrust of respectively 4.7N and 5.8N. These are roughly the operating conditions that the system was designed for when operating on a drone.
For the performance measurements, six different rotor diameters D_r between 127.2 mm - 124.9 mm are tested, both in open air and inside a duct. This corresponds to tip gap ratios δ^*_{tip} between 0.625% and 2.422% inside he duct. For comparison purposes, the load-cell experiments are repeated for a standard reference rotor for open air that is commercially available.

For the static pressure, PIV and acoustic measurements, only the cases inside the duct with rotor diameter D_r=127.2mm and D_r=125.4mm are investigated, which corresponds to tip gaps δ^*_{tip}=0.625% and δ^*_{tip}=2.031%. In this report, these two cases are referred to as the 'small tip gap' and 'large tip gap' cases. A single rotational speed of Ω=11000 RPM is considered for the PIV experiments, and for the acoustic and static-pressure experiments Ω=11000 RPM and Ω=12000 RPM are considered (as these are the intended operating conditions of the ducted rotor system).

Table 4.1: Oversight of the operating conditions for all the experiments

Constant: 1 setting
Varied: 2 settings
Varied: >2 settings

Variables:	Performance characterization	Static-pressure measurements	Flow measurements using PIV	Noise measurements
Configuration: (open air or ducted)	Open air, Ducted	Ducted	Ducted	Ducted
Rotor design:	Custom rotor, Reference rotor	Custom rotor	Custom rotor	Custom rotor
Rotor diameter and tip gap:	6 different rotor diameters / tip gaps	6 different rotor diameters / tip gaps	2 different rotor diameters / tip gaps	2 different rotor diameters / tip gaps
Rotational speed:	2000–14000 RPM, steps of 1000 RPM	11000 RPM and 13000 RPM	11000 RPM	12000 RPM and 13000 RPM
Type of measurement:	Time-averaged	Time-averaged	Time-averaged, Phaselock at Θ=45°, Θ=90°, and Θ=135°	Time-averaged

5

Results and discussion

In this chapter, the results of the experimental campaign are analysed and discussed.

In section 5.1, the aerodynamic performance of the ducted rotor system is characterized. The performance curves (Ω v.s. C_T, C_P and FM) are compared to the case in open air, and to a reference rotor that is commercially available.

In section 5.2 it is described how the performance of the ducted rotor (C_T and FM, and the portion of thrust generated by the duct) changes if the tip gap is varied.

In section 5.3, the static pressure distributions over the duct profile for different tip gaps are presented and analysed. The duct thrust calculated from the integrated pressure is compared to the duct thrust results of the load-cell experiments, to analyse how well these results agree.

The next two sections contain the results of the PIV measurments. It is described how the velocity field inside the duct changes for two different tip gaps (section 5.4), and how the tip gap affects the trajectory and breakdown of the rotor tip vortices (section 5.5). It is also analysed and discussed how these changes in the flow field are linked to the observations of the static-pressure distribution and performance curves.

In he final section (5.6), the preliminary results of the noise measurements are presented. The overall sound pressure level is compared for two different tip gaps, at constant Ω and constant level of thrust. Furthermore it is analysed how the noise spectrum changes with the tip gap.

5.1. Aerodynamic performance of the ducted rotor system

As explained in section 4.1, a custom designed ducted rotor system of a drone is investigated throughout this study. This section describes the performance of this ducted rotor system. The performance curves of the custom designed rotor are shown for the case in open air and inside the duct. The tip gap is not varied yet in this section. Only the rotor with largest diameter (D_r=127.2mm) is examined, which corresponds to a tip gap ratio δ^*_{tip} of 0.625%. Furthermore, the results are compared to a reference rotor that is designed for open air: the commercially available DAL5045B2 5-inch rotor [27], which is used on MAV quadcopters in hover and has the exact same rotor diameter D_r as the custom designed rotor.

For the load-cell experiments each measurement is conducted in threefold, and the average is used for the final results. The standard deviation of these threefold measurements turned out to be so small that the error bars are smaller than the plot-markers. Therefore, for all the presented graphs in section 5.1 and 5.2, the error bars are not included in the figures.

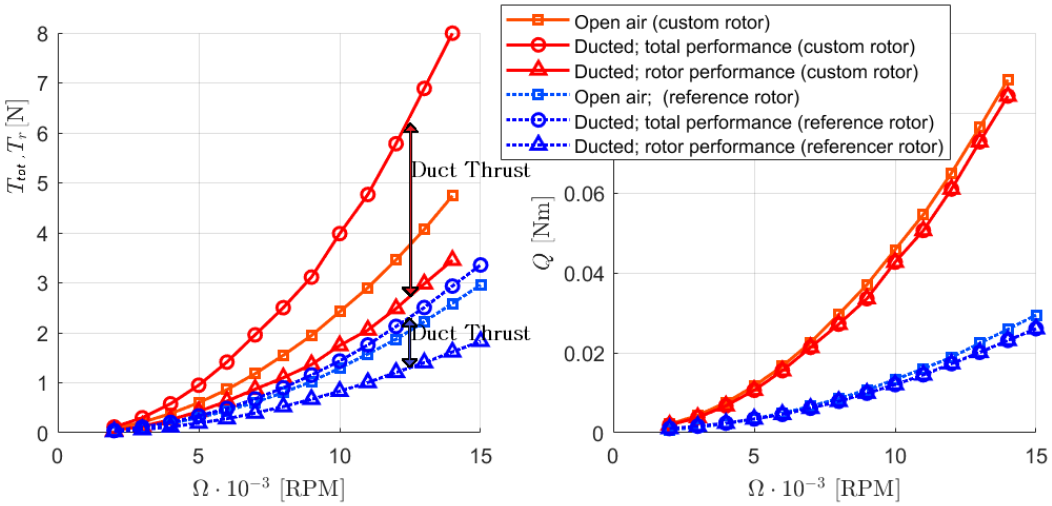

Figure 5.1: Load-cell measurements: Ω vs thrust T and torque Q. Rotor diameter D_r=127.2mm, tipgap ratio δ^*_{tip}=0.625%

Figure 5.1 shows the directly measured torque and thrust for the custom rotor and reference rotor, inside the duct and in open air. When comparing the custom and reference rotor, it can be seen that the custom rotor has a higher loading (both thrust and torque) for all cases. This is as expected, because compared to the reference rotor it has a much more aggressive angle of attack, and also a wider chord towards the blade tip (as explained in section 4.1). For both rotors, the duct itself generates a considerable amount of thrust (indicated with the arrows in figure 5.1). When comparing the ducted case and open air case, it can be seen that both rotors produce much less thrust themselves when placed inside the duct. Interestingly, the rotor torque is not as much affected, with only a small torque decrease for the ducted case compared to the open air case.
Instead of comparing the directly measured thrust and torque, a better way to analyse the performance of the different configurations is by considering the thrust coefficient C_T, power coefficient C_P and figure of merit FM (defined in equation set 3.2 on page 13). In figure 5.2 these coefficients are plotted against Ω. When analysing these results, the following observations are made:

- **Dependency on rotational speed:**
  When observing the performance curves of figure 5.2, it can be seen that the coefficients (C_T, C_P and FM) are strongly dependant on the rotational speed up to Ω=5000 RPM. For higher Ω, the performance does not strongly depend anymore on the rotational speed; only a small increase of performance (lower C_P, higher C_T and FM) occurs for increasing Ω above 5000 RPM.
- **Thrust performance of the duct:**
  Looking at the C_T curves in figure 5.2, it can be seen that for the ducted configurations the duct itself generates a considerable amount of thrust. The thrust generated by the duct is the distance between the total performance curve and the rotor performance curve (as earlier illustrated in figure 5.1). For the custom rotor, about 55% of the total thrust is generated by the duct. For the reference rotor the duct generates up to 45% of the total thrust. These numbers are in line with the earlier studies of Pereira [26] and Martin and Tung [23].

- **Aerodynamic efficiency of the different configurations**
  As explained in section 3.1, the figure of merit FM expresses the aerodynamic efficiency of a rotor. It describes the ratio of the power needed for a certain amount of thrust, relative to the power of an ideal actuator disc with the same area. Looking at the FM curves in figure 5.2, the ducted rotor configurations outperform the rotors in open air. The ducted custom rotor has the best overall performance with a FM around 1.0. It is about 40% more efficient then the reference rotor in open air ($FM \approx 0.6$), and about 20% more efficient compared to the reference rotor in the same duct ($FM \approx 0.8$).

  The latter underlines the importance of using the custom rotor for the current study, instead of simply placing a standard rotor in a duct. Contrary to the reference rotor, the custom rotor operates at roughly the right angle of attack along the entire span of the blade when placed inside a duct. Furthermore, the wider chord towards the tip of the custom rotor enables the duct to generate more thrust. These features are essential for investigating and evaluating the flow inside the duct for different tip gaps. As expected, the custom rotor is very inefficient in open air (compared to the reference rotor), because now the angle of attack is too large and the wider chord towards the tip causes more tip losses.

  Furthermore, these results underline the conclusion that a well designed ducted rotor is significantly more efficient than a rotor in open air. To place the performance of the ducted custom rotor and open air reference rotor of figure 5.2 in perspective; The reference rotor and custom rotor operate at a Reynolds number (at 75% of the blade span) between 25k and 75k for Ω between 5000 RPM and 11000 RPM. At these operating conditions, the reference rotor has a maximum figure of merit of 0.62. The highest recorded FM in literature for a small-scale low-Reynolds (Re_c<30k) rotor in open air is 0.67 [36] [6], which is fairly close to the measured FM of the reference rotor. Compared to these efficiencies for rotors in open air, the aerodynamic efficiency of the ducted custom rotor is significantly higher with a measured FM up to 1.02. These numbers (FM above 1.0 for ducted rotors and a maximum FM below 0.7 for rotors in open air) are in line with other studies [23] [2].

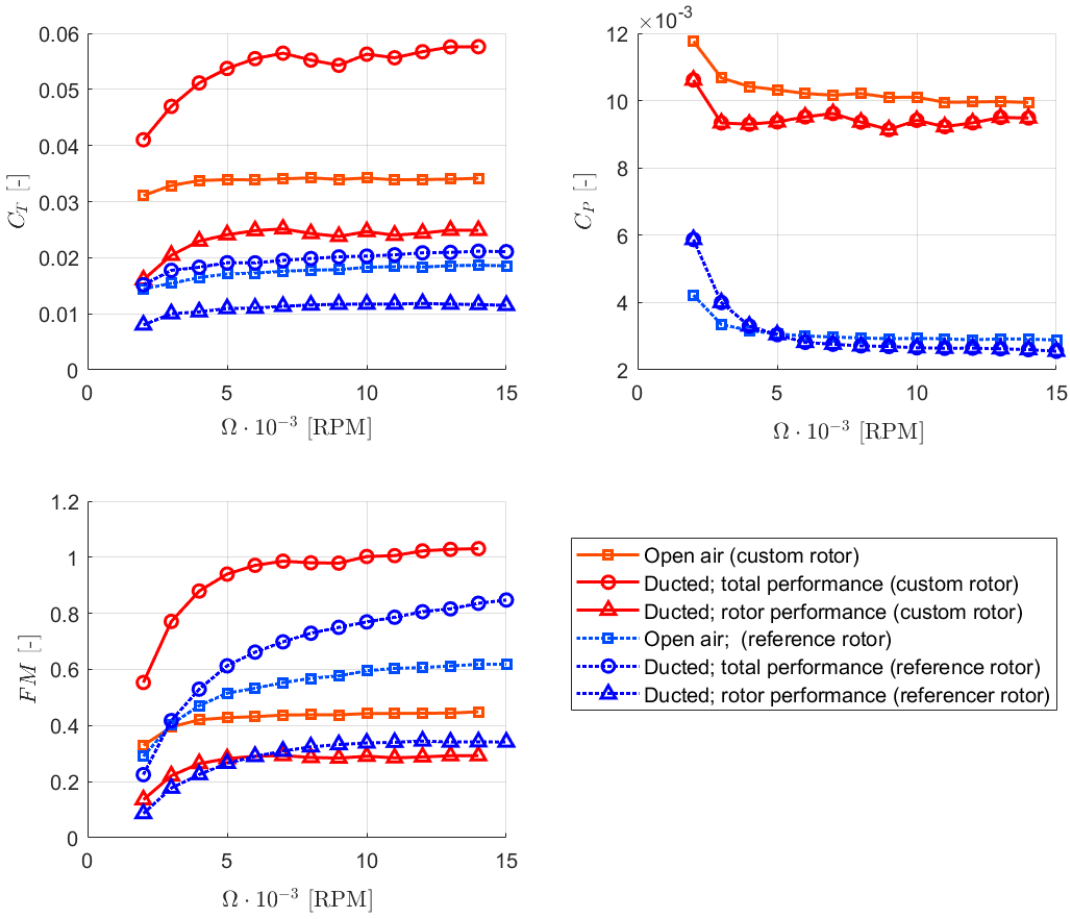

Figure 5.2: Performance coefficients derived from the load cell measurements: rotation speed Ω vs thrust coef. C_T, power coef. C_P, and figure of merit FM. Rotor diameter D_r=127.2mm, tipgap ratio δ^*_{tip}=0.625%.

- **Performance of the rotor itself in open air v.s. inside a duct:**
  The performance of the rotor itself (excluding the duct thrust) decreases for the ducted case compared to the open air case. Figure 5.2 shows that for both the reference rotor and custom rotor, the rotor produces significantly less thrust inside a duct. The mechanical power is also slightly lower due to a reduction in the torque load, but not as much compared to the thrust. Therefore the FM decreases, which means that the rotors are less efficient inside a duct compared to open air (if the duct thrust is excluded).
  An interesting question is why this happens. For the reference rotor an inferior performance in the duct can be expected, because its blade geometry was optimized for open air. For the custom rotor however this observation is unexpected. Its design was optimized for the ducted case, with a much higher angle of attack and wider chord towards the blade tip. These features are clearly sub-optimal for operation in open air, but somehow the performance in open air is still better then the performance in a duct.
  In the study of Pereira [26], a similar trend was observed. Four different rotors (at collective blade angles of 10°, 20°, 30° and 40°) were investigated in open air and inside 10 different ducts. For all cases, the rotor performance was worse in the duct compared to open air. Pereira attributed this observation to the increased axial velocity (as explained in section 2.3 of this report), because the difference became smaller for the rotors with larger angle of attack (and almost negligible for the rotor with the highest blade pitch).
  It is hypothesized as follows why the custom rotor performs worse inside a duct than in open air: The custom rotor was not optimized for its isolated performance, but optimized to maximize the FM *together with the duct thrust.* Apparently, for a ducted rotor system it can be beneficial for the total performance to increase the blade pitch beyond a point that is optimal for the performance of the rotor itself. The optimal angle of attack α of an arbitrary airfoil is at the location of L/D_{max} (for example, see page 5-4 of [1]). An optimal rotor normally operates as closely as possible to this α along the entire span of the blade. For a ducted rotor however it can be beneficial to operate at a higher α (beyond L/D_{max}), such that C_l increases and more air is accelerated into the duct. This then enables the duct to generate more thrust, which compensates for the sub-optimal performance of the rotor itself.

- **Figure of Merit above 1.0**
  In figure 5.2, the ducted custom rotor has a FM above 1.0. This means that it outperforms an ideal actuator disc, which is theoretically impossible. The caveat is that for the calculations of the performance coefficients, the area of the duct throat is used. This is the same definition that is used in other studies [23][26]. If instead of the duct throat diameter the duct outer diameter is used for the calculations, the FM drops below 1.0. The difference between these definitions is illustrated in figure 5.3. In the rest of this report, the area that corresponds to the duct throat diameter is used to calculate the coefficients. It is only a matter of definition, but it is important to be aware of it when comparing the performance of ducted rotors and rotors in open air.

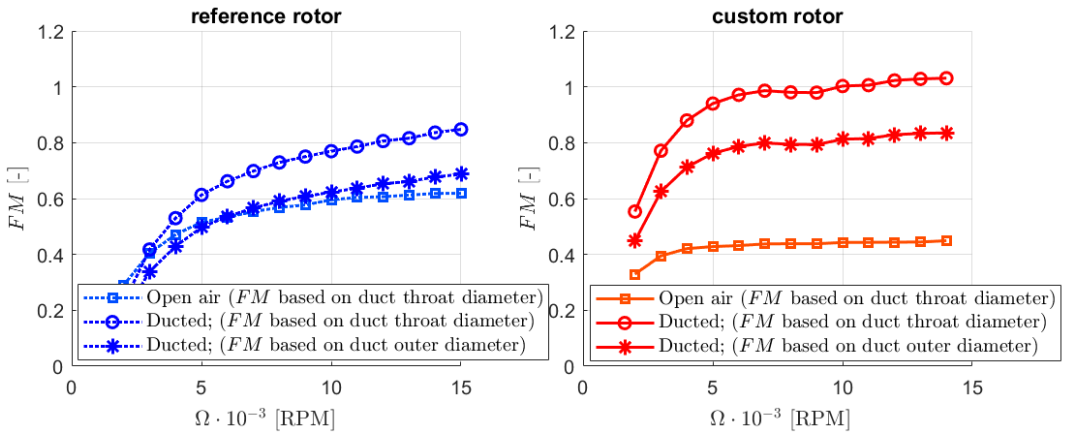

Figure 5.3: Rotational speed Ω plotted v.s. figure of merit FM, for different definitions of the area A in the calculations. The area based on rotor diameter is the definition that is handled throughout the rest of this report.

5.2. Effect of the tip gap on the aerodynamic performance

In previous section (5.1), the aerodynamic performance of the ducted rotor system was characterized. In this section it is described how this performance changes if the tip gap is varied.

In figure 5.4 it is shown how the thrust coefficient C_T, power coefficient C_P and figure of merit FM change with the tip gap ratio δ^*_{tip}, at a rotational speed of Ω=11000 RPM for the custom rotor. The rotor diameters that correspond to the tip gap ratios are depicted at the top of each graph. Looking at these results, the following observations and analyses are made:

- **Effect of the rotor diameter on performance**
  As explained in section 4.6, the tip gap is varied by changing the rotor diameter. To isolate how the tip gap alone affects the performance of a ducted rotor, it is important to investigate how much the difference of the rotor diameter contributes to the performance changes. Therefore, the performance of the rotor for different diameters is also plotted for the case in open air (see figure 5.4). It can be seen that a larger rotor slightly increases the thrust and mechancial power, but the differences are very small. Therefore, it can be assumed that the effect of the rotor diameter is negligible, and that observed aerodynamic changes for different δ^*_{tip} in this study are indeed a result of a changing tip gap.

- **Effect of the tip gap on rotor performance**
  An interesting question is how the tip gap affects the performance of the rotor itself in a duct (excluding the thrust generated by the duct). In figure 5.4, it can be seen that thrust coefficient C_T of the rotor in a duct is not affected by the tip gap ratio. The power coefficient C_P decreases slightly for larger tip gap ratios, but the difference is not large.
  These observations are similar to the results presented in the studies of Pereira [26] and Martin and Tung [23], where the tip gap also mostly affected the duct thrust and not the rotor performance. In the study of Akturk and Camci [3] however, it was shown that increasing the tip gap significantly affects the rotor performance, due to increased interaction losses between the blade tip and leakage flow of the preceding blade. These different conclusions are probably related to the fact that Akturk and Camci used an 8-bladed rotor, whereas the other studies (and the current study) investigated a 2-bladed rotor. If the blade number is decreased, the spacing between a rotor blade tip and the vortex of the preceding blade increases, which also decreases the losses that are related to their interaction.

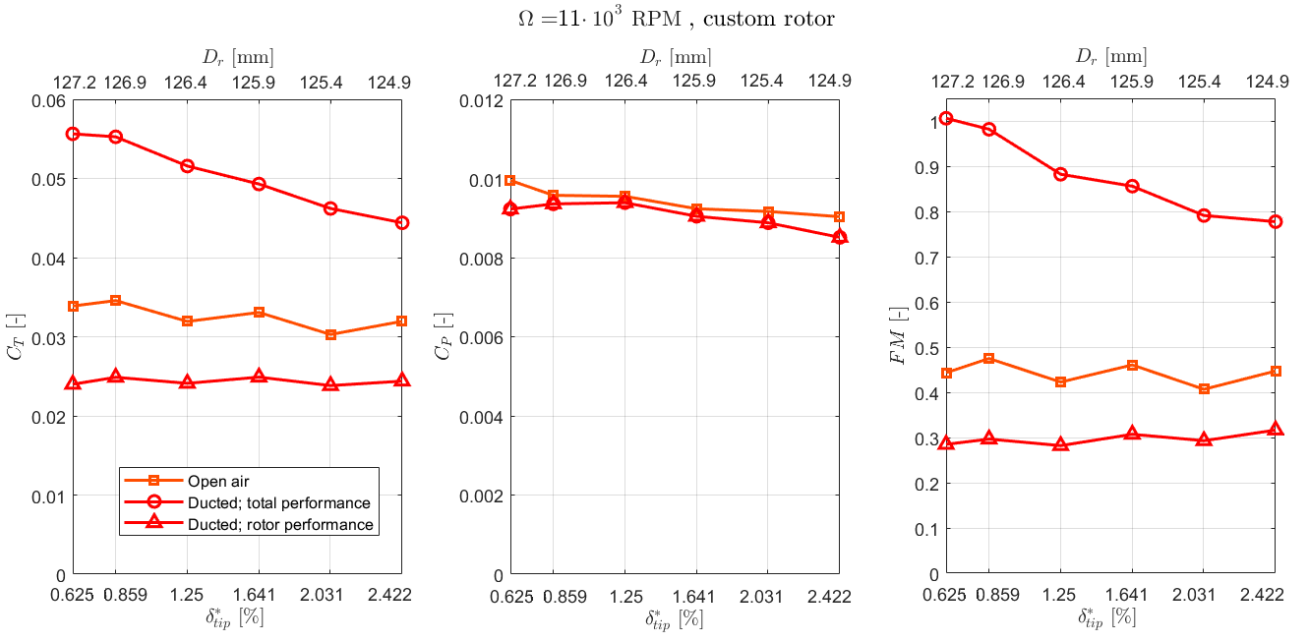

Figure 5.4: Effect of the tip gap ratio on the performance of the ducted rotor

- **Effect of the tip gap on the thrust generated by the duct**
  Looking at figure 5.4, it can be seen that – contrary to the rotor performance – the performance of the duct is strongly affected by the tip gap ratio. This is illustrated more clearly in figure 5.5: The duct thrust decreases with roughly 40% (from 2.7N to 1.6N) if the tip gap ratio is increased from 0.625% to 2.422%, while the rotor thrust remains unaffected. The increase of duct thrust for a smaller tip gap causes the total thrust coefficient C_T of the ducted rotor to increase from 0.044 to 0.057, and the figure of merit FM to increase from 0.78 to 1.0. It can be concluded that the performance increase for smaller tip gaps is completely caused by an enhanced thrust performance of the duct.
  The observation that the duct thrust strongly increases for smaller tip gaps was also observed in earlier studies of Pereira [26], Martin and Tung [23] and Akturk and Camci [4]. As explained in section 1.2, the goal of the current study is to get a better understanding of the physical mechanism behind this trend. This analysis is presented in section 5.3, 5.4 and 5.5, based results of the static-pressure measurements and PIV measurements.

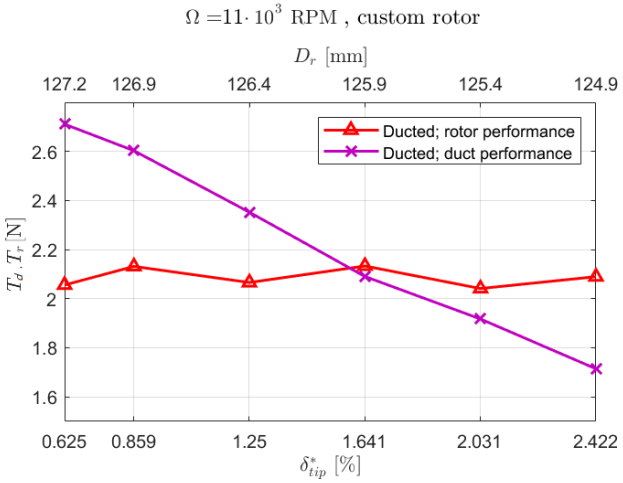

Figure 5.5: Effect of the tip gap ratio on the measured thrust components (duct thrust T_d, rotor thrust T_r) of the ducted rotor system

- **Deviation in the geometry of the left- and right-spinning rotors**
  For the load-cell experiments, six different rotors with six different diameters are investigated. Three of those were left-turning rotors, and three right-turning rotors. This was chosen because only these 6 rotors were available, and it should not matter for the results. However, the performance curves of the isolated rotor in figure 5.4 show a certain 'wiggle'. After further investigation, it turned out that this is caused by a small geometrical difference in the left-turning and right-turning rotors. This is illustrated more clearly in figure 5.6. The left- and right-turning rotor are produced with two different molds, and apparently there is a small deviation between their shapes. For the PIV and acoustic experiments – where only 2 different tip gaps are considered– it was decided to investigate the δ^*_{tip}=0.625% and δ^*_{tip}=2.031% cases, such that the same (left-spinning) rotors are used.

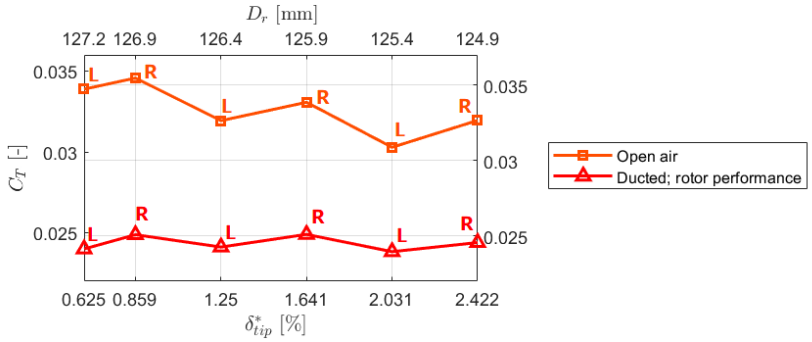

Figure 5.6: Zoomed in plot of the rotor diameter v.s. C_T, indicating that the left-turning (L) and right-turning (R) rotors are not perfectly symmetric

- **Sensitivity to the alignment of the rotor inside the duct**
  As shown in figure 5.4 the tip gap ratio δ^*_{tip} is varied between 0.625% and 2.422%. This corresponds to tip gaps δ_{tip} between 0.8mm and 3.1mm, with increments of 0.5mm. Given these small differences, it is very important to precisely center the rotor in the duct, such that the tip gap is exactly the same at all sides. A setup with a mockup-frame and displacement gauge were used to realize this precise centric alignment.
  The thrust measurements of the two load-cells that hold the duct (see figure 4.2 on page 27) were compared to check if the alignment was good. As shown in figure 5.7, the measured force for the aligned configuration (no offset) is exactly the same on the left and right side of the duct, which indicates that the duct was well aligned. For comparison, the results are also plotted for a configuration where the rotor is intentionally placed 2.2mm off-center (to the right). Clearly, the right side of the duct now generates more thrust, because the tip gap is smaller on this side.

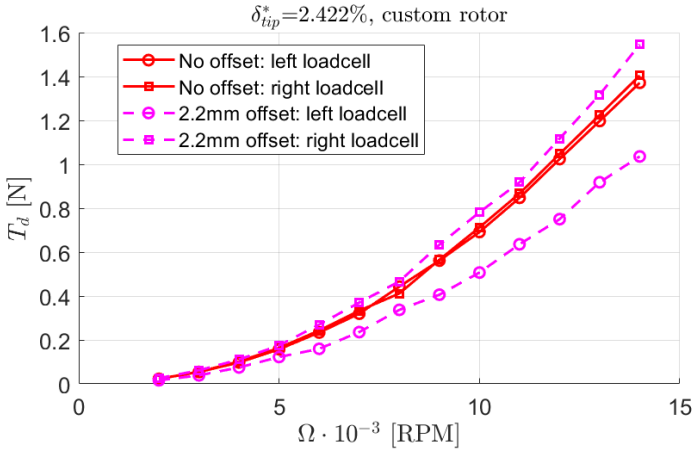

Figure 5.7: Force of the two loadcells that measure the thrust of the duct T_d (left and right), for a perfectly centered ducted rotor (no offset) and a configuration where the rotor is placed off-center (2.2mm offset)

5.3. Pressure distribution over the duct wall

In this section it is presented what the pressure distribution over the duct profile looks like, and how it changes for different tip gaps. These results are based on the static-pressure measurements, described in section 4.3.

In figure 5.8, the pressure distribution is plotted for six different tip gap ratio's δ^*_{tip}. In the top graph, the pressure distribution is visualized by plotting the contours directly on the cross-section of the duct. In the two graphs on the bottom, the relative pressure ($p_{atm} - p_{stat}$) and pressure coefficient $C_{p,stat}$ are plotted against the duct length coordinate L. As defined in equation 4.1 on page 28, the coefficient $C_{p,stat}$ is obtained by dividing the relative pressure with the dynamic pressure at the blade tips. If the pressure is integrated over the duct surface, the duct thrust can be calculated. In table 5.1, the duct thrust based on the integrated pressure is shown together with the directly measured results of the load-cell measurements.

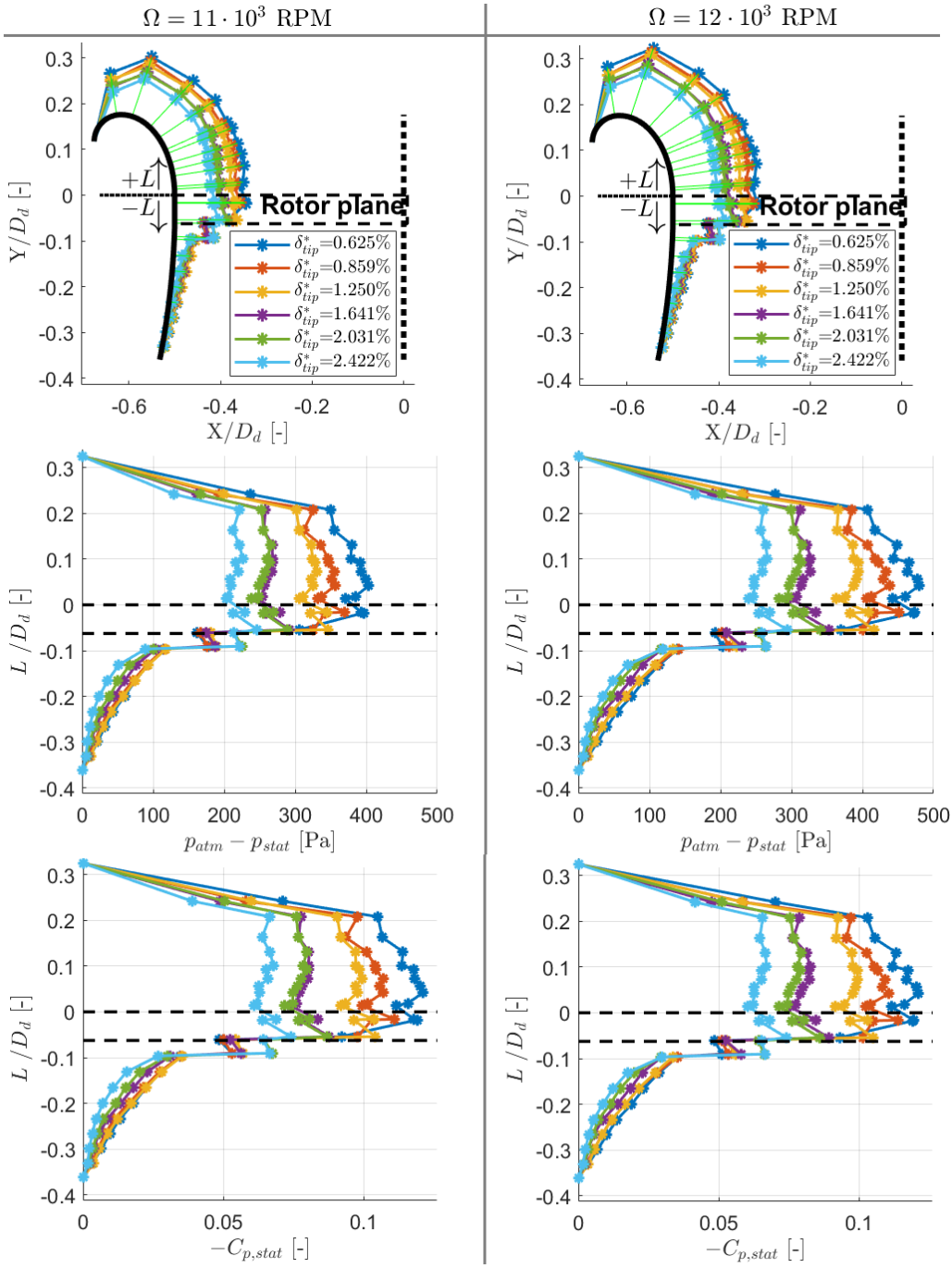

Figure 5.8: Pressure distribution over the duct profile for different tip gap ratio's, for Ω=11000 RPM and Ω=12000 RPM

The following observations and analyses are made based on the pressure distribution results presented in figure 5.8 and table 5.1:

- **Dependency of the static pressure distribution on rotational speed**
  When comparing the results of Ω=11000 RPM and Ω=12000 RPM, it can be seen that – as expected – the pressure relative to the ambient pressure decreases for a higher rotational speed Ω. The distribution of the pressure coefficient $C_{p,stat}$ is however almost identical for the two different Ω cases.

- **General description of the pressure distribution over the duct wall**
  Figure 5.8 shows that the static pressure is lower than the ambient pressure along the entire length of the duct wall. There is a strong and constant suction zone over the inlet lip. The pressure increases rapidly at the height of the rotor blade tip trailing edge (Y/D_d=-0.07). This sudden increase is related to the pressure difference over the rotor blade. After the rotor plane, a small secondary suction zone is observed (at Y/D_d=-0.1). This local low pressure zone can be related to the presence a rotor tip vortex close to the duct wall. After the secondary suction zone, the pressure increases in the diffuser. It can be seen that at the outlet of the duct (Y/D_d=-0.35), the pressure is almost equal to the ambient pressure. As explained in the theory of section 2.4, this means that the diffuser is designed well and expands the flow as desired.

- **Effect of the tip gap on the pressure distribution**
  Looking at figure 5.8, it can be seen that decreasing the tip gap decreases the pressure over the duct profile. The stronger suction at the inlet lip is in line with the earlier observed increase of duct thrust for smaller tip gaps (see section 5.2). The secondary suction zone (at Y/D_d=-0.1) is the only location where the static-pressure is lower for a larger tip gap. This underlines the earlier conclusion that this secondary suction zone is related to the presence of a tip vortex close to the duct wall. Apart from having an offset, the shape of the pressure distribution does not change significantly for different tip gaps. Only for the smallest tip gap case (δ^*_{tip}=0.625%), a small difference can be seen at the height of the rotor plane: At Y/D_d=-0.7, the pressure increases beyond the values of the δ^*_{tip}=0.859% and δ^*_{tip}=1.250% cases (for both Ω=11000 RPM and Ω=12000 RPM). This may indicate that for the δ^*_{tip}=0.625% case, the tip gap is so small that the characteristics of the tip leakage flow are different compared to all other tip gap cases.

- **Contribution to duct thrust by the inlet lip and diffuser**
  The inlet lip ($L > 0$) is the only location where the vectors normal to the surface are pointing in thrust direction. In the diffuser ($L < 0$), the vectors are pointing downwards, meaning that the suction over the duct diffuser has a negative contribution to the total duct thrust. In table 5.1, it can seen what the contribution of the inlet lip and diffuser to the total thrust are. It can be seen that the negative thrust contribution of the diffuser is insignificant compared to the positive thrust of the inlet lip. Still, one could argue that removing the diffuser would we better as it has a negative contribution to the thrust. This is however not true, because the diffuser enables the inlet lip of the duct to generate more thrust. As explained in section 2.4, the diffuser helps to accelerate the air through the duct by expanding the flow, and an increased flow acceleration through the inlet causes stronger suction at the inlet lip. Another way to see it is that the diffuser supports the low pressure distribution at the inlet lip; without a diffuser, the static pressure cannot suddenly jump from its current value to the ambient pressure at Y/D_d=-0.07. Instead, the suction all over the inlet lip would decrease, which means that the duct generates less thrust.

- **Comparison of the static-pressure experiments and load-cell experiments**
  When comparing the thrust computed from the integrated static-pressure distributions with the directly measured thrust of the load-cell experiments (see table 5.1), it can be seen that the results match very well, which confirms that the experiments have been conducted correctly. The maximum relative difference between the two methods is roughly 5%. This difference is probably caused by some small differences in the experimental setup. For example, two different 3d-printed ducts are used for the static-pressure and load-cell experiments. A small deviation of the two products could lead to differences in the performance. Furthermore, contrary to the load-cell measurements, the contribution of the friction drag to the resulting force on the duct is not included in the calculations based on the static-pressure measurements.

Table 5.1: Comparison of the duct thrust from the static-pressure and load-cell measurements, at an Ω=11000 RPM (a) and Ω=12000 RPM (b)

RPM=11k	Thrust (Static-pressure) [N]			Thrust (Load cell) [N]
	Inlet lip	Diffuser	Total	Total
δ^*_{tip}=0.625 %	2.9381	-0.0724	2.8657	2.7109
δ^*_{tip}=0.859 %	2.6760	-0.0664	2.6096	2.6029
δ^*_{tip}=1.250 %	2.4867	-0.0713	2.4154	2.3522
δ^*_{tip}=1.641 %	2.1482	-0.0553	2.0928	2.0903
δ^*_{tip}=2.031 %	2.0421	-0.0509	1.9913	1.9172
δ^*_{tip}=2.422 %	1.7801	-0.0389	1.7412	1.7143

(a)

RPM=12k	Thrust (Static-pressure) [N]			Thrust (Load cell) [N]
	Inlet lip	Diffuser	Total	Total
δ^*_{tip}=0.625 %	3.4697	-0.0891	3.3805	3.2978
δ^*_{tip}=0.859 %	3.2212	-0.0809	3.1403	3.1303
δ^*_{tip}=1.250 %	2.9772	-0.0816	2.8955	2.7800
δ^*_{tip}=1.641 %	2.5656	-0.0658	2.4998	2.5000
δ^*_{tip}=2.031 %	2.4518	-0.0600	2.3918	2.2948
δ^*_{tip}=2.422 %	2.1465	-0.0512	2.0953	2.0711

(b)

5.4. Velocity field in the mid-plane of the the duct

In this section the results of the PIV-measurements are presented. The velocity-field in the mid-plane of the duct (the X-Y plane) is shown for two different tip gap cases: the case with large tip gap (δ^*_{tip}=2.031%) and small tip gap (δ^*_{tip}=0.625%). It is described how the flow field in the duct changes with the tip gap, and how these observations can be related to the earlier presented results of the performance characterization and the static-pressure measurements.

As explained in section 4.4, two different measurements were used to separately capture the velocity fields in the duct inlet lip (upstream of the rotor) and in the duct diffuser (downstream of the rotor). For the results presented in this section, the data of these two separate measurements are combined into one figure (see figure 5.10 and 5.13). It should be noted that the experimental-setup for these measurements are not exactly the same, with the main difference that the center beam holding the motor is positioned upstream or downstream for the two different configurations (see figure 4.6 on page 30).

5.4.1. Phase-locked velocity field (θ=90°)

The phaselocked measurements at a rotor phase position of θ=90° give the most accurate results, because this is the only position where the reflections of the rotor did not disturb the PIV measurements. As shown in figure 5.9, at θ=90° the rotor blades are positioned perpendicular to the laser sheet. For all other positions, the rotor blades appear behind the laser sheet, which disturbs the measurements. For example, looking at the θ=45° image in figure 5.9, the blade appears behind the sheet for camera 2. The laser reflections on the blade are so bright that the illuminated particles in front it often cannot be distinguished (even after post-processing the images). For some of the measurements, this causes local areas with a non-physical velocity to appear. As this issue did not play any role for the phase-locked measurements at θ=90°, these are the results that are primarily used for the analysis and discussion of the flow-field in the duct for different tip gaps.

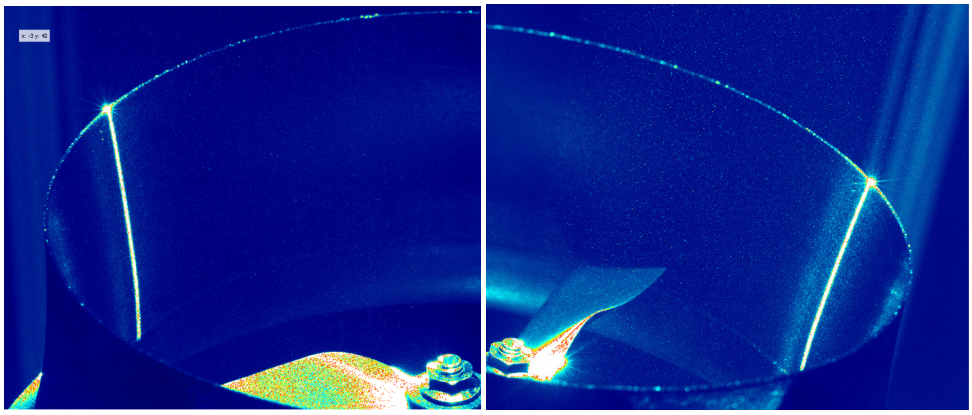

(a) Camera 1 (θ=45°)

(b) Camera 2 (θ=45°)

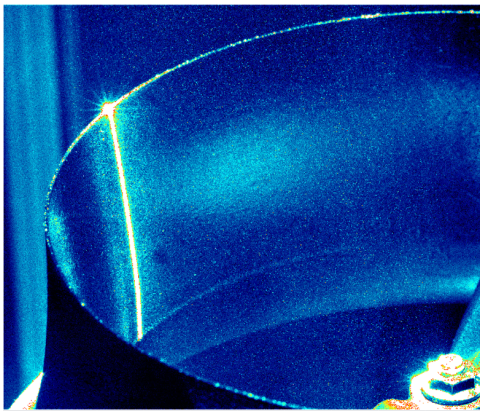

(c) Camera 1 (θ=90°)

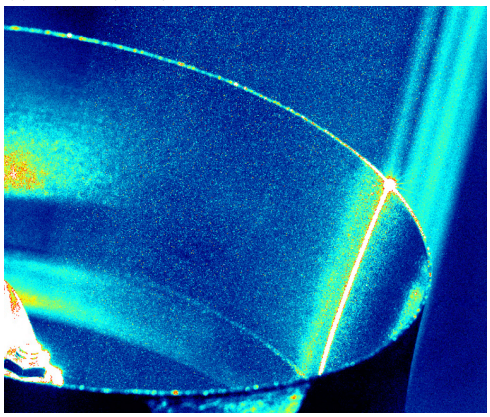

(d) Camera 2 (θ=90°)

Figure 5.9: Images of the two camera's of the stereo-PIV experiments, for a rotor phase position of θ=45° and θ=90°

In figure 5.10 and 5.11 , the contours of the total velocity V_{tot} and out-of-plane vorticity ω_z are plotted for a rotor phase of 90°. The velocity field presented is the average of 500 measurements at a rotor position of 90°. A one-per-revolution optical encoder was used to trigger the measurement at the right rotor phase θ. However, due to an inconsistency in the rotational speed of the rotor (±80 at Ω=11000 RPM), there was also a deviation in the phase position of the rotor of roughly ±7°. This means that the results presented in figure 5.10 are in fact the average of 500 measurements with a rotor phase θ between 83° and 97°. This deviation affects the results, for example because it slightly spreads the position of the rotor tip vortices in axial direction.

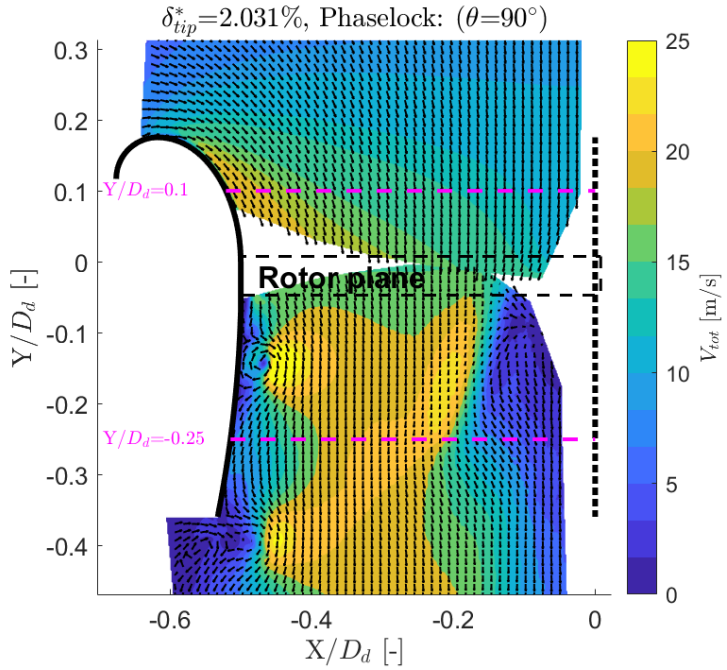

(a)

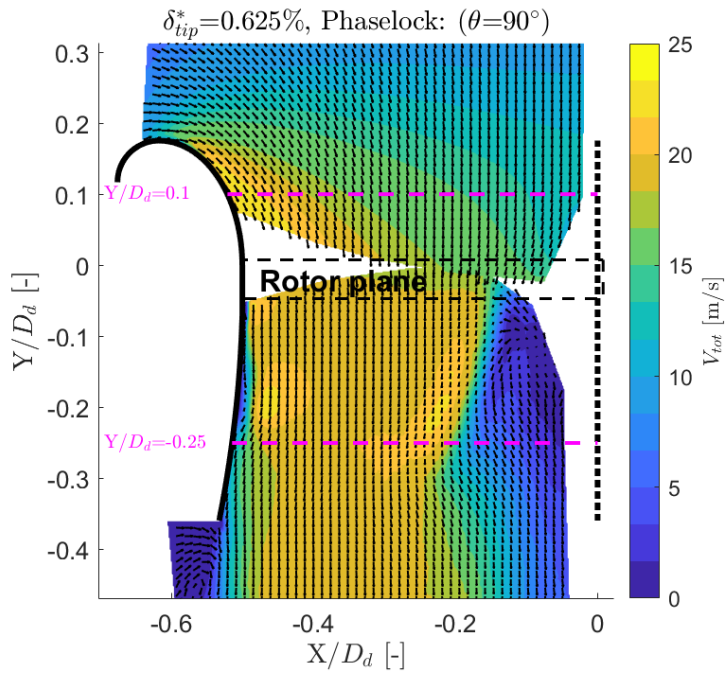

(b)

Figure 5.10: Phase-locked total velocity in the duct (average of 500 measurements at rotor phase θ=90°) at Ω=11000 RPM, for two different tip gap ratios: δ^*_{tip}=2.031% (a) and δ^*_{tip}=0.6251% (b)

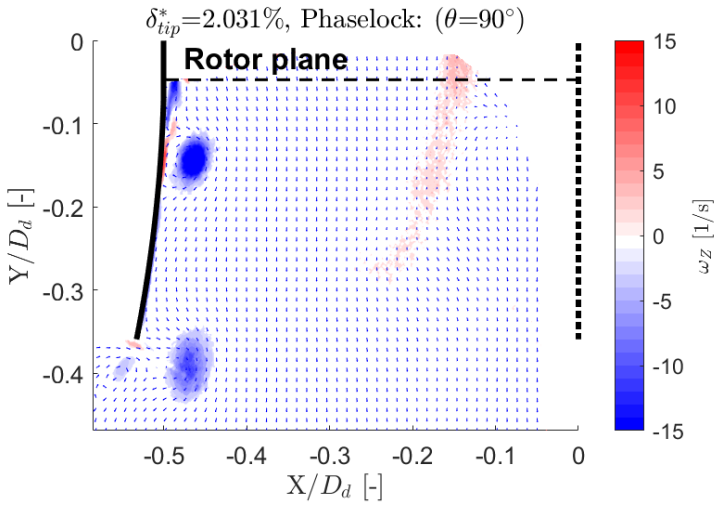

(a)

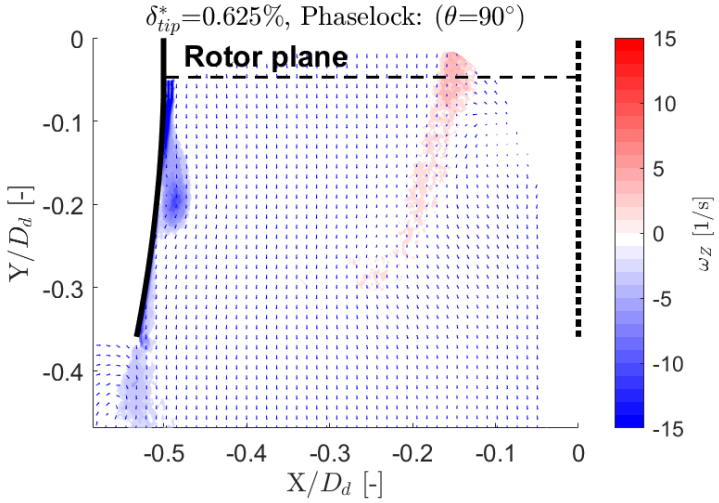

(b)

Figure 5.11: Phase-locked Vorticity ω_z in the duct for rotor phase θ=90° at Ω=11000 RPM, for two different tip gap ratios: δ^*_{tip}=2.031% (a) and δ^*_{tip}=0.6251% (b)

Looking at the velocity and vorticity contour plots for the small and large tip gap case in figure 5.10 and 5.11, the following observations and analyses are made:

- **Attenuated rotor tip vortices for a smaller tip gap**
  In figure 5.10 it is immediately noticeable that for the large tip case two rotor tip vortices are present (at Y/D_d=-0.14 and Y/D_d=-0.4). For the small tip gap case however, only a small remainder of the vortex can be seen at Y/D_d=-0.2. This means that for the small tip gap case, the rotor tip vortex breaks down before reaching the duct outlet. This can be seen more clearly in figure 5.11, where the vorticity contours of ω_z are plotted. The weak vorticity at Y/D_d=-0.2 is spreads out significantly in Y-direction. This partially happens because of the deviation in the rotor phase θ of $\pm 7^\circ$. Apart from the rotor tip vortices, also a rotor hub vortex can be observed that is similar for the two tip gap cases.

  For the large tip gap case, the presence of the strong vortex causes a zone of reversed flow in the boundary layer of the duct; at Y/D_d=-0.14, all vectors close all wall are pointed upwards. This observation of a locally reversed flow over the diffuser wall due to the presence of a rotor tip vortex is in line with the findings of earlier studies [7] [23] (see section 3.2.2). For the small tip gap case however, no reversed flow is observed. Close to the wall the velocity becomes almost zero, but all vectors are still pointing downwards. In section 5.5 it is described in more detail how the trajectory and breakdown of the rotor tip vortices is affected by the tip gap.

- **Higher velocity for a smaller tip gap**
  Looking at figure 5.10, it can be seen that the axial velocity ($-V_y$) is much larger almost everywhere in the duct for the small tip gap case. For the large tip gap, zones of lower velocity are present in-between the two vortices in the diffuser. Furthermore, a zone of low velocity can be seen immediately downstream of the rotor plane. Upstream of the rotor there is also a velocity increase for the smaller tip gap, which interestingly is not limited to the zone close to the duct wall. It was expected that close to the inlet lip, the velocity would increase with a smaller tip gap due to a reduction of the tip leakage flow [4] (see section 3.2.4). Figure 5.10 shows however that not only the flow on the outside (close to the duct wall) has a higher velocity, but also the flow in the middle of the duct inlet (up to X/D_d=-0.2).

  The higher velocity in the duct inlet is directly related to the earlier findings of the performance characterization and static-pressure measurements (section 5.2 and 5.3); with a smaller tip gap more air is accelerated in the duct, which increases the suction at the inlet lip and enables the duct to generate more thrust. An interesting question is what physical mechanism causes the observed flow acceleration in the duct for smaller tip gaps. Based on the results presented in section 5.4 and 5.5, it is hypothesized that the flow acceleration for smaller tip gaps is related to the following phenomena:

  - With a small tip gap, there is less tip leakage flow between the rotor blade tip and the duct wall. The end of the rotor blade is sealed better by the closer proximity of the duct wall, which prevents the rolling up of a strong tip vortex from the pressure to suction side of the blade. Besides preventing the formation of tip vortices, the better sealing also helps to directly accelerate more air into the duct.
  - The tip vortices that are convected along the diffuser wall slow down the airflow in the diffuser. This happens especially for the case with a large tip gap, where a strong vortex is present until the very end of the duct. The outer side of the vortex induces a velocity opposite to the axial flow direction, which causes a withdrawal of momentum from the boundary layer. This zone of lower velocity close to the diffuser wall (see figure 5.13) causes the vortices to be convected slower downstream compared to the case with small tip gap (see figure 5.15 on page 53).
  - With a small tip gap, the (remainder of) the rotor tip vortices follow the contour of the duct diffuser better than with a large tip gap. This can be seen in figure 5.15 on page 53; For the small tip gap case, the vortices break down fast, and are located close to the diffuser wall. For the large tip gap case however, the strong tip vortices have a slighlty contracting trajectory, instead of following the outward shape of the duct diffuser. This means that for the large tip gap case the diffuser cannot effectively expand the flow, and as explained in section 2.4 this expansion in the diffuser has an upstream effect of the flow accelaration through the duct. This observation can also be related to the static-pressure profiles presented in section 5.3, where for a larger tip gap the pressure is higher along the diffuser wall.

5.4.2. Mean velocity field (θ= random)

As mentioned in previous section (5.4.1), the PIV-results for rotor phases other than θ=90° contain inaccuracies related to laser reflections on the rotor. These inaccuracies also affected the results of the mean velocity fields that are presented in this section. In appendix A it is explained in more detail to what extend the mean velocity field is accurate.

In figure 5.13 the mean velocity field for the large and small tip gap case are presented. Figure 5.12 shows the difference between the phase-locked (θ=90°) and mean (θ= random) velocity fields. Looking at these figures, the following observations are made:

- **Comparison of the phase-locked an mean velocity fields**
  Looking at figure 5.12, it can be seen that the phase-locked and mean velocity fields are very different downstream of the rotor. This is related to the presence of tip vortices for the phase-locked results, which dissapear when the mean velocity field is developed. Therefore, both the rotor tip and hub vortices are clearly visible in the relative velocity field of figure 5.12. Upstream of the rotor, there is not a large difference between the mean and phase-locked velocity fields. A maximum difference of 0.9m/s is observed. Only very close to the duct inlet lip a larger difference can be seen, but as explained in section 5.4.3 the data very close to the duct wall is not very reliable due to the brightness of the laser reflection on the duct.
- **Zone of low velocity along the diffuser wall for a larger tip gap**
  For the larger tip gap case, there is a zone of low velocity close to the diffuser wall. This band of low velocity is much thinner for the small tip gap case. As explained in previous section, this is related to the presence of tip vortices that are convected along the diffuser wall, and their interaction with boundary layer.
- **Increased velocity upstream of the rotor for a smaller tip gap**
  Similarly to the results of previous section, the velocity upstream of the rotor is much higher for the smaller tip gap case. This velocity increase is not limited to the zone close to the duct wall, but is also present in the center of the duct.

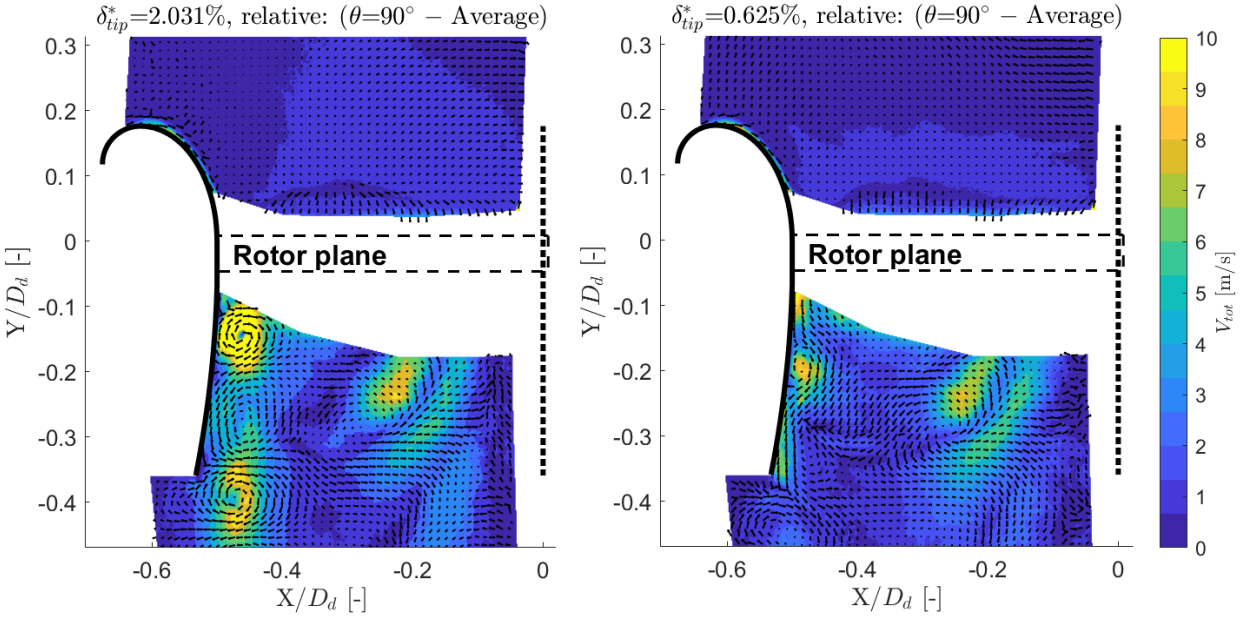

Figure 5.12: Difference between the phase-locked (θ=90°) and mean velocity field (θ=random) at Ω=11000 RPM, for two different tip gap ratios: δ^*_{tip}=2.031% and δ^*_{tip}=0.6251%

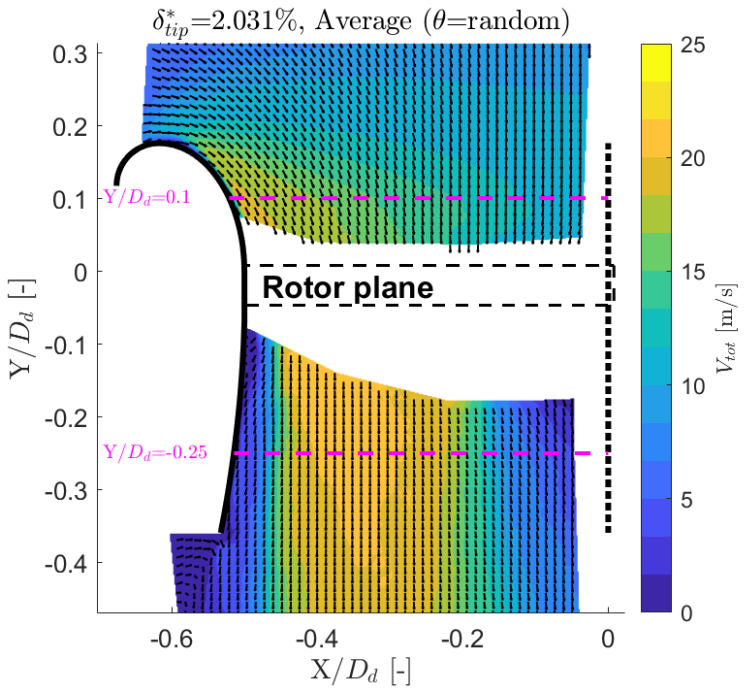

(a)

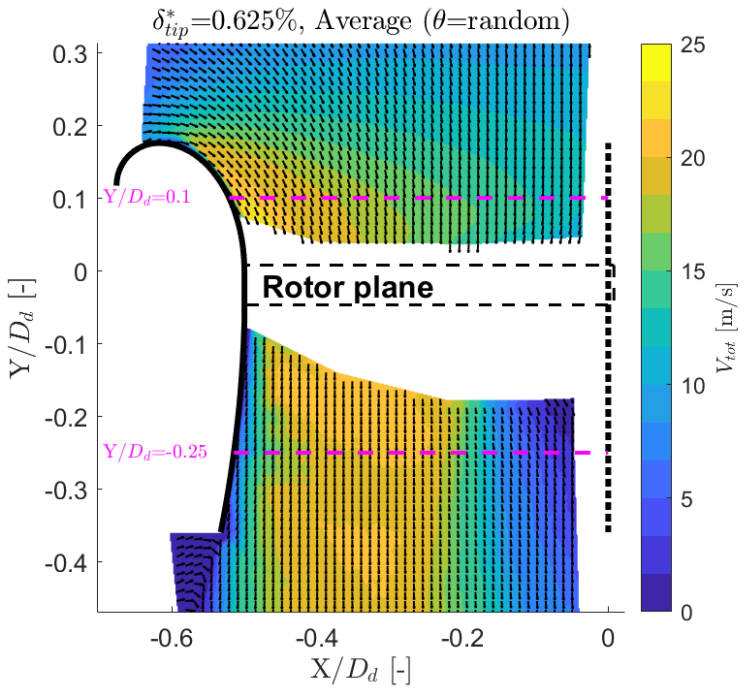

(b)

Figure 5.13: Mean total velocity in the duct (average of 500 measurements at random rotor phases) at Ω=11000 RPM, for two different tip gap ratios: δ^*_{tip}=2.031% (a) and δ^*_{tip}=0.6251% (b)

5.4.3. Velocity distribution plots: unreliability of data close to the duct wall

In the earlier presented phase-locked and mean velocity fields (figure 5.10 on page 46 and figure 5.13 on page 50), dashed lines are drawn at Y/D_d=0.1 and Y/D_d=-0.25. In this subsection, the velocity distributions along these lines are plotted and analyzed. In figure 5.14, the axial velocity component V_y is plotted for the phase-locked and mean results of the large and small tip gap case. They mostly present the same information as the contour plots of figure 5.10 and 5.13, but in these plots it is easier to directly read how much the velocity differs for the various configurations. For example, it can be seen more clearly than in the contour plots, that for a smaller tip gap the velocity is increased all the way up to the duct center, and not just on the outside.

An interesting question is whether the boundary layer profiles are visible in these plots. If the boundary layer profiles are correctly visible, they could be used to align the position of the duct wall more precisely in the velocity fields (this is done manually until now). To investigate this, the velocity close to the duct wall (marked with the green dotted region) was plotted on a semi log-scale for several data sets. An example of this is shown at the right side of figure 5.14. The log-scale is useful, for example because in a turbulent boundary layer flow a layer exists where the average velocity is proportional to the logarithm of the distance to the wall [22]. After plotting the curves on a semi log-scale, it however became clear that the velocity information close to the duct wall is unreliable. Namely, for repeated datasets of the exact same configuration, the curves were very different when approaching the last millimeter close to the duct wall. Moreover, none of the boundary layer profile rules could be consistently be recognized in any of the plots. After looking more closely into the PIV results, it became clear that the data of roughly the first 1.5 millimeter is disturbed by the reflection of the laser on the duct wall. Due to the high intensity of the reflection, the particles in close proximity are sometimes invisible. Instead, the algorithm detects the static reflection of the 3d printed duct texture as illuminated particles (which don't move), leading to non-physical velocities. Attempts to improve this with more post-processing steps were proven unsuccessful.

Clearly, to properly investigate the boundary layer profiles, the velocity distribution should be plotted normal to the duct wall (which is not exactly the case for the Y/D_d=0.1 and Y/D_d=-0.25 lines). However, when it was discovered that the laser reflections disturb the data close to the wall in anyway, it was decided to simply conclude that velocity data in the 1st 1.5 millimeter is just not reliable. This means that the boundary layer characteristics cannot be derived from the current PIV measurements.

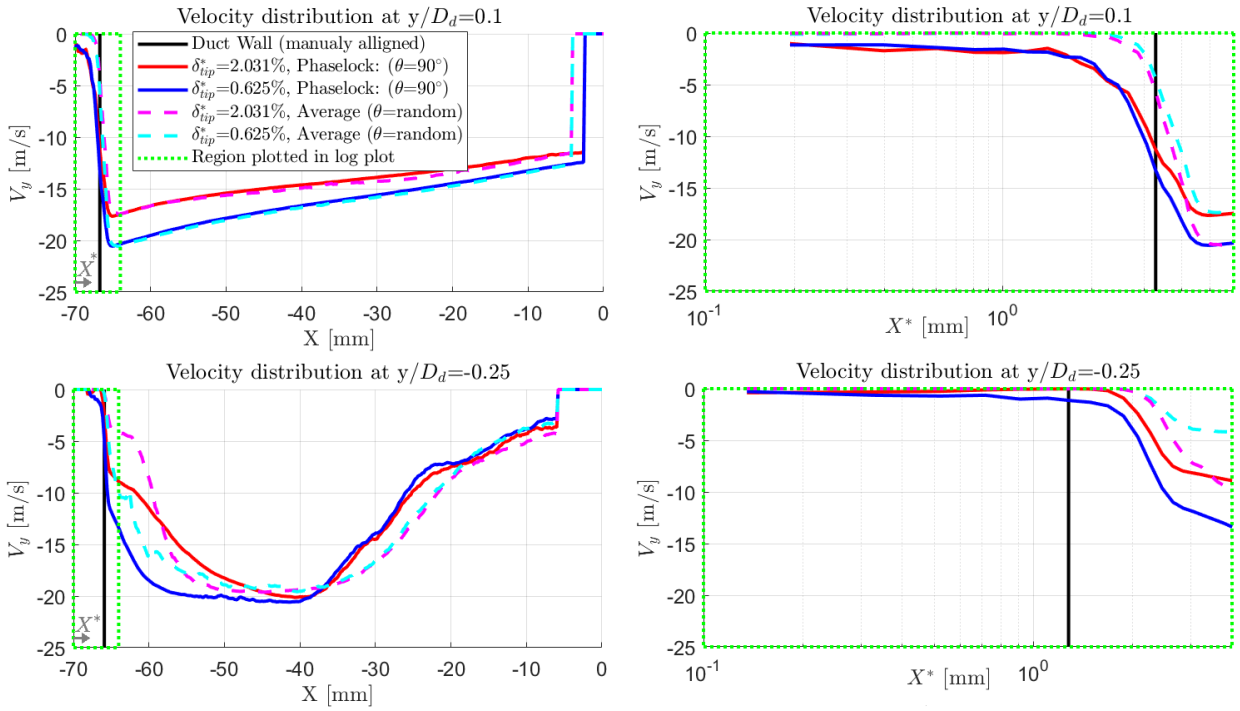

Figure 5.14: Distribution of the velocity in Y-direction at Y/D_d =0.1 and Y/D_d=-0.25, for the phase-locked and mean velocity fields, of two different tip gap ratios at Ω=11000 RPM.

5.5. Rotor tip vortex trajectory and breakdown

This section describes how the trajectory and breakdown of the rotor tip vortices are affected by the tip gap.

As explained in section 5.4.1, only the PIV measurements at a rotor phase of θ=90° are not disturbed by the laser reflections on the rotor and duct. This causes the velocity field to have inaccurate data in some local areas of the mid-plane of the duct for other rotor phases (see and appendix A). However, for the rotor phases θ=45° and θ=135°, these reflections were only present near the center of the rotor hub. On the outside (close to the duct wall), no disturbing reflections were present for the phase-locked experiments at θ=45° and θ=135°. This means that the data of these experiments is still suitable to analyse the trajectory of the rotor tip vortices along the duct diffuser wall.

In figure 5.15, the vorticity contours ω_z are plotted for three rotor phases: θ=45°, θ=90° and θ=135°. For each rotor phase, the resulting vorticity field is based on the average of 500 phase-locked measurements. As mentioned earlier in section 5.4.1, there is a deviation in the phase position of the rotor of roughly ±7°, which effectively spreads the vortex cores in axial direction. By plotting the results of multiple rotor phases in on figure, the evolution of the vortices can be tracked. Furthermore, in figure 5.16, the velocity fields at θ=45° and θ=90° zoomed in at the vortex cores are shown. Based on figure 5.15 and 5.16, the following main observations and analyses are made:

- **Initial strength of the tip vortices**
  When comparing the strength of the vortices right after the rotor plane in figure 5.15, it can be seen that the vortices are much more distinct for the large tip gap case. The zoomed in velocity contours of figure 5.16 show this as well: for the large tip gap case a very clear vortex can be seen at θ=45°. For the small tip gap case on the contrary, the vortex at θ=45° is not so clear, with only a very small zone very the vectors are pointing upwards. As mentioned earlier there is less leakage flow if the tip gap is decreased. The closer proximity of the duct wall seals the gap, and prevents the rolling up of a strong vortex from the pressure side of the blade to the suction side.

- **Convection speed of the tip vortices**
  Not only the strength, but also the spacing of the rotor tip vortices is affected by the tip gap. When comparing the height of the vortices of each phase θ in figure 5.15, it can be seen that the vortices are convected downstream much faster if the tip gap is smaller. For example, the vortex core of θ=135° is positioned at Y/D_d=-0.2 for the large tip gap, but already at Y/D_d=-0.27 for the small tip gap. As explained in section 5.4.1, this is related to the fact that the vortices decelerate the flow close to the duct wall, because they induce a velocity opposite to the flow direction in the boundary layer (see illustration in figure 3.7 on page 19). This effect is more pronounce for the large tip gap case, because the vortices are much stronger here.

- **Trajectory of the tip vortices**
  Figure 5.15 shows that also the trajectory of the vortices is affected by the tip gap. For the small tip gap, the vorticity of each rotor phase θ is located very close to the duct wall. The last visible remainder of the vortex (at θ=135°) still follows the expanding shape of the diffuser. For the large tip gap on the contrary, the vortices have a slightly contracting trajectory. Already the first vortex (at θ=45°) is located further from the wall compared to the small tip gap case, and the distance to the duct wall increases if the vortex is convected downstream. As explained in section 5.4.1, this is disadvantageous for the performance of the duct because it reduces the capability of the diffuser to expand and accelerate the flow through the duct.

- **Breakdown of the tip vortices**
  In figure 5.15 and 5.16 it is immediately noticeable that for the small tip gap the tip vortices completely break down around Y/D_d=-0.2, whereas for the large tip gap the vortices are clearly visible beyond the outlet of the duct. This is in line with earlier studies [32] [5] where a faster breakdown of the vortices was related to the closer proximity of the duct wall (see section 3.2.3).

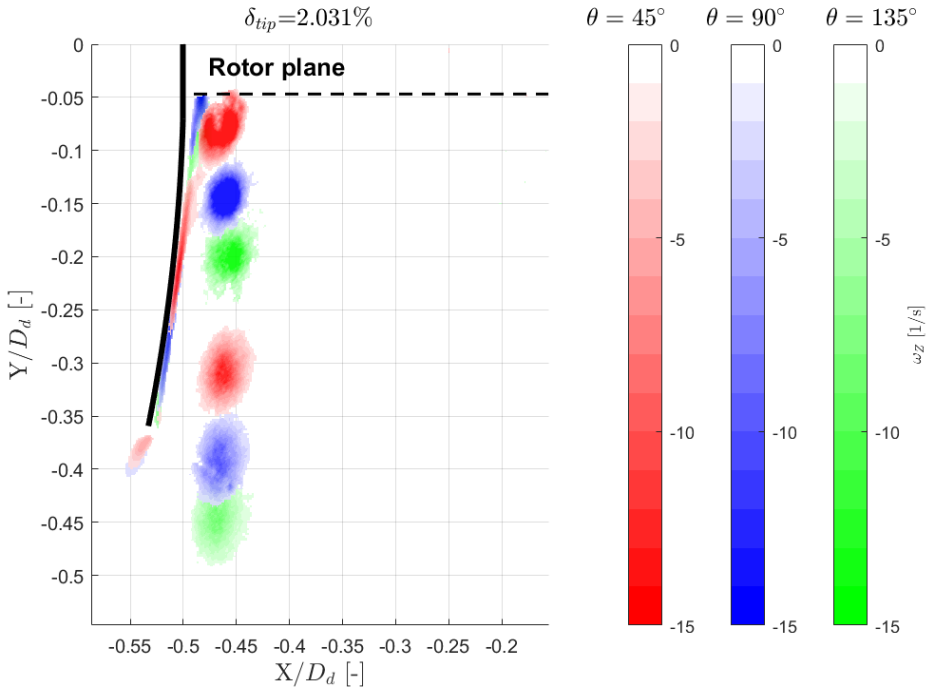

(a)

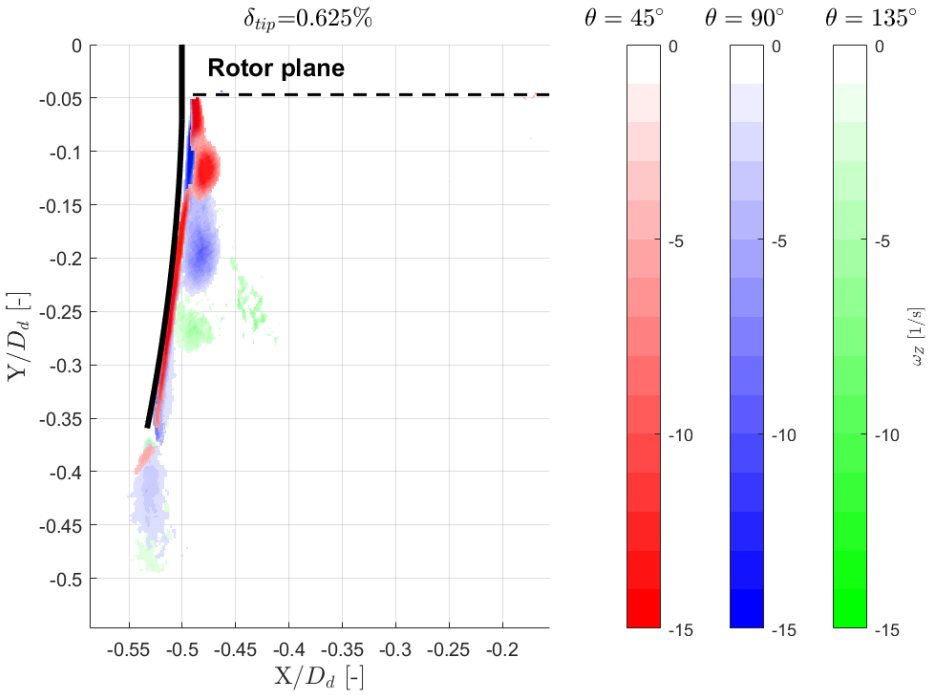

(b)

Figure 5.15: Phase-locked Vorticity ω_z in the duct for rotor phase θ=45°,θ=90° and θ=135° at Ω=11000 RPM, for two different tip gap ratios: δ^*_{tip}=2.031% (a) and δ^*_{tip}=0.6251% (b)

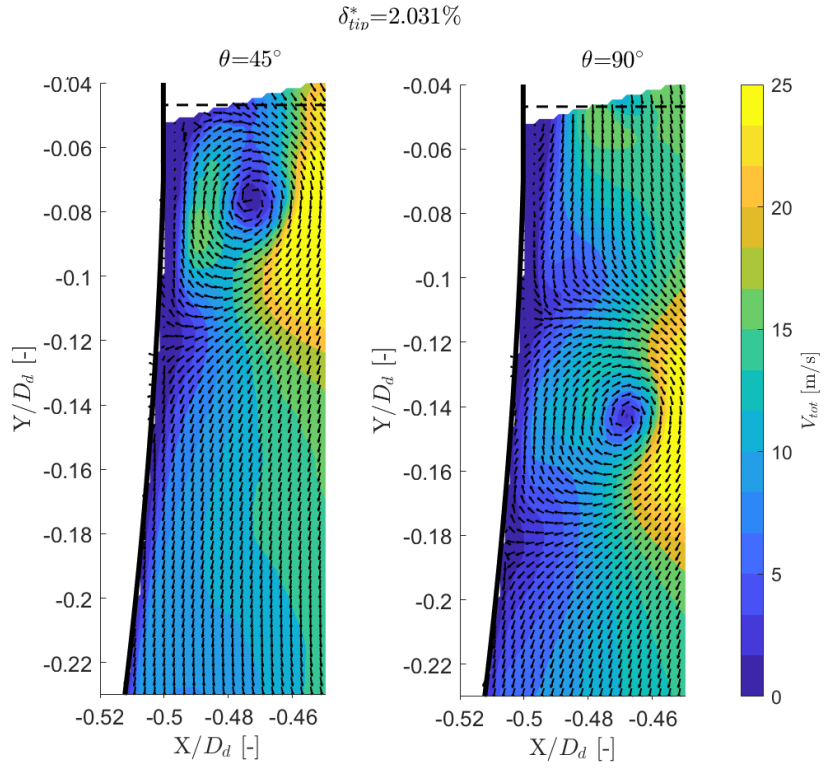

(a)

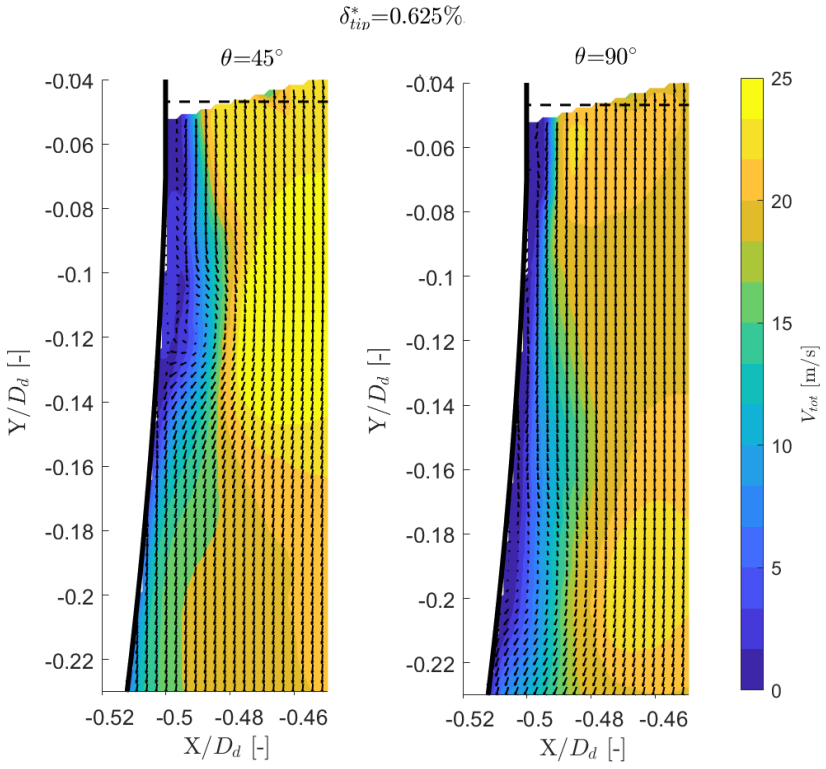

(b)

Figure 5.16: Total velocity in the duct (Zoomed in) at two different rotor phases θ and Ω=11000 RPM, for two different tip gap ratios: δ^*_{tip}=2.031% (a) and δ^*_{tip}=0.6251% (b)

5.6. Preliminary results: effect of the tip gap on the aeroacoustic noise

Even though the current study mainly focuses on the aerodynamics of ducted rotors in hover, at the end of the experimental campaign some aeroacoustic experiments were performed as well. As explained in section 4.5, the far-field noise of the ducted rotor was measured with a microphone array for two different tip gaps. In this section these preliminary results are presented.

In order to measure only the aeroacoustic noise of the ducted rotor, it has to be ensured that other noise sources such as the motor are not dominating the acoustics. In figure 5.17, the sound pressure level spectrum of the ducted rotor is compared with that of only the spinning motor, at two different microphone positions. It can be seen that the noise of the motor only is much lower than the noise of the ducted rotor, which allows to make the assumption for all other results that the measured total noise is indeed the aeroacoustic noise of the ducted rotor system.
Furthermore, as mentioned earlier in section 4.5, the facility for the acoustic experiments has anechoic properties only above 100 Hz. To account for this, a filter is applied to delete the noise below 100Hz. Figure 5.17 shows how this filter affects the SPL spectrum of the ducted rotor system. This filter is applied to all results presented later in this section.

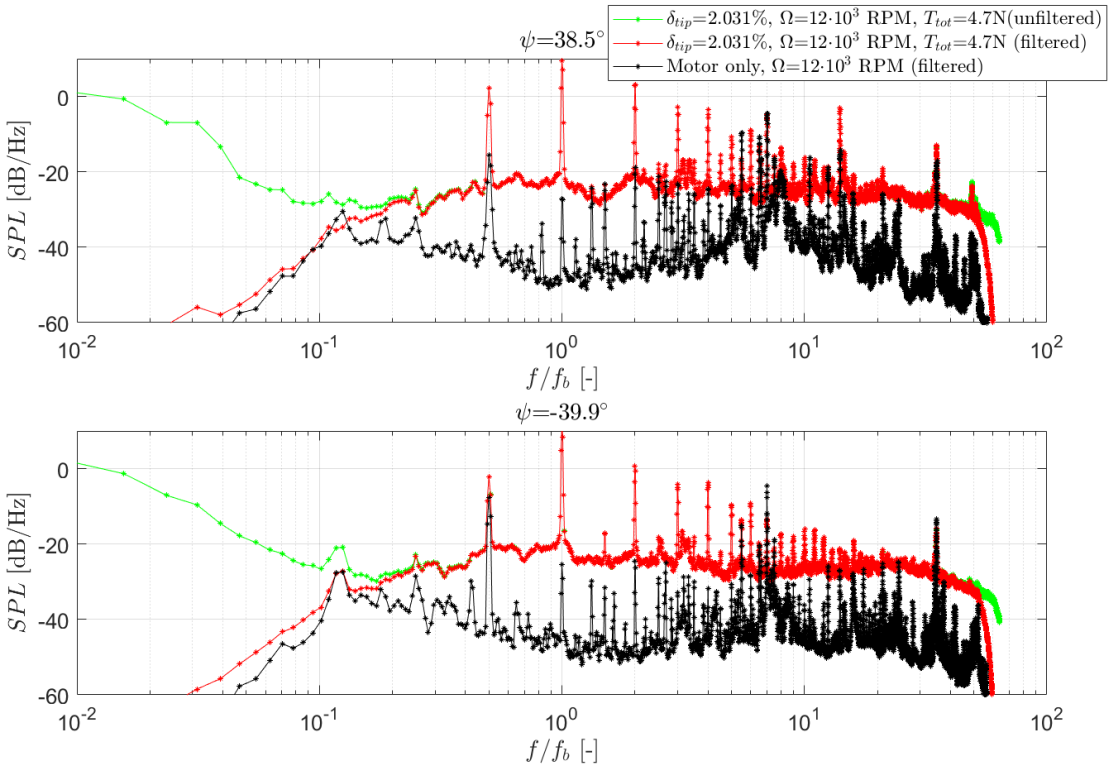

Figure 5.17: Sound pressure level spectrum for the ducted rotor and motor only configurations, at microphone positions ψ=38.5° and ψ=-39.9°

A straight-forward way to investigate the noise of a ducted rotor for different tip gaps, is by comparing the two tip gap cases at the same rotational speed Ω. This gives the best insight in how the aeroacoustic noise physically changes with the tip gap, because at constant Ω the blade pass frequency f_b is constant as well. However, as shown in the results of section 5.2, changing the tip gap also strongly affects the total thrust of the ducted rotor. Arguably, a fairer way to compare the noise for different tip gaps, is by keeping the total thrust of the system constant. Namely, in practice an aerial vehicle in hover operates at a constant level of thrust (equal to its weight). If the noise of two different configurations is compared at a different level of thrust, it means that for one of the configurations the rotational speed could be lowered, which then also lowers the noise.

Therefore, in this section the noise for the two different tip gap cases is compared at the same rotational speed as well as the same level of thrust. The case with large tip gap (δ^*_{tip}=2.031%) is evaluated at a rotational speed of 12000 RPM and a total thrust of 4.7N. The small tip gap case (δ^*_{tip}=0.625%) is evaluated at the same rotational speed of 12000 RPM, but also at 11000 RPM such that the total thrust is equal to 4.7N. In figure 5.18 it is illustrated how these operating conditions enable to compare at the same rotational speed and level of thrust.
Figure 5.19 shows the noise directivity of the ducted rotor for two different tip gaps, compared at the same rotational speed and level of thrust. Here, the overall sound pressure level ($OASPL$) is plotted for all the microphone positions in the array. The results in figure 5.19 present the sound level at a distance of 10 times the duct throat diameter D_d. Based on the the results presented in figure 5.19, the following observations and analyses are made regarding the effect of the tip gap on the aeroacoustic noise:

- **Directivity pattern:**
  Figure 5.19 shows that the directivity pattern is the same for all tip gaps and operating conditions. Two lobes of higher noise are identified upstream ($+\psi$) and downstream ($-\psi$) of the rotor. In the middle (at ψ=0°, the overal sound pressure level is very low. This local zone of lower noise can be related to the shielding effect of the duct, as observed in an earlier study of Malgoezar et al. [21].

- **Effect of the tip gap on the overall sound pressure level:**
  When comparing the overall sound pressure level for different tip gaps at the same rotational speed Ω in figure 5.19, it can be seen that the small tip gap case produces significantly more noise in every direction (between 1.5-2 dB). On the contrary, when the comparison is performed at the same level of total thrust, the small tip gap case leads to a lower noise in almost every direction (except for the lowest microphone position).

The directivity plot of figure 5.18 clearly presents the relation between the tip gap and the total noise of the ducted rotor system. It is however hard to derive from this plot how and why the aeroacoustic noise changes with the tip gap. A deeper insight into the aeroacoustic noise can be obtained by considering the SPL-spectra instead of the integrated overall sound pressure level $OASPL$. Namely, by analysing the frequency characteristics of the noise, it is possible to relate the observed noise changes to certain physical aerodynamic mechanisms. Even though a thorough analysis of the noise falls outside the scope of the current study, the noise spectra of the microphones at ψ=38.5° and ψ=-39.9° are included in appendix B. The main observation here is that the high frequency broadband noise always increases with a smaller tip gap, but no conclusions are drawn about the physical cause of this effect.

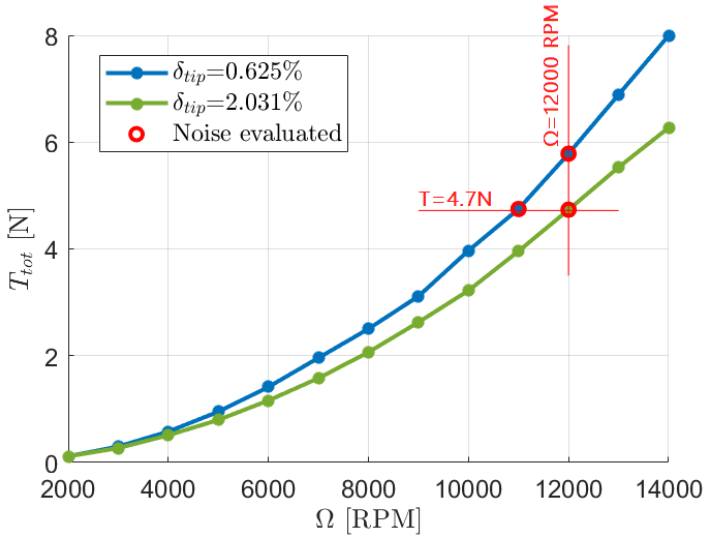

Figure 5.18: Rotational speed plotted v.s. total thrust for the ducted rotor with two different tip gaps. The red marked operating points are evaluated in the acoustic experiments

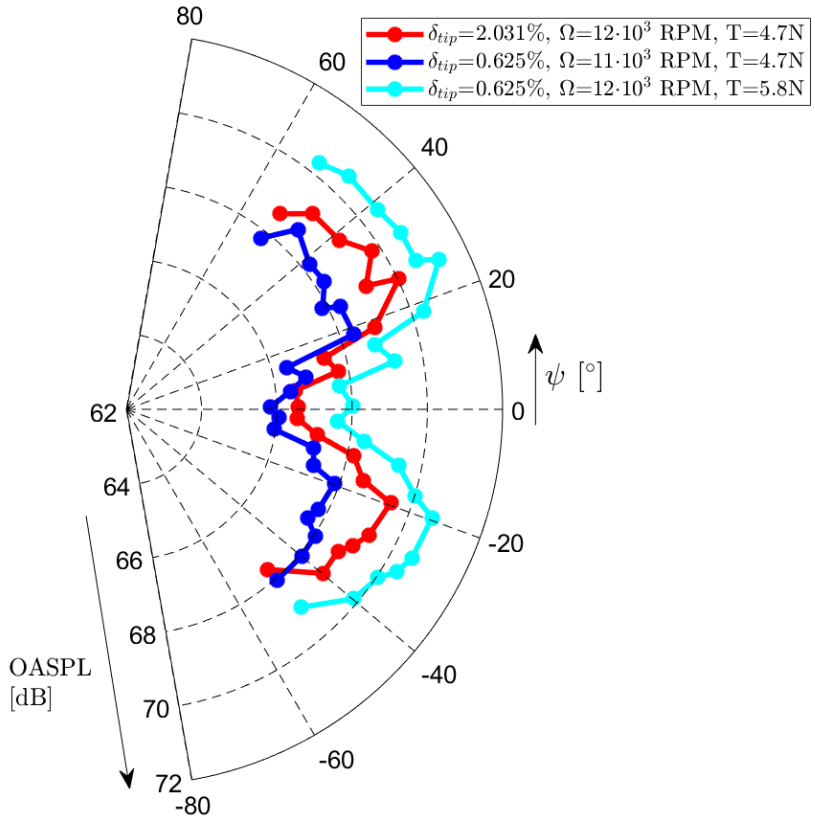

Figure 5.19: Ducted rotor noise directivity for two different tip gaps, at a distance of $10D_d$. The two tip gap cases are compared at the same rotational speed (Ω=12000 RPM) and the same level of thrust (T_{tot}=4.7N)

6

Conclusions and recommendations

6.1. Conclusions

With the rapidly evolving markets for Urban Air Mobility (UAM) and Micro Air Vehicles (MAV), there is a growing demand for efficient propulsion systems that operate primarily in hover. These developments have led the ducted rotor configuration to emerge as a popular design solution. The performance of a ducted rotor is subject to the complex aerodynamic interaction between the rotor and duct. The degree of interaction between rotor and duct strongly depends on the tip gap δ_{tip}, which is defined as the radial distance between the rotor blade tip and the circumferential wall of the duct. The tip gap is therefore a major parameter in the design of a ducted rotor system.

The aim of the current study is to investigate in detail how the tip gap affects the aerodynamic performance of a small-scale ducted rotor in hover. In order to achieve this, three types of experiments are performed on a single ducted rotor system: The performance of the ducted rotor system is characterized through force measurements with load-cells, the pressure distribution over the duct profile is measured with static-pressure tabs in the duct inner-wall, and the flow field inside the duct is retrieved and analyzed using PIV- (particle image velocimetry) measurements. The main parameter varied throughout these experiments is the size of the tip gap. Additionally, a set of acoustic experiments is performed to investigate if and how the tip gap affects the aeroacoustic far field noise of the ducted rotor. Based on the results of all these experiments, the following conclusions are drawn:

Aerodynamic performance of the ducted rotor sytem:

- The ducted rotor system investigated in this study has a significantly higher aerodynamic efficiency compared to a reference rotor in open air. With a figure of merit FM above 1, the ducted rotor system outperforms rotors in open air, which typically operate at a FM between 0.6 and 0.67 for small-scale and low-Re configurations.
- When investigating the performance of ducted rotors, it is important to use a rotor whose blade geometry is designed to operate inside a duct. This ensures that the rotor operates at roughly the right angle of attack along the entire span of the blade, which is essential for investigating and evaluating the flow inside the duct for different tip gaps. Moreover, quantitative comparisons (for example the noise level of different configurations) can only be performed in a fair way if the system operates at its intended design conditions. The ducted rotor investigated in this study has a 20% higher FM compared to a standard reference rotor in the same duct, which underlines the importance of selecting the right rotor geometry when investigating a ducted rotor configuration.
- Up to 55% of the total thrust of the ducted rotor is generated by the duct itself. The duct thrust is caused by the suction at the inlet lip, where the vectors normal to the duct profile are pointed in thrust-direction. In the diffuser on the contrary, these vectors normal to the duct profile are pointed downwards (opposite to the thrust-direction). Even though this causes the duct to generate a small amount of negative thrust, its presence is critical for the below-the-rotor pressure recovery and for establishing a high axial throughflow.

- The efficiency (figure of merit FM) of the rotor itself (excluding the duct thrust) is lower inside a duct compared to its performance in open air. This observation is consistent with several other studies. The performance decrease is caused by the increased axial velocity inside a duct compared to open air. The same velocity increase is however also related to a lower pressure at the duct inlet lip, which increases the duct thrust. Therefore, when including the duct thrust, the overall performance of the ducted rotor system is still better compared to the case in open air.

Effect of the tip gap on the aerodynamic performance:

- The tip gap has a very significant effect on the thrust generated by the duct. If the tip gap ratio is increased from 0.625% to 2.422%, the duct generates roughly 40% less thrust. This causes the figure of merit FM of the ducted rotor system to decrease from 1.02 to 0.78.
- Surprisingly, the tip gap does not strongly affect the performance of the rotor itself. The thrust coefficient of the rotor remains constant for different tip gaps, and the power coefficient only slightly decreases when increasing the tip gap ratio from 0.625% to 2.422%. The relatively small effect of the tip gap on the rotor performance is related to the fact that the rotor has only 2 blades. For a rotor with a higher blade-number, the performance is more likely to be prone to the size of the tip gap.
- The characteristics of the rotor tip vortices strongly depend on the tip gap. With a small tip gap ratio (δ^*_{tip}=0.625%), a weak vortex is identified right after the rotor plane, which completely breaks down halfway through the duct. The (remainder of) the vortex has a trajectory that follows the expanding contour of the diffuser well. With a large tip gap ratio (δ^*_{tip}=2.013%) on the contrary, a strong vortex can be observed that does not break down (even not after leaving the duct). The trajectory of this vortex is slightly contracting, which means that the vortex 'separates' from the diffuser. Furthermore, the vortices are also convected downstream slower with a large tap compared to a small tip gap (which means they are spaced more closely together).
- When decreasing the tip gap ratio from 2.013% to 0.625%, a higher axial velocity is observed almost everywhere in the duct. The velocity increase is especially strong on the outside (close to the duct wall), but is also clearly present all the way to the duct center. It is hypothesized that the increased velocity is related to three phenomena. Firstly, a smaller tip gap seals the suction and pressure side of the rotor better, which reduces the presence of a tip leakage flow and the formation of tip vortices. Secondly, the tip vortices convected along the diffuser decelerate the flow close to the duct wall, because here they induce a velocity opposite to the axial flow direction. This causes a thick layer of low velocity to appear close to the diffuser wall for the large tip gap case. Thirdly, the diffuser cannot effectively expand the flow for the large tip gap case, which is indicated by the contracting trajectory of the rotor tip vortices, as well as the collapsed pressure distribution profiles. This then affects the velocity distribution upstream in the duct.
  The observed velocity increase for a smaller tip gap directly relates to the lower measured static-pressure all over the duct profile. Especially at the duct inlet lip the pressure strongly decreases, which increases the suction force. This explains the 40% increase of duct thrust for the smaller tip gap case.

Effect of the tip gap on the aeroacoustic noise:

- When evaluating the aeroacoustic noise of the ducted rotor system at constant rotational speed (Ω=12000 RPM), a smalller tip gap leads to a noise increase in all directions. Decreasing the tip gap ratio δ^*_{tip} from 2.031% to 0.625% increases the overall sound pressure level $OASPL$ between 1.5 and 2 dB.
- On the contrary, when evaluating the aeroacoustic noise of the ducted rotor system at constant thrust (T=4.7N), a smaller tip gap leads to a decrease of noise in almost all directions of about 1dB. Only for the most downstream positioned microphone (ψ=-49°), the small tip gap case has a higher $OASPL$ than the large tip gap case.
- When comparing the noise spectra of the two different tip gap cases (δ^*_{tip}=2.031% and δ^*_{tip}=0.625%), the most distinct difference is that the configuration with smaller tip gap always produces more broadband noise at high frequencies (above 8 times the blade pass frequency). This is the case for both the comparison at constant rotational speed and constant level of thrust, and is observed at all microphones positions. The physical mechanism that is responsible for this increase in broadband noise is not clearly identified.

6.2. Recommendations

The following recommendations are given for future studies in the field of ducted rotor aerodynamics and aeroacoustics:

- For the PIV measurements, the reflections of the laser on the duct wall and rotor blade impeded the accuracy of the velocity fields. For rotor phases other than θ=90°, this caused inaccuracies to appear at some local zones the middle of the velocity field. Furthermore, the velocity data in the first 1.5mm close to the duct wall turned out to be unreliable, which made it impossible to analyse the velocity profiles in the boundary layer. All these issues are related to the reflectivity of the duct and rotor material. Therefore, for future studies it is strongly recommended to put more effort in darkening the duct and rotor before conducting the PIV measurements. This will improve the accuracy of the results, and saves a lot of time in the post-processing of the PIV data.

- For the current study, only the perfect hover flight condition was considered for all experiments. In practice however, aerial vehicles also have some forward velocity when flying around. Therefore it would be interesting to extend the work of the current study by performing the same experiments with various free-stream velocities.

- This study highlights that ducted rotors in hover significantly outperform rotors in open air. The performance increase is mainly related to the suction at the inlet lip, which enables the duct to generate a large amount of thrust. The optimal geometry of the duct has been investigated in several studies, but only for conventional (airfoil-like) shapes. There are very few studies that have considered completely new geometries, such as a double stacked inlet lip. It would be interesting to investigate if its possible to further improve the performance of a ducted rotor with unconventional ideas that are based on the same basic concept: namely the placement of an additional geometry in the low pressure zone upstream of the rotor, such that effectively a force in the thrust direction is generated.

- In this study, the aeroacoustic performance of the ducted rotor system was only briefly investigated, because the main focus was to investigate the aerodynamic performance. Some preliminary results were presented of the noise for two different tip gaps, which showed that the tip gap has an effect on the overall sound pressure level. However, no conclusions were drawn about the physical mechanisms that underlie these noise changes. An increase of broadband noise was consistently observed for smaller tip gaps (see appendix B), but no physical explanation was provided for this observation.
  In existing literature there also seems to be no consensus as to how the tip gap affects the aeroacoustic noise of a ducted rotor system. Several studies mention a change in the aeroacoustic noise that is associated with rotor-duct interaction [21] [32] [5] [31]. Even though for all these studies a noise increase is observed with the (nearer) presence of a duct, the frequency characteristics and magnitude of the noise changes are completely different.
  This lack of clarity provides a clear basis for a new study into the aeroacoustic performance of ducted rotors. The preliminary results of the current study could be expanded, such that a thorough analysis can be performed about how and why the tip gap affects the noise of the system. Ultimately, a better understanding on this topic can contribute to improving the design of ducted rotors for noise.

A

Inaccuracy of PIV results for certain rotor phase positions

As mentioned in section 5.4.1, for all rotor positions other than θ=90°, the reflections on the rotor blade interfered with the results of the PIV experiments. Therefore, the phase-locked velocity fields at θ=90° are presented as the most accurate results in the main body of this report. However, in section 5.4.2 the mean velocity field was still presented for comparison. In this appendix it is briefly described what parts of the mean velocity fields are inaccurate due to the laser reflections on the rotor blade.

In figure A.1 it is shown what the original results of the mean velocity field look like. The red circles indicate the areas where the derived velocity field is strongly affected by the laser reflections.

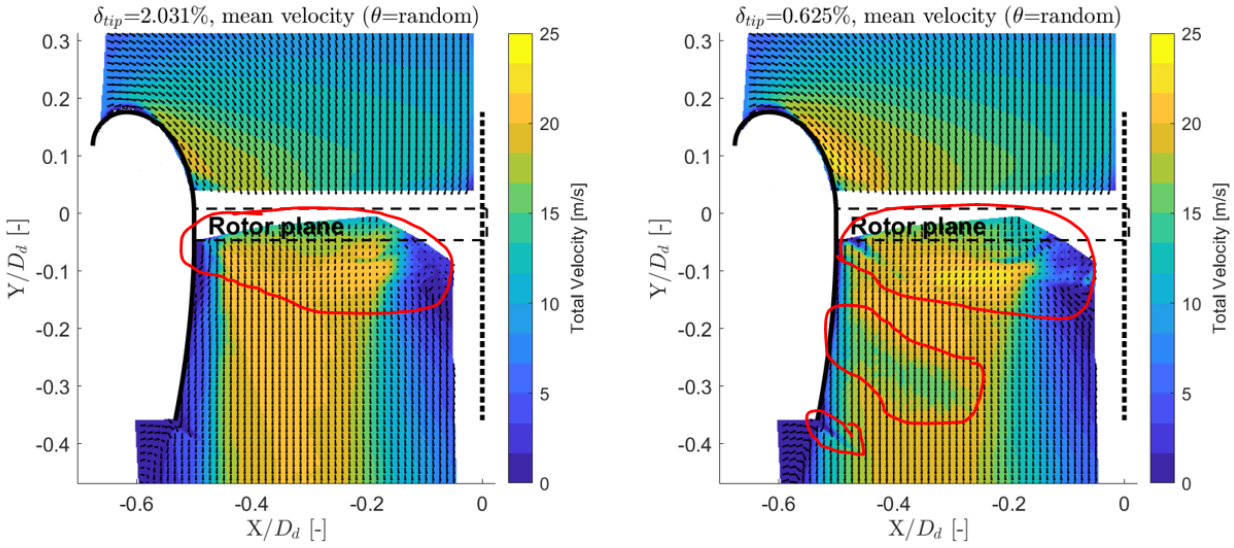

Figure A.1: Original results of the mean total velocity in the duct. The red circles indicate the zones with inaccuracies that are caused by the reflections of the rotor blade

Figure A.2 shows the adapted results, which are the same results that are presented in the main body of this report (section 5.4.2). The results have been improved compared to figure A.1, by masking large areas where the reflections on the rotor disturbed the PIV measurements. Furthermore, manual post-processing steps were used to improve the non-physical low velocity zone between Y/D_d=-0.2 and Y/D_d=-0.3: some images with extreme reflections were removed manually, and additional time-substract filters were applied to some subsets of the 500 random measurements to improve the visibility of particles in front of reflections. It can be seen that these steps improved the results, but still some zones with inaccurate data remain (indicated by the red circle). Moreover, apart from these clearly visible inaccuracies, it is well possible that the data elsewhere

in the velocity field is also (slightly) affected. Therefore, the absolute values of the mean velocity field are not completely reliable. It can however still be used to analyse the main differences between the large and small tip gap case. Also, the mean velocity upstream of the rotor is completely reliable, because no issues with reflections occurred here.

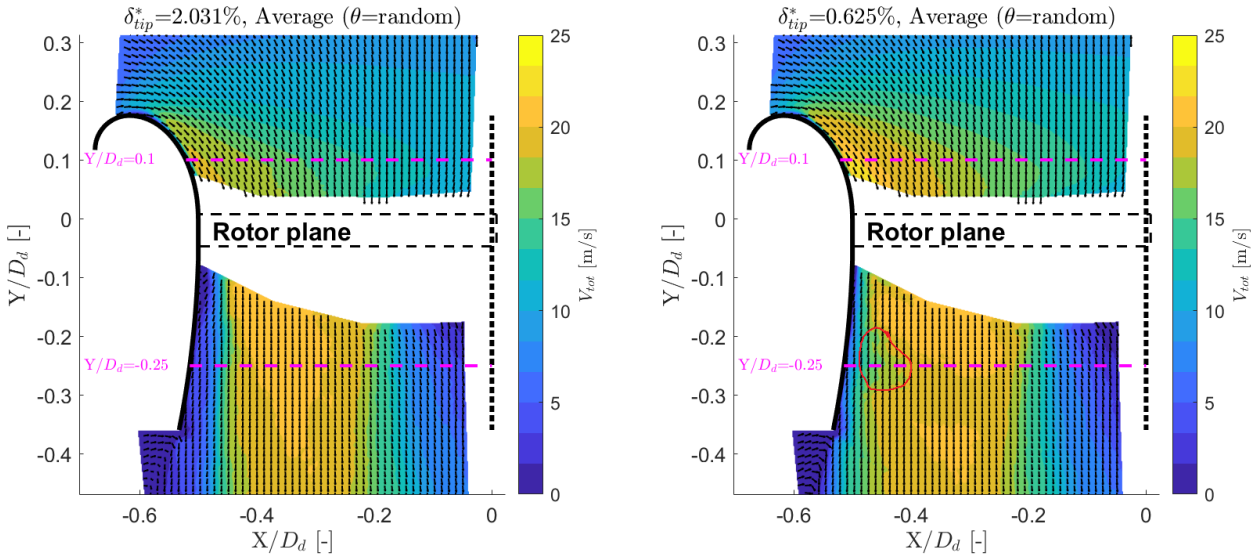

Figure A.2: Adapted results of the mean total velocity in the duct. The red circle indicates the zone with inaccurate results that could not be resolved with specific post-processing steps

B

Noise spectra

In the main body of this report, some preliminary results of the acoustic experiments are presented (see section 5.6). It is shown how the overall noise of the ducted rotor system changes with the tip gap, when comparing the two cases at constant rotational speed and constant level of thrust. In the figure 5.18 of section 5.6, the overall sound pressure level $OASPL$ is plotted for all microphone positions in a directivity plot. As explained section 4.5, the $OASPL$ is obtained by integrating the sound pressure level SPL over all frequencies. In this appendix, the SPL-spectra are included for the microphones at ψ=38.5° and ψ=-39.9°.

Figure B.1 shows the comparison of the two tip gap cases at constant rotational speed, and figure B.2 shows the comparison at constant level of thrust. In these figures, the frequency on the x-axis is divided by the blade pass frequency f_b, such that the tonal peaks can easily be identified.

When compared at the same rotational speed (see figure B.1), the smaller tip gap leads to a slightly higher sound pressure level across the complete spectrum. The most distinct difference is that at higher frequencies (above 8 times f_b), there is significantly more broadband noise for the small tip gap case. When compared at the same thrust (see figure B.2), the smaller tip gap case has a slightly lower sound pressure level across most of the spectrum. The highest peak at the blade pass frequency is also significantly lower, due to the decreased rotational speed. For high frequencies however, the small tip gap case has significantly more broadband noise, similarly to the comparison at constant rotational speed. When comparing the results of the upstream (ψ=38.5°) and downstream (ψ=-39.9°) located microphones, no major differences are observed in the characteristics of the sound pressure level spectra.

Considering all noise spectra, the most distinct difference between the small and large tip gap cases, is that a smaller tip gap increases the broadband noise above $8 \cdot f_b$ (both when comparing at the same rotational speed and same level of thrust). This conclusion is in line with the results presented in the study of Avallone et al.[5], who also observed an increase of high frequency broadband noise when the tip gap is decreased. In the study of Avallone et al., the increased broadband noise was associated to a larger intensity of velocity fluctuations along the duct diffuser, due to earlier flow separation for the smaller tip gap case. This explanation does however not apply to the current study. As shown in section 5.4 and 5.5, there are much more velocity fluctuations along the duct diffuser wall for the large tip gap case, due to the presence of the tip vortices. Therefore it remains unclear what physical flow effect causes the observed increase of high frequency broadband noise for smaller tip gaps in this study. Moreover, for the study of Avallone et al. a ducted wind-turbine was investigated instead of a ducted rotor, which makes it risky to make direct comparisons between these two completely different cases.

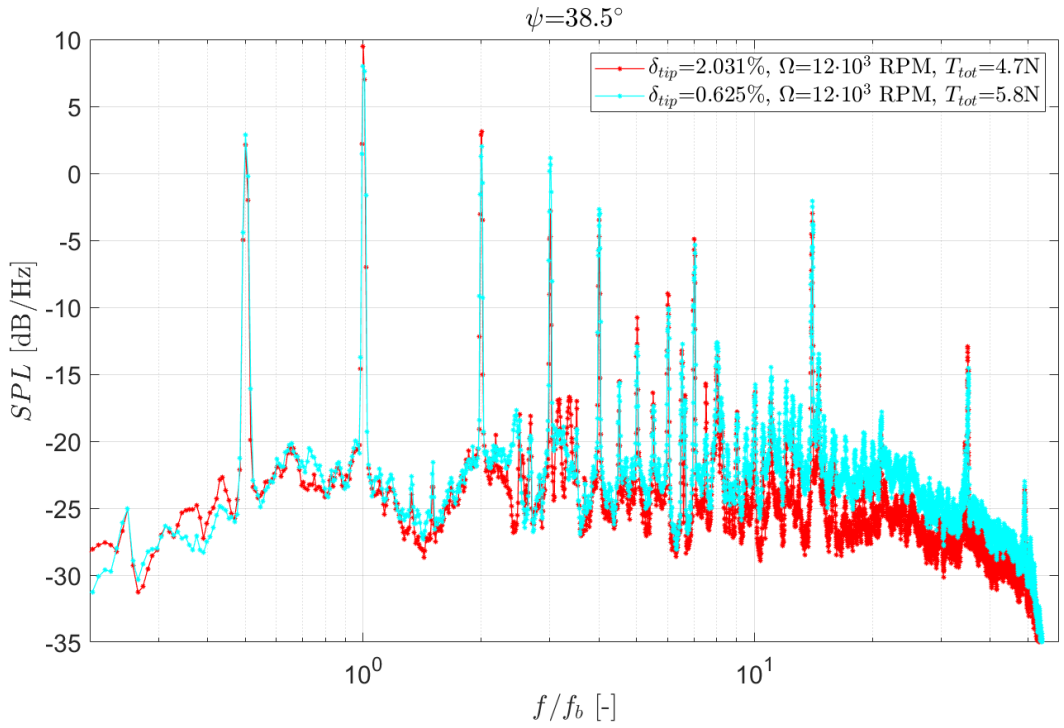

(a)

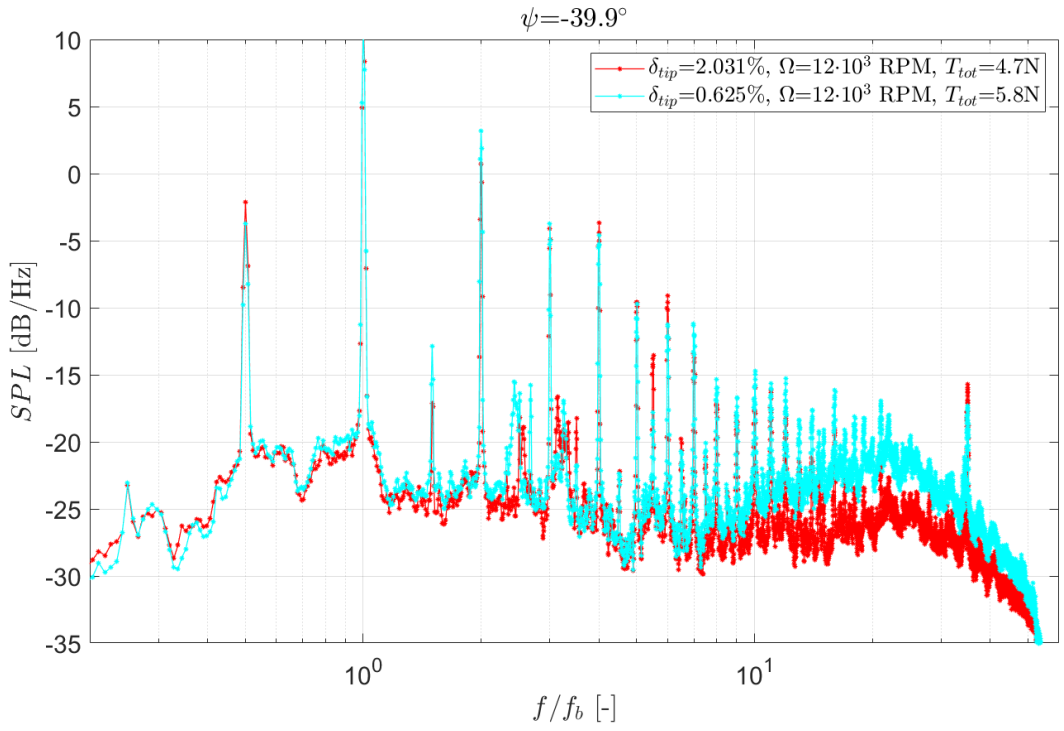

(b)

Figure B.1: Sound pressure level spectrum for the small and large tip gap case, compared at the same rotational speed (Ω=12000 RPM), and for two microphone positions at a distance of $10D_d$. The blade pass frequency f_b is 400Hz

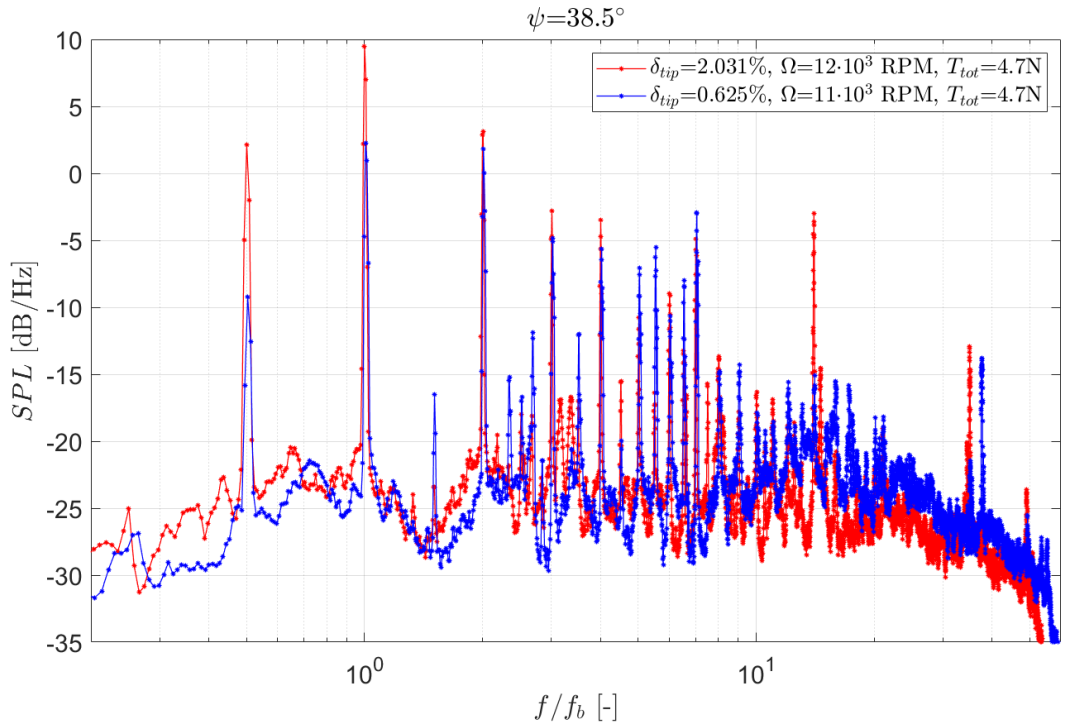

(a)

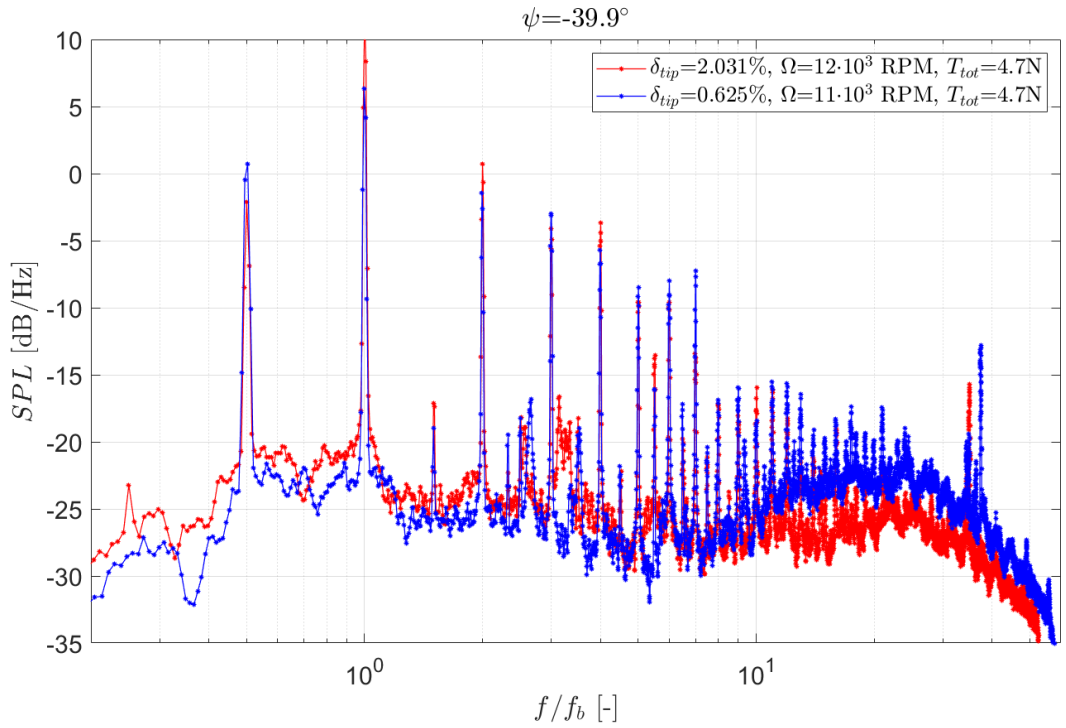

(b)

Figure B.2: Sound pressure level spectrum for the small and large tip gap case, compared at the same thrust (T_{tot}=4.7N), and for two microphone positions at a distance of $10D_d$.The blade pass frequencies f_b are 400Hz and 433.3Hz

Bibliography

[1] Federal Aviation Administration. *Pilot's Handbook of Aeronautical Knowledge*. U.S. Dept. of Transportation, Federal Aviation Administration, 2016. ISBN 9781619544734. URL https://www.faa.gov/regulations_policies/handbooks_manuals/aviation/phak/media/pilot_handbook.pdf.

[2] J. Ahn and K. Lee. *Performance Prediction and Design of a Ducted Fan System*. doi: 10.2514/6.2004-4196. URL https://arc.aiaa.org/doi/abs/10.2514/6.2004-4196.

[3] A. Akturk and C. Camci. Experimental and computational assessment of a ducted-fan rotor flow model. *Journal of Aircraft*, 49:885–897, 05 2012. doi: 10.2514/1.C031562.

[4] A. Akturk and C. Camci. Tip Clearance Investigation of a Ducted Fan Used in VTOL Unmanned Aerial Vehicles—Part I: Baseline Experiments and Computational Validation. *Journal of Turbomachinery*, 136 (2), 09 2013. ISSN 0889-504X. doi: 10.1115/1.4023468. URL https://doi.org/10.1115/1.4023468.021004.

[5] F. Avallone, D. Ragni, and D. Casalino. On the effect of the tip-clearance ratio on the aeroacoustics of a diffuser-augmented wind turbine. *Renewable Energy*, 152:1317–1327, 2020. ISSN 0960-1481. doi: https://doi.org/10.1016/j.renene.2020.01.064. URL https://www.sciencedirect.com/science/article/pii/S0960148120300768.

[6] M. Benedict, J. Winslow, Z. Hasnain, and I. Chopra. Experimental investigation of micro air vehicle scale helicopter rotor in hover. *International Journal of Micro Air Vehicles*, 7(3):231–255, 2015. doi: 10.1260/1756-8293.7.3.231. URL https://doi.org/10.1260/1756-8293.7.3.231.

[7] H. Bento, R. de Vries, and L. Veldhuis. Aerodynamic performance and interaction effects of circular and square ducted propellers. *AIAA Scitech 2020 Forum Orlando*, 2020.

[8] D. Bies, C. Hansen, and C. Howard. *Engineering Noise Control, Fifth Edition*. 11 2017. ISBN 1498724051.

[9] E. Branlard. *Momentum Theory*, pages 157–180. 04 2017. ISBN 978-3-319-55163-0. doi: 10.1007/978-3-319-55164-7_9.

[10] R. Deters, G. Ananda, and M. Selig. Reynolds number effects on the performance of small-scale propellers. 06 2014. ISBN 978-1-62410-288-2. doi: 10.2514/6.2014-2151.

[11] M. Drela. Xfoil formulation. *MIT Aero and Astro*, 11 2001. URL https://web.mit.edu/drela/Public/web/xfoil/.

[12] M. Drela. Qprop formulation. *MIT Aero and Astro*, 06 2006. URL http://web.mit.edu/drela/Public/web/qprop/qprop_theory.pdf.

[13] Flyability, 2019. URL https://www.flyability.com/.

[14] Aerodynamcis for Students. Blade element theory for propellers. URL http://www.aerodynamics4students.com/propulsion/blade-element-propeller-theory.php.

[15] W. Hongwei, Z. Huang, G. Jian, and X. Hongliang. The optical flow method research of particle image velocimetry. *Procedia Engineering*, 99:918–924, 12 2015. doi: 10.1016/j.proeng.2014.12.622.

[16] V. Hrishikeshavan, J. Black, and I. Chopra. Design and performance of a quad shrouded rotor micro air vehicle. *Journal of Aircraft*, 51:779–791, 03 2014. doi: 10.2514/1.C032463.

[17] J. Salomon J. Ledoux, S. Riffo. Analysis of the blade element momentum theory. *hal-02550763*, 2020. URL https://hal.archives-ouvertes.fr/hal-02550763v1.

[18] C. Keys, M. Sheffler, S. Weinier, and R. Herminway. Lh wind tunnel testing: Key to advanced aerodynamic design. *American Helicopter Society 47th Annual Forum Proceedings*, 152:77–87, 1991.

[19] P. Lampart. Tip leakage flows in turbines. *TASK QUARTERLY*, 10:139–175, 01 2006.

[20] J. Leishman. *Principles of Helicopter Aerodynamics*. Cambridge University Press NY, 2000.

[21] A. Malgoezar, A. Vieira, M. Snellen, D. Simons, and L. Veldhuis. Experimental characterization of noise radiation from a ducted propeller of an unmanned aerial vehicle. *International Journal of Aeroacoustics*, 18:372–391, 2019. doi: 10.1177/1475472X19852952.

[22] B. Mandal and H.P. Mazumdar. The importance of the law of the wall. *International Journal of Applied Mechanics and Engineering*, 20, 12 2015. doi: 10.1515/ijame-2015-0055.

[23] P. Martin and C. Tung. Performance and flowfield measurements on a 10-inch ducted rotor vtol uav. *NASA Technical Reports*, 06 2004. URL https://ntrs.nasa.gov/citations/20050009943.

[24] S. Mohsen A. Moghadam, M. Meinke, and W. Schröder. Analysis of tip-leakage flow in an axial fan at varying tip-gap sizes and operating conditions. *Computers and Fluids*, 183:107–129, 2019. ISSN 0045-7930. doi: https://doi.org/10.1016/j.compfluid.2019.01.014. URL https://www.sciencedirect.com/science/article/pii/S0045793019300088.

[25] S. Ning. A simple solution method for the blade element momentum equations with guaranteed convergence. *Wind Energy*, 17, 07 2013. doi: 10.1002/we.1636.

[26] J. Pereira. *Hover and wind-tunnel testing of shrouded rotors for improved micro air vehicle design*. PhD thesis, Department of Aerospace Engineering, University of Maryland, College Park, MD, 01 2008.

[27] Dal Props, 2021. URL https://www.dalprops.com/collections/bi-blade-5.

[28] M. Raffel, C. Willert, S. Wereley, and J. Kompenhans. *Particle Image Velocimetry: A Practical Guide*. 01 2007. ISBN 978-3-540-72307-3. doi: 10.1007/978-3-540-72308-0.

[29] S.F. Ramdin. Prandtl tip lsos factor assessed. *TU Delft repository*, 01 2017. URL https://repository.tudelft.nl/islandora/object/uuid:3eda6d83-9aaa-4632-8037-b44107a084e3.

[30] C. Rotaru and M. Todorov. Chapter 2: Helicopter flight physics. 2018. doi: https://doi.org/10.1016/j.renene.2020.01.064. URL https://www.intechopen.com/books/flight-physics-models-techniques-and-technologies/helicopter-flight-physics.

[31] P. Santosh. Noise generation mechanisms in short ducted rotors. Master's thesis, The Pennsylvania State University, College of Engineering, 08 2011.

[32] D. Shukla and N. Komerath. Rotor–duct aerodynamic and acoustic interactions at low reynolds number. *Experiments in Fluids*, 60:885–897, 05 2019. doi: 10.1007/s00348-018-2668-z.

[33] Vertical Flight Society. Press release: The electric vtol news tops 100 aircraft in directory, 2018. URL https://vtol.org/news/press-release-the-electric-vtol-news-tops-100-aircraft-in-directory.

[34] J. A. Storer and N. A. Cumpsty. Tip Leakage Flow in Axial Compressors. *Journal of Turbomachinery*, 113 (2):252–259, 04 1991. ISSN 0889-504X. doi: 10.1115/1.2929095. URL https://doi.org/10.1115/1.2929095.

[35] J. Taghinezhad, R. Alimardani, H. Mosazadeh, and M. Masdari. Ducted wind turbines a review. 04 2019.

[36] T. Tulwin. Low reynolds number rotor blade aerodynamic analysis. *MATEC Web of Conferences*, 252: 04006, 01 2019. doi: 10.1051/matecconf/201925204006.

[37] S. Yilmaz, D. Erdem, and M.S. Kavsaoglu. Performance of a ducted propeller designed for uav applications at zero angle of attack flight: An experimental study. *Journal of Visualization*, 45:376–386, 2015. doi: https://doi.org/10.1016/j.ast.2015.06.005. URL https://www.sciencedirect.com/science/article/pii/S1270963815001820.